CERN/LHCC 2017-003
LHCb EoI
08 February 2017

LHCb UPGRADE II

Opportunities in flavour physics,
and beyond, in the HL-LHC era

Expression of Interest

EUROPEAN ORGANIZATION FOR NUCLEAR RESEARCH (CERN)

CERN-LHCC-2017-003
February 8, 2017

Expression of Interest for a Phase-II LHCb Upgrade

Opportunities in flavour physics, and beyond, in the HL-LHC era

The LHCb collaboration

Abstract

A Phase-II Upgrade is proposed for the LHCb experiment in order to take full advantage of the flavour-physics opportunities at the HL-LHC, and other topics that can be studied with a forward spectrometer. This Upgrade, which will be installed in Long Shutdown 4 of the LHC (2030), will build on the strengths of the current experiment and the Phase-I Upgrade, but will consist of re-designed sub-systems that can operate at a luminosity of $2 \times 10^{34}\,\mathrm{cm}^{-2}\mathrm{s}^{-1}$, ten times that of the Phase-I Upgrade detector. New and improved detector components will increase the intrinsic performance of the experiment in certain key areas. In particular the installation of a tungsten sampling electromagnetic calorimeter will widen LHCb's capabilities for decays involving π^0 and η mesons, electrons, and photons from loop-level penguin processes. The physics motivation is presented, and the prospects for operating the LHCb Interaction Point at high luminosity are assessed. The challenges for the detector are described and possible solutions are discussed. Finally, the key R&D areas are summarised, together with a set of initial modifications suitable for implementation during Long Shutdown 3 (2024–2026).

LHCb collaboration

I. Bediaga, J.M. De Miranda, A. Gomes[a], A. Massafferri, J. Molina Rodriguez, A.C. dos Reis, A.B. Rodrigues, V. Salustino Guimaraes, l. Soares Lavra, R. Tourinho Jadallah Aoude [1] *Centro Brasileiro de Pesquisas Físicas (CBPF), Rio de Janeiro, Brazil*

S. Amato, A. Bursche, K. Carvalho Akiba, F. Da Cunha Marinho, L. De Paula, F. Ferreira Rodrigues, M. Gandelman, A. Hicheur, J.H. Lopes, D. Martins Tostes, I. Nasteva, J.M. Otalora Goicochea, E. Polycarpo, C. Potterat, M.S. Rangel, L. Silva de Oliveira, B. Souza De Paula [2] *Universidade Federal do Rio de Janeiro (UFRJ), Rio de Janeiro, Brazil*

L. An, A. Davis, Y. Gao, F. Jiang, T. Li, X. Liu, Z. Yang, L. Zhang, X. Zhu [3] *Center for High Energy Physics, Tsinghua University, Beijing, China*

L. Beaucourt, M. Chefdeville, D. Decamp, N. Déléage, Ph. Ghez, J.F. Marchand, M.-N. Minard, B. Pietrzyk, S. T'Jampens, V. Tisserand, E. Tournefier, Z. Xu [4] *LAPP, Université Savoie Mont-Blanc, CNRS/IN2P3, Annecy-Le-Vieux, France*

Z. Ajaltouni, M. Baalouch, E. Cogneras, O. Deschamps, G. Gazzoni, C. Hadjivasiliou, P. Henrard, M. Kozeiha, R. Lefèvre, J. Maratas[v], S. Monteil, P. Perret, M. Vernet [5] *Clermont Université, Université Blaise Pascal, CNRS/IN2P3, LPC, Clermont-Ferrand, France*

J. Arnau Romeu, E. Aslanides, J. Cogan, K. De Bruyn, R. Le Gac, O. Leroy, G. Mancinelli, M. Martin, J. Serrano, A. Tayduganov, A. Tsaregorodtsev [6] *CPPM, Aix-Marseille Université, CNRS/IN2P3, Marseille, France*

Y. Amhis, V. Balagura[c], S. Barsuk, F. Bossu, D. Chamont, F. Fleuret[b], J. Lefrançois, Y. Li, F. Machefert, L.M. Massacrier, E. Maurice[b], R. Quagliani[48], V. Renaudin, P. Robbe, M.-H. Schune, B. Viaud, M.A. Winn, G. Wormser, Y. Zhang [7] *LAL, Université Paris-Sud, CNRS/IN2P3, Orsay, France*

E. Ben-Haim, P. Billoir, M. Charles, L. Del Buono, V.V. Gligorov, A. Mogini, F. Polci [8] *LPNHE, Université Pierre et Marie Curie, Université Paris Diderot, CNRS/IN2P3, Paris, France*

S. Beranek, M. Boubdir, R. Greim, A. Heister, T. Kirn, C. Langenbruch, S. Nieswand, S. Schael, T.A. Verlage, C. Voß [9] *I. Physikalisches Institut, RWTH Aachen University, Aachen, Germany*

J. Albrecht, A. Birnkraut, M. Deckenhoff, M. Demmer, U. Eitschberger, R. Ekelhof, L. Gavardi, F. Kruse, F. Meier, J. Müller, V. Müller, R. Niet, S. Reichert, M. Schellenberg, M. Schlupp, T. Schmelzer, K. Schubert, B. Spaan, H. Stevens, T. Tekampe, J. Wishahi [10] *Fakultät Physik, Technische Universität Dortmund, Dortmund, Germany*

J. Blouw[†], H.-P. Dembinski, T. Klimkovich, D. Popov[40], M. Schmelling, M. Zavertyaev[c] [11] *Max-Planck-Institut für Kernphysik (MPIK), Heidelberg, Germany*

P. d'Argent, S. Bachmann, S. Braun, A. Comerma-Montells, M. De Cian, M. Dziewiecki, S. Esen, D. Gerick, E. Gersabeck, X. Han, S. Hansmann-Menzemer, M. Kecke, B. Khanji, M. Kolpin, R. Kopecna, K. Kreplin, B. Leverington, J. Marks, D.S. Mitzel, S. Neubert, M. Neuner, T. Nikodem, A. Piucci, M. Stahl, S. Stemmle, U. Uwer, M. Vesterinen, A. Zhelezov [12] *Physikalisches Institut, Ruprecht-Karls-Universität Heidelberg, Heidelberg, Germany*

R. McNulty, J.W. Ronayne, R. Wallace [13] *School of Physics, University College Dublin, Dublin, Ireland*

M. De Serio[d], R.A. Fini, A. Palano[d], M. Pappagallo[d], A. Pastore[d], S. Simone[d] [14] *Sezione INFN di Bari, Bari, Italy*

F. Betti, A. Carbone[e], A. Falabella, F. Ferrari, D. Galli[e], U. Marconi, M. Mussini, C. Patrignani[e], V. Vagnoni[40], G. Valenti, S. Zucchelli [15] *Sezione INFN di Bologna, Bologna, Italy*

W. Bonivento, S. Cadeddu, A. Cardini, L. Casu, V. Cogoni[f], D. Brundu, M. Fontana[40], P. Griffith, A. Lai, A. Loi, G. Manca[f], D. Marras, R. Oldeman[f], B. Saitta[f], C. Vacca[f] [16]*Sezione INFN di Cagliari, Cagliari, Italy*

M. Andreotti[g], W. Baldini, C. Bozzi[40], R. Calabrese[g], M. Corvo[g], M. Fiore[g], M. Fiorini[g], E. Luppi[g], L.L. Pappalardo[g], B.G. Siddi[40], G. Tellarini[g], L. Tomassetti[g], S. Vecchi [17]*Sezione INFN di Ferrara, Ferrara, Italy*

L. Anderlini, A. Bizzeti[u], G. Graziani, G. Passaleva, M. Veltri[r] [18]*Sezione INFN di Firenze, Firenze, Italy*

M. Anelli, A. Balla, G. Bencivenni, P. Campana, M. Carletti, P. Ciambrone, P. De Simone, P. Di Nezza, G. Felici, M. Gatta, G. Morello, S. Ogilvy, M. Palutan[40], M Poli Lener, M. Rotondo, M. Santimaria, A. Saputi, A. Sarti[k], F. Sborzacchi, B. Sciascia, R. Vazquez Gomez [19]*Laboratori Nazionali dell'INFN di Frascati, Frascati, Italy*

R. Cardinale[h], G. Cavallero, F. Fontanelli[h], A. Petrolini[h], A. Pistone [20]*Sezione INFN di Genova, Genova, Italy*

N. Belloli[i], A. Borgheresi[i], M. Calvi[i], P. Carniti[i], L. Cassina[i], D. Fazzini[i], C. Gotti[i], L. Grillo[40,i], C. Matteuzzi, P. Seyfert [21]*Sezione INFN di Milano Bicocca, Milano, Italy*

B. Dey, M. Citterio, S. Coelli, J. Fu[q], A. Merli[q,40], N. Neri[40], M. Petruzzo[q] [22]*Sezione INFN di Milano, Milano, Italy*

S. Amerio, A. Bertolin, S. Gallorini, D. Lucchesi[o], A. Lupato, E. Michielin, M. Morandin, L. Sestini, G. Simi[o] [23]*Sezione INFN di Padova, Padova, Italy*

F. Bedeschi, R. Cenci[t], A. Lusiani, P. Marino[t], M.J. Morello[t], G. Punzi[p], M. Rama, S. Stracka[p], J. Walsh [24]*Sezione INFN di Pisa, Pisa, Italy*

G. Carboni[j], E. Furfaro[j], E. Santovetti[j], A. Satta [25]*Sezione INFN di Roma Tor Vergata, Roma, Italy*

G. Auriemma, V. Bocci, P. Fresch, G. Martellotti, G. Penso, D. Pinci, R. Santacesaria, C. Satriano[s], A. Sciubba[k] [26]*Sezione INFN di Roma La Sapienza, Roma, Italy*

M. Baszczyk, W. Kucewicz[l], M. Kucharczyk, T. Lesiak, M. Pikies, M. Witek [27]*Henryk Niewodniczanski Institute of Nuclear Physics Polish Academy of Sciences, Kraków, Poland*

A. Dendek, M. Firlej, T. Fiutowski, M. Idzik, P. Morawski, J. Moron, A. Oblakowska-Mucha, B. Rachwal, K. Swientek, T. Szumlak [28]*AGH - University of Science and Technology, Faculty of Physics and Applied Computer Science, Kraków, Poland*

V. Batozskaya, K. Klimaszewski, W. Krzemien, K. Kurek, D. Melnychuk, M. Szczekowski, A. Ukleja, W. Wislicki [29]*National Center for Nuclear Research (NCBJ), Warsaw, Poland*

L. Cojocariu, L. Giubega, A. Grecu, F. Maciuc, V. Placinta, B. Popovici, S. Stoica, M. Straticiuc [30]*Horia Hulubei National Institute of Physics and Nuclear Engineering, Bucharest-Magurele, Romania*

G. Alkhazov, N. Bondar, A. Chubykin, A. Dzyuba, S. Kotriakhova, O. Maev, N. Sagidova, Y. Shcheglov, A. Vorobyev [31]*Petersburg Nuclear Physics Institute (PNPI), Gatchina, Russia*

F. Baryshnikov, I. Belyaev, I. Bordyuzhin, V. Egorychev, D. Golubkov, A. Kosmyntseva, T. Kvaratskheliya[40], E. Sadykhov, D. Savrina[33], A. Semennikov [32]*Institute of Theoretical and Experimental Physics (ITEP), Moscow, Russia*

A. Berezhnoy, I.V. Gorelov, A. Kozachuk, A. Leflat[40], N. Nikitin, V. Volkov, V. Zhukov [33]*Institute of Nuclear Physics, Moscow State University (SINP MSU), Moscow, Russia*

S. Filippov, E. Gushchin, L. Kravchuk [34] *Institute for Nuclear Research of the Russian Academy of Sciences (INR RAN), Moscow, Russia*

A. Baranov, M. Borisyak, D. Derkach, M. Hushchyn, E. Khairullin, T. Likhomanenko[68], F. Ratnikov, A. Rogozhnikov, A. Ustyuzhanin [35] *Yandex School of Data Analysis, Moscow, Russia*

A. Bondar[w], S. Eidelman[w], P. Krokovny[w], V. Kudryavtsev[w], T. Maltsev, L. Shekhtman[w], V. Vorobyev[w], X. Yuan[w] [36] *Budker Institute of Nuclear Physics (SB RAS), Novosibirsk, Russia*

A. Artamonov, K. Belous, R. Dzhelyadin, Yu. Guz, A. Novoselov, V. Obraztsov, A. Popov, S. Poslavskii, V. Romanovskiy, M. Shapkin, O. Stenyakin, O. Yushchenko [37] *Institute for High Energy Physics (IHEP), Protvino, Russia*

A. Badalov, M. Calvo Gomez[m], A. Camboni, S. Coquereau, G. Fernandez, L. Garrido, D. Gascon, R. Graciani Diaz, E. Graugés, C. Marin Benito, E. Picatoste Olloqui, V. Rives Molina, D. Sanchez Gonzalo, X. Vilasis-Cardona[m] [38] *ICCUB, Universitat de Barcelona, Barcelona, Spain*

B. Adeva, M. Borsato, V. Chobanova, X. Cid Vidal, A. Dosil Suárez, A. Fernandez Prieto, A. Gallas Torreira, J. García Pardiñas, E. Lemos Cid, M. Lucio Martinez, D. Martinez Santos, M. Plo Casasus, J. Prisciandaro, M. Ramos Pernas, A. Romero Vidal, J.J. Saborido Silva, B. Sanmartin Sedes, C. Santamarina Rios, P. Vazquez Regueiro, C. Vázquez Sierra, M. Vieites Diaz [39] *Universidad de Santiago de Compostela, Santiago de Compostela, Spain*

R. Aaij, F. Alessio, C. Barschel, M.-O. Bettler, J. Buytaert, D.H. Campora Perez, M. Cattaneo, Ph. Charpentier, M. Clemencic, J. Closier, P. Collins, A. Contu, G. Coombs, G. Corti, B. Couturier, C. D'Ambrosio, A. Di Canto, H. Dijkstra, F. Dordei, K. Dungs, P. Durante, A. Dziurda, C. Färber, M. Ferro-Luzzi, K. Fohl, R. Forty, M. Frank, C. Frei, W. Funk, C. Gaspar, L.A. Granado Cardoso, T. Gys, C. Haen, M. Hatch, E. van Herwijnen, R. Jacobsson, D. Johnson, C. Joram, B. Jost, M. Karacson, D. Lacarrere, F. Lemaitre, R. Lindner, O. Lupton, R. Matev, Z. Mathe, N. Neufeld, A. Otto, A. Pearce, M. Pepe Altarelli, S. Perazzini, T. Poikela, S. Ponce, M. Rihl, S. Roiser, T. Ruf, H. Schindler, B. Schmidt, A. Schopper, R. Schwemmer, S. Sridharan, F. Stagni, S. Stahl, F. Teubert, E. Thomas, D. Tonelli, A. Trisovic, A. Valassi, S. Valat, J.V. Viana Barbosa, B. Voneki, M. Whitehead, M. Williams, K. Wyllie [40] *European Organization for Nuclear Research (CERN), Geneva, Switzerland*

G. Andreassi, V. Battista, A. Bay, V. Bellee, F. Blanc, L. Castillo Garcia, M. Dorigo, C. Fitzpatrick, S. Gianì, O.G. Girard, G. Haefeli, T. Head, H. Hopchev, C. Khurewathanakul, I. Komarov, A.K. Kuonen, M. Marinangeli, M. Martinelli, B. Maurin, T. Nakada, T.D. Nguyen, C. Nguyen-Mau[n], P.R. Pais, L. Pescatore, O. Schneider, M. Schubiger, P. Stefko, M.E. Stramaglia, M. Tobin, S. Tourneur, K. Trabelsi, M.T. Tran [41] *Institute of Physics, Ecole Polytechnique Fédérale de Lausanne (EPFL), Lausanne, Switzerland*

R. Bernet, C. Betancourt, Ia. Bezshyiko, E. Bowen, M. Chrzaszcz[27], E. Graverini, F. Lionetto, A. Mauri, K. Müller, P. Owen, A. Puig Navarro, N. Serra, R. Silva Coutinho, O. Steinkamp, B. Storaci, U. Straumann, M. Tresch, A. Vollhardt, A. Weiden [42] *Physik-Institut, Universität Zürich, Zürich, Switzerland*

S. Ali, F. Archilli, L.J. Bel, S. Benson, M. van Beuzekom, G. Ciezarek, E. Dall'Occo, P.N.Y. David, L. Dufour, E. Govorkova, W. Hulsbergen, E. Jans, P. Koppenburg, J. van Leerdam, M. Merk, M. Mulder, A. Pellegrino, J. van Tilburg, P. Tsopelas, N. Tuning, M. van Veghel, J.A. de Vries [43] *Nikhef National Institute for Subatomic Physics, Amsterdam, The Netherlands*

T. Ketel, G. Raven, V. Syropoulos [44] *Nikhef National Institute for Subatomic Physics and VU University Amsterdam, Amsterdam, The Netherlands*

A. Dovbnya, S. Kandybei, I. Raniuk, I. Shapoval [45] *NSC Kharkiv Institute of Physics and Technology (NSC KIPT), Kharkiv, Ukraine*

S. Koliiev, V. Pugatch [46] *Institute for Nuclear Research of the National Academy of Sciences (KINR), Kyiv, Ukraine*

S. Bifani, G. Chatzikonstantinidis, N. Farley, C. Lazzeroni, A. Mazurov, A. Sergi, N.K. Watson, M.P. Williams, T. Williams, K.A. Zarebski [47] *University of Birmingham, Birmingham, United Kingdom*

M. Adinolfi, E. Buchanan, A. Cook, J. Dalseno, S.T. Harnew, J.M. Kariuki, P. Naik, K. Petridis, G.J. Pomery, E. Price, C. Prouve, J.H. Rademacker, S. Richards, D.M. Saunders, N. Skidmore, J.J. Velthuis [48] *H.H. Wills Physics Laboratory, University of Bristol, Bristol, United Kingdom*

H.V. Cliff, H.M. Evans, J. Garra Tico, P.J. Garsed, V. Gibson, S.C. Haines, C.R. Jones, M. Kenzie, M. Sirendi, J. Smith, S. Tolk, A. Tully, M. Vitti, D.R. Ward, S.A. Wotton [49] *Cavendish Laboratory, University of Cambridge, Cambridge, United Kingdom*

J.J. Back, T. Blake, C.M. Costa Sobral, A. Crocombe, T. Gershon, M. Kreps, T. Latham, D. Loh, A. Mathad, D.P. O'Hanlon, A. Poluektov[36], W. Qian, C. Wallace, J. Wicht [50] *Department of Physics, University of Warwick, Coventry, United Kingdom*

S. Easo, R. Nandakumar, A. Papanestis, S. Ricciardi, F.F. Wilson [51] *STFC Rutherford Appleton Laboratory, Didcot, United Kingdom*

L. Carson, P.E.L. Clarke, G.A. Cowan, D.C. Craik, M. Ebert, S. Eisenhardt, D. Ferguson, S. Gambetta, K. Gizdov, H. Luo, A.B. Morris, F. Muheim, M. Needham, S. Playfer, I.T. Smith [52] *School of Physics and Astronomy, University of Edinburgh, Edinburgh, United Kingdom*

M. Alexander, J. Beddow, C.T. Dean, L. Eklund, S. Karodia, I. Longstaff, M. Schiller, F.J.P. Soler, P. Spradlin, M. Traill, K. Wraight [53] *School of Physics and Astronomy, University of Glasgow, Glasgow, United Kingdom*

T.J.V. Bowcock, G. Casse, F. Dettori, K. Dreimanis, S. Farry, R. Fay, V. Franco Lima, K. Hennessy, D. Hutchcroft, K. Rinnert, T. Shears, H.M. Wark [54] *Oliver Lodge Laboratory, University of Liverpool, Liverpool, United Kingdom*

P. Alvarez Cartelle, S. Baker, S. Cunliffe, R. Currie, U. Egede, A. Golutvin[40], T. Humair, M. McCann[40], M. Patel, F. Redi, E. Smith, M. Smith, S. Stefkova, W. Sutcliffe, M.J. Tilley, D. Websdale [55] *Imperial College London, London, United Kingdom*

R.B. Appleby, I. Babuschkin, R.J. Barlow, W. Barter, A. Bitadze, S. Borghi, J. Brodzicka, C. Burr, L. Capriotti, S. Chen, S. De Capua, G. Dujany, M. Gersabeck, J. Harrison, C. Hombach, S. Klaver, G. Lafferty, K. Maguire, A. McNab, D. Müller, C. Parkes, P. Rodriguez Perez† [56] *School of Physics and Astronomy, University of Manchester, Manchester, United Kingdom*

S.-F. Cheung, T. Evans, P. Gandini, B.R. Gruberg Cazon, T. Hadavizadeh, N. Harnew, D. Hill, J. Jalocha, M. John, N. Jurik, S. Malde, A. Nandi, A. Rollings, S. Topp-Joergensen, M. Van Dijk, G. Veneziano, G. Wilkinson[40] [57] *Department of Physics, University of Oxford, Oxford, United Kingdom*

T. Boettcher, P. Ilten, M. Williams [58] *Massachusetts Institute of Technology, Cambridge, MA, United States*

S. Akar, A.A. Alves Jr, V. Coco, Z.-C. Huard, B. Meadows, C. Pappenheimer, E. Rodrigues, H.F. Schreiner, M.D. Sokoloff [59] *University of Cincinnati, Cincinnati, OH, United States*

J.E. Andrews, B. Hamilton, A. Jawahery, W. Parker, J. Wimberley, Z Yang [60] *University of Maryland, College Park, MD, United States*

M. Artuso, B. Batsukh, A. Beiter, S. Blusk, T. Britton, S. Ely, D.C. Forshaw, M. Kelsey, Z. Li, P. Manning, R. Mountain, I. Polyakov, M.S. Rudolph, T. Skwarnicki, S. Stone, F. Toriello, A. Venkateswaran, J. Wang, M. Wilkinson, Z. Xing, Y. Yao [61] *Syracuse University, Syracuse, NY, United States*

C. Baesso, M. Cruz Torres, C. Göbel [62] *Pontifícia Universidade Católica do Rio de Janeiro (PUC-Rio), Rio de Janeiro, Brazil, associated to Institute* [2]

J. He, X. Lyu, C. Qian, D. Vieira, Y. Zheng [63] *University of Chinese Academy of Sciences, Beijing, China, associated to Institute* [3]

L. Sun [64] *School of Physics and Technology, Wuhan University, Wuhan, China, associated to Institute* [3]

Y. Xie, H. Yin, J. Yu [65] *Institute of Particle Physics, Central China Normal University, Wuhan, Hubei, China, associated to Institute* [3]

D.A. Milanes, I.A. Monroy, J.A. Rodriguez Lopez [66] *Departamento de Fisica , Universidad Nacional de Colombia, Bogota, Colombia, associated to Institute* [8]

O. Grünberg, M. Heß, H. Viemann, R. Waldi [67] *Institut für Physik, Universität Rostock, Rostock, Germany, associated to Institute* [11]

A. Malinin, O. Morgunova, A. Nogay, A. Petrov, V. Shevchenko [68] *National Research Centre Kurchatov Institute, Moscow, Russia, associated to Institute* [30]

L.M. Garcia Martin, L. Henry, F. Martinez Vidal, A. Oyanguren, C. Remon Alepuz, P. Ruiz Valls, C. Sanchez Mayordomo [69] *Instituto de Fisica Corpuscular, Centro Mixto Universidad de Valencia - CSIC, Valencia, Spain, associated to Institute* [35]

C.J.G. Onderwater [70] *Van Swinderen Institute, University of Groningen, Groningen, The Netherlands, associated to Institute* [23]

[a] *Universidade Federal do Triângulo Mineiro (UFTM), Uberaba-MG, Brazil*
[b] *Laboratoire Leprince-Ringuet, Palaiseau, France*
[c] *P.N. Lebedev Physical Institute, Russian Academy of Science (LPI RAS), Moscow, Russia*
[d] *Università di Bari, Bari, Italy*
[e] *Università di Bologna, Bologna, Italy*
[f] *Università di Cagliari, Cagliari, Italy*
[g] *Università di Ferrara, Ferrara, Italy*
[h] *Università di Genova, Genova, Italy*
[i] *Università di Milano Bicocca, Milano, Italy*
[j] *Università di Roma Tor Vergata, Roma, Italy*
[k] *Università di Roma La Sapienza, Roma, Italy*
[l] *AGH - University of Science and Technology, Faculty of Computer Science, Electronics and Telecommunications, Kraków, Poland*
[m] *LIFAELS, La Salle, Universitat Ramon Llull, Barcelona, Spain*
[n] *Hanoi University of Science, Hanoi, Viet Nam*
[o] *Università di Padova, Padova, Italy*
[p] *Università di Pisa, Pisa, Italy*
[q] *Università degli Studi di Milano, Milano, Italy*
[r] *Università di Urbino, Urbino, Italy*
[s] *Università della Basilicata, Potenza, Italy*
[t] *Scuola Normale Superiore, Pisa, Italy*
[u] *Università di Modena e Reggio Emilia, Modena, Italy*
[v] *Iligan Institute of Technology (IIT), Iligan, Philippines*
[w] *Novosibirsk State University, Novosibirsk, Russia*

[†] *Deceased*

Contents

Chapter 1

Executive summary

Overview

It is proposed to upgrade the LHCb experiment in order to take full advantage of the flavour-physics opportunities at the High Luminosity LHC (HL-LHC). A detector will be installed for the beginning of Run 5, currently scheduled to begin in 2031, which can operate at luminosities of around $2 \times 10^{34}\,\mathrm{cm}^{-2}\mathrm{s}^{-1}$ and be suitable for a comprehensive range of flavour physics measurements, as well as spectroscopy studies and other physics in the forward direction. The project will be a Phase-II Upgrade and build on the achievements of both the current detector and the Phase-I Upgrade, which is currently under construction. New attributes will also enhance the detector's capabilities to a wider range of physics signatures. Valuable preparatory work can be performed in Long Shutdown 3 (LS3) (2024–2026), which will have benefits for Phase-I performance. The Phase-II Upgrade will allow the experiment to accumulate data corresponding to a minimum of $300\,\mathrm{fb}^{-1}$, and enable many important observables to be measured with a precision unattainable at any other experiment. This project will extend the HL-LHC's capabilities to search for physics beyond the Standard Model (SM), and implements the highest-priority recommendation of the European Strategy for Particle Physics (Update 2013) [1], which is to exploit the full potential of the LHC for a variety of physics goals, including flavour.

Flavour physics and the LHCb experiment

The precise measurement of flavour-changing transitions in hadrons is a long-established and powerful tool to seek out manifestations of new physics phenomena. The mass scales that can be probed in loop-level processes are far higher than those that can be accessed in direct searches for on-shell particles. Furthermore, many of the open questions in fundamental physics reside in the flavour sector. Why are there three generations of fermions and what is responsible for their hierarchy of masses? What determines the characteristic structure of the Cabibbo-Kobayashi-Maskawa (CKM) matrix? What is the nature and origin of the *CP* violation that is responsible for the baryon-antibaryon asymmetry of the universe?

The LHCb experiment has demonstrated emphatically that the LHC is an ideal laboratory for quark-flavour physics. Significant achievements include the discovery of the ultra-rare decay $B^0_s \to \mu^+\mu^-$ [2–5], the first single-experiment observation of charm mixing [6], and the world's most precise measurements of both the CKM angle γ [7] and the B^0_s weak-phase ϕ_s [8, 9]. The experimental attributes that have made these measurements possible have also allowed LHCb

to make major advances in hadron spectroscopy, for example the first discovery of pentaquark states [10], as well as unique contributions to electroweak, QCD and heavy ion physics (*e.g.* Refs. [11–13]), topics which were not considered when the detector was being designed.

The current LHCb detector, operating at a luminosity of $\sim 4 \times 10^{32}\,\mathrm{cm}^{-2}\mathrm{s}^{-1}$, will continue data taking until the end of Run 2 of the LHC, in 2018. During Long Shutdown 2 (LS2) it will be replaced by an upgraded experiment, referred to in this document as the Phase-I Upgrade. This Upgrade will employ a full software trigger, which will provide significantly increased efficiency in hadronic final states, and allow the experiment to function effectively at the higher luminosity of $2 \times 10^{33}\,\mathrm{cm}^{-2}\mathrm{s}^{-1}$. In order to read out the experiment at the crossing rate of the LHC and to operate at this higher luminosity, most of the sub-detectors will be replaced, as will all of the frontend electronics and data-acquisition system. In particular, a pixel Vertex Locator (VELO), a silicon tracking station before the magnet (UT) and a large-scale downstream Scintillating Fibre (SciFi) tracker system will be installed. The evolving design of the Phase-I Upgrade has been presented in several documents [14–20] and progress towards construction and installation has been reported regularly to the LHCC. By the end of LHC Run 4, in 2029, the experiment will have accumulated a data sample of around $50\,\mathrm{fb}^{-1}$. Further data taking with the Phase-I detector will not be attractive beyond this date, on account of the excessive 'data-doubling' time, and many of its components will have reached the end of their natural life span in terms of radiation exposure.

The Phase-I Upgrade will greatly improve the sensitivity of many flavour studies, as will the Belle-II experiment at KEK [21], which is scheduled to have finished data taking by the mid 2020s. However, the precision on a host of important, theoretically clean, measurements will still be limited by statistics, and other observables associated with highly suppressed processes will be poorly known. There is therefore a strong motivation for building a Phase-II Upgrade, which will fully realise the flavour potential of the HL-LHC.

The LHCb Phase-II Upgrade

Studies indicate that HL-LHC will be able to supply peak luminosities to Interaction Point 8 (IP8), where LHCb is located, of around $2 \times 10^{34}\,\mathrm{cm}^{-2}\mathrm{s}^{-1}$ at start of fill. A detector with the capability to operate in this environment could accumulate an annual integrated luminosity of up to seven times larger than that collected by the Phase-I Upgrade. The lifetime of the inner triplets at IP8, with appropriate shielding in place, is expected to correspond to an integrated luminosity of $300\,\mathrm{fb}^{-1}$. This total, achievable within the planned HL-LHC operation schedule, sets the baseline target for the Phase-II Upgrade data taking, although improved understanding of the triplets' response to radiation damage may allow this value to be raised.

The Phase-II Upgrade will be capable of a broad spectrum of important flavour-physics measurements. The key goals are as follows:

- A comprehensive measurement programme of observables in a wide range of $b \to s l^+ l^-$ and $b \to d l^+ l^-$ transitions, many not accessible in the current experiment or Phase-I Upgrade, employing both muon and electron modes;
- Measurements of the *CP*-violating phases γ and ϕ_s with a precision of 0.4° and 3 mrad, respectively;
- Measurement of $R \equiv \mathcal{B}(B^0 \to \mu^+\mu^-)/\mathcal{B}(B_s^0 \to \mu^+\mu^-)$ with an uncertainty of 20%, and the first precise measurements of associated $B_s^0 \to \mu^+\mu^-$ observables;

- A wide-ranging set of lepton-universality tests in $b \to cl^- \bar{\nu}_l$ decays, exploiting the full range of b-hadrons;
- CP-violation studies in charm with 10^{-5} precision.

In addition, the Phase-II Upgrade will be capable of major discoveries in hadron spectroscopy, and pursuing a wide and unique programme of general physics measurements, complementary to those of ATLAS and CMS.

Although the HL-LHC will begin operation with Run 4 in 2026, the Phase-II Upgrade will not be installed until Long Shutdown 4, which takes place in 2030. [1] This offset is to allow the Phase-I Upgrade to complete its programme, and to allow sufficient time for the appropriate R&D and construction activities to take place. Nonetheless, LS3, scheduled for 2024-2026, provides an ideal opportunity for preparatory activities, together with consolidation work and modest improvements to the Phase-I detector that can also be regarded as first steps towards the Phase-II project. Table 1.1 summarises the periods of operation of the various phases of the LHCb experiment, and the data taking parameters.

Table 1.1: Summary of LHCb pp data taking and running conditions for the current experiment, the Phase-I and Phase-II Upgrades. The future years of data taking will be interrupted by Long Shutdowns 2, 3, 4 and 5, currently scheduled to take place in 2019-2020, 2024-2026, 2030 and 2034, respectively [22].

	LHC Run	Period of data taking	Maximum $\mathcal{L}$ $[\mathrm{cm}^{-2}\mathrm{s}^{-1}]$	Cumulative $\int \mathcal{L}\,dt$ $[\mathrm{fb}^{-1}]$
Current detector	1 & 2	2010–2012, 2015–2018	4×10^{32}	8
Phase-I Upgrade	3 & 4	2021–2023, 2026–2029	2×10^{33}	50
Phase-II Upgrade	5 $\to$	2031–2033, 2035 $\to$	2×10^{34}	300

The challenges of performing precision flavour physics at the high luminosities under consideration are daunting. The mean number of interactions, μ, in each event will be around 50. The increased particle multiplicity and rates will present significant problems for all detectors, as will the increased radiation damage for certain components. A thorough study, involving both simulation and detector R&D, will be required to find realisable designs for each sub-system. Nonetheless, promising potential solutions may already be identified. An essential attribute, not present in the current detector or the Phase-I Upgrade, will be precise timing, in the VELO detector, and also downstream of the magnet for both charged tracks and neutrals. This information, if it approaches a resolution of a few tens of ps per particle, will allow charged tracks and photons to be associated to the correct interaction vertex, thereby suppressing combinatoric background and also allowing for time-dependent CP measurements.

The detector design outlined in this document would deliver a similar performance to the Phase-I Upgrade, with the potential to exceed it in certain key attributes, bringing significant physics gains in addition to those coming from the increased integrated luminosity. In particular, a high granularity tungsten sampling electromagnetic calorimeter will extend the experiment's capabilities in final states involving photons, π^0 mesons and electrons, with which many important

[1] This Long Shutdown is currently scheduled to last only one year [22], but would need to be extended to at least 18 months to allow the Phase-II Upgrade to be installed.

studies may be conducted. By instrumenting the side walls of the dipole, the tracking acceptance can be significantly increased for soft tracks, improving the experiment's efficiency for high multiplicity decays. The downstream fast-timing capabilities required for rejecting combinatoric background can also be used for improving particle identification at low momentum. In addition, improvements can be foreseen in the RICH system and the VELO. The initial steps of a limited number of these detector upgrade projects could already be installed during LS3, allowing the Phase-I experiment to improve its physics reach during Run 4.

This document is organised as follows. The motivation for a high-precision flavour-physics programme at the HL-LHC is presented in Chapter 2, together with a discussion of other interesting physics topics. The capabilities of the accelerator for delivering high-luminosity collisions at IP8 and the implications for the machine components are briefly summarised in Chapter 3. The requirements on the detector and initial thoughts on possible solutions for each sub-system are discussed in Chapter 4, while in Chapter 5 the R&D plans are outlined, and a selection of potential first steps to be taken in LS3 is given.

Chapter 2

Physics opportunities

2.1 Flavour physics in the HL-LHC era

The HL-LHC era will begin with Run 4, currently scheduled to start in 2026. By this time the Belle-II experiment at KEK is expected to have finished operation, having collected around $50\,\text{ab}^{-1}$ of integrated luminosity. The only running experiments worldwide capable of performing b-physics measurements will be at CERN, namely the ongoing LHCb Phase-I Upgrade, and the General Purpose Detectors, ATLAS and CMS. The latter two experiments will themselves have been upgraded in preparation for the higher luminosities and the harsher environment of the new machine, with the goal of accumulating an integrated luminosity of $3000\,\text{fb}^{-1}$ each.

LHCb [23] is designed to reach much lower p_{T} thresholds than ATLAS or CMS, which leads to a higher efficiency for reconstructing the decay products of b- and c-hadrons. This attribute is complemented by excellent vertex and proper time resolution, provided by the VELO detector, which are vital assets for flavour studies. In addition, LHCb is unique among the LHC experiments in having hadron identification across a wide momentum spectrum and, from Run 3 onwards, will be alone in having a fully software-based trigger able to perform offline-like selections at the full LHC crossing rate.

The LHCb Phase-I Upgrade will continue data taking until the end of Run 4, after which it will become too time-consuming to accumulate significantly larger samples, and when the radiation dose will have reached the design values for several critical sub-systems. However, notwithstanding the improvement in knowledge that can be expected from the Phase-I Upgrade, and from Belle II, there will be strong arguments to continue flavour physics studies at the LHC with a dedicated experiment. This realisation motivates the current proposal, for a Phase-II Upgrade of LHCb that will operate at luminosities of around $2 \times 10^{34}\,\text{cm}^{-2}\text{s}^{-1}$ and thereby exploit the full flavour-physics potential of the HL-LHC. A comprehensive programme of highly sensitive flavour studies will become possible, which will complement the improved knowledge of the Higgs couplings that will be achieved by ATLAS and CMS.

Many studies of suppressed decays of heavy-flavour hadrons and τ-leptons, which are of great interest in probing for New Physics (NP) effects, are limited by the sample sizes available and will greatly benefit from the significant increase in integrated luminosity that the Phase-II Upgrade will enable. Similarly, some of the most interesting measurements of weak phases, for example the unitarity-triangle angle γ and the B_s^0 mixing phase ϕ_s, are not limited by systematic uncertainties and so can be determined with even higher precision in the HL-LHC era. Such

measurements will allow LHCb to probe the CKM paradigm at the level of the SM theoretical predictions. Furthermore, a significant increase in the data sample will allow a wider range of decay modes and observables to be measured. In addition to the increased statistical precision that the Phase-II experiment will bring, the increased range of measurements will permit searches for patterns of correlated deviations from the SM across a wide range of observables, which will be invaluable in distinguishing between viable NP models. Finally, the Phase-II Upgrade will widen the physics opportunities in many areas beyond flavour, such as hadron spectroscopy and studies of SM processes in the forward region.

In the following discussion it is assumed that the experiment will collect $300\,\text{fb}^{-1}$ of integrated luminosity and the Phase-II detector will have a similar performance to the Phase-I Upgrade in the parameters that are important for flavour physics. In fact, as is explained in Chapter 4, it is proposed to extend the experiment's capabilities in certain key areas, in particular sensitivity to π^0 and η mesons, photons and electrons, and to low-momentum charged tracks. These improvements are expected to have a significant impact on the physics reach beyond the increase in statistical power that the Phase-II Upgrade will bring.

2.2 Rare processes and lepton-universality tests

The study of semileptonic $b \to s l^+ l^-$ transitions, in which the dilepton pair is not produced in the decay of a hadronic resonance, offers a rich set of observables that probe and constrain [24] viable NP models in a complementary way to the study of $B^0_s \to \mu^+\mu^-$ and the radiative process $b \to s\gamma$. LHCb has already reported important results for many of these modes [25–31], most notably $B^0 \to K^{(*)}\mu^+\mu^-$ and $B^0 \to K^{(*)}e^+e^-$. The main systematic uncertainties are expected to scale with integrated luminosity, motivating continued study of these decay channels at the Phase-II Upgrade. Recent measurements have prompted discussion about the size of possible charm-loop effects, which may introduce additional theoretical uncertainties in the interpretation of the observables. Data-driven methods to control such effects are being developed, *e.g.* Ref. [32], and can be fully exploited with the Phase-II Upgrade data sample. The improvement in statistical precision for quantities already under study can be assessed from Fig. 2.1(a), which compares the Run-1 sensitivity for the $B^0 \to K^*\mu^+\mu^-$ observable P'_5 in bins of the dimuon invariant-mass squared, q^2, with that expected in the Phase-II Upgrade. The region $4 < q^2 < 8\,\text{GeV}^2/c^4$, where there currently exists a discrepancy between data and prediction, will be mapped out with very high precision using the larger data set. More importantly, new observables, particularly in the B^0_s and Λ^0_b sectors, will be measured with excellent sensitivity for the first time, for example those accessible in a flavour-tagged time-dependent analysis of the decay $B^0_s \to \phi\mu^+\mu^-$.

Since any plausible NP model should affect all $b \to s l^+ l^-$ transitions in a coherent way, this comprehensive study will allow for a powerful global test of any observed deviations from the SM picture of the kind which current measurements may hint at (*e.g.* see Ref. [35, 36]). The Phase-II Upgrade will not only improve the statistical sensitivity of such a global test of the SM. By allowing many of the most suppressed observables in $b \to s l^+ l^-$ transitions to be measured for the first time, it will also reduce the dependence of such tests on the accuracy of the theoretical prediction of any single observable, allowing for much greater confidence in the interpretation of the results. Since the analyses will be performed for both electron and muon final states, all measurements will also be naturally interpretable as tests of $e - \mu$ lepton universality. By way of example, Fig. 2.1(b) displays the results of a simulation study closely

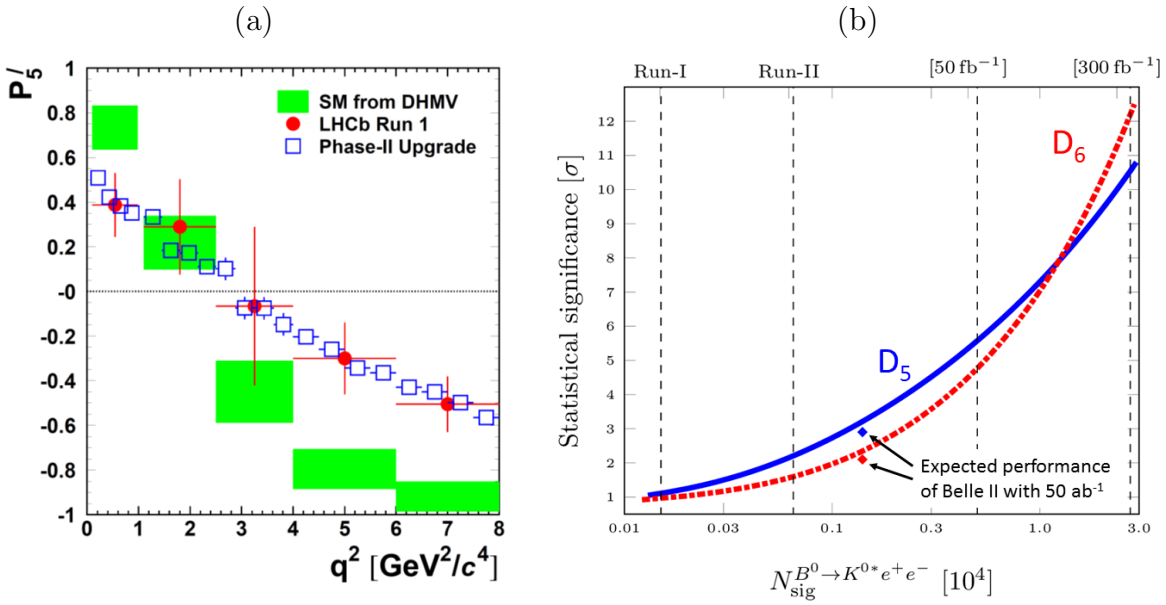

Figure 2.1: Electroweak penguin studies at the Phase-II Upgrade. (a) P'_5 vs. q^2, showing the LHCb Run-1 results [25] and those of a simulated experiment with 300 fb^{-1}, assuming the same central values. The SM predictions, with the currently assigned uncertainties, come from Ref. [33]. (b) significance of the measured values of S_5 and S_6, quantifying lepton-universality violation in $B^0 \to K^*\mu^+\mu^-$ and $B^0 \to K^*e^+e^-$ decays, as a function of sample size, assuming a NP scenario defined in Ref. [34]. The correspondence with the different running periods of LHCb is indicated, as is the expected performance of Belle II.

based on that presented in Ref. [34], showing the significance of the measurement of the observable D_5, which is closely related to the differences in behaviour for P'_5 between muon and electron modes, and is expected to be vanishingly small in the SM. Also shown is the significance on the measurement of the observable D_6, again very close to 0 in the SM. The generated values for D_5 and D_6 are set to non-zero NP numbers compatible with current constraints [34]. The expected significances are shown as a function of $B^0 \to K^*e^+e^-$ sample size. Also indicated is the correspondence between the sample size and the running period of LHCb, as extrapolated from Run-1 measurements [28] and taking no account of possible improvements to the ECAL during Phase II. For this NP scenario, and for many others with smaller lepton-universality violating contributions, the Phase-II Upgrade will be required to observe a clear effect.

Similar arguments hold for studies of $b \to dl^+l^-$ transitions, albeit with lower statistical precision, as may be illustrated with a few examples. The angular analysis of the $b \to dl^+l^-$ decay $B_s^0 \to \overline{K}^{*0}\mu^+\mu^-$ with the data sample collected by the Phase-II Upgrade is expected to become more precise than the Run-1 result for the $b \to sl^+l^-$ process $B^0 \to K^{*0}\mu^+\mu^-$, enabling a powerful comparison between different flavour transitions. A time-dependent analysis will become feasible for the mode $B^0 \to \rho^0\mu^+\mu^-$. The large sample sizes, coupled with the improved π^0-reconstruction that is foreseen from an upgraded ECAL (see Sec. 4.3.3), will allow for isospin tests in $B \to \rho\mu^+\mu^-$ and $B \to \pi\mu^+\mu^-$ decays.

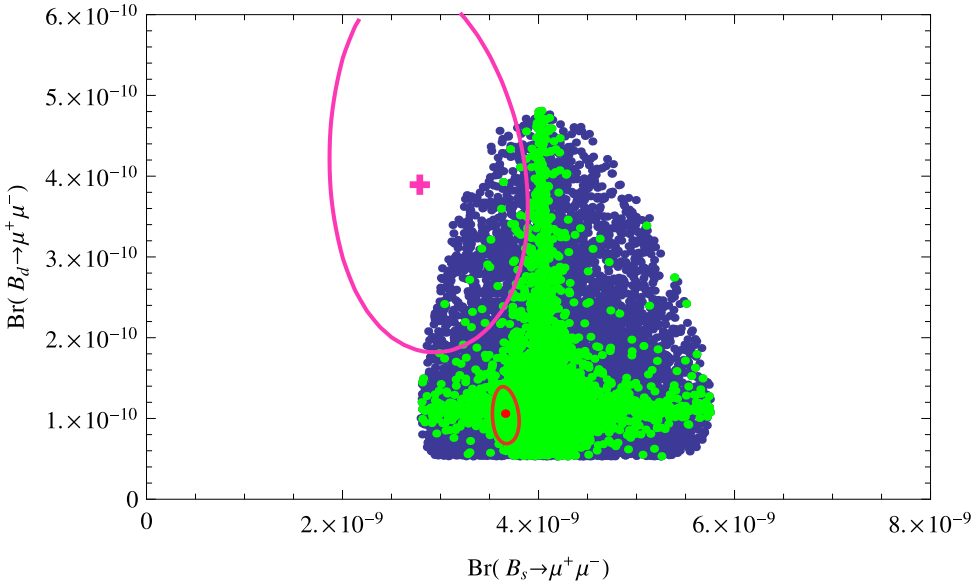

Figure 2.2: $\mathcal{B}(B_s^0 \to \mu^+\mu^-)$ vs $\mathcal{B}(B^0 \to \mu^+\mu^-)$ as computed using new sources of flavour-changing neutral currents, as discussed in Ref. [41]. The green points are the subset consistent with other measurements. The red point is the SM prediction. The pink contour corresponds to the 68% C.L. region determined by the Run-1 measurements [2–4] and the red contour corresponds to future measurements centred at the SM prediction with a $\sim 14\%$ precision on R.

The upgraded ECAL will also be very valuable in improving the sensitivity of the experiment to studies of $b \to s\gamma$ and $b \to d\gamma$ processes. The Phase-II Upgrade will be unique in allowing precision measurements of time-dependent $b \to s\gamma$ observables in the decay of B_s^0 hadrons, for example enabling the photon polarisation in $B_s^0 \to \phi\gamma$ [37] to be measured with a sensitivity comparable to the precision on the SM prediction for the first time, and also making accessible polarisation measurements with rare baryon decays, such as $\Lambda_b^0 \to \Lambda\gamma$, $\Xi_b \to \Xi\gamma$ and $\Omega_b \to \Omega\gamma$.

Lepton universality studies in $b \to c l^- \bar{\nu}$ transitions are of growing interest and provide complementary constraints on possible NP models. Recent measurements of $R_{D^{(*)}} \equiv \mathcal{B}(B \to D^{(*)}\tau^-\bar{\nu_\tau})/\mathcal{B}(B \to D^{(*)}\mu^-\bar{\nu_\mu})$, both at the B-factories [38, 39] and LHCb [40], have indicated some tension with the SM. The Phase-II Upgrade will allow LHCb to test both $\tau - \mu$ and $\mu - e$ universality in $b \to c l^- \bar{\nu}$ transitions at better than the percent level across the full range of decaying b-hadrons, and in particular will allow precision measurements of $\tau - \mu$ universality in B_c^+ decays for the first time. The yields of $B \to D^{(*)}\tau^-\bar{\nu_\tau}$ decays will be sufficiently large to allow for precise polarisation studies of the final-state particles, which are complementary to the measurement of $R_{D^{(*)}}$. Again, a global analysis will be crucial for not only testing the SM, but also discriminating between different models of NP.

The very rare decay $B_s^0 \to \mu^+\mu^-$ has been successfully observed at the LHC, and its branching ratio measured to be consistent with the SM predictions with a precision of 23% [2–5]. The rate of the decay $B^0 \to \mu^+\mu^-$ is suppressed by a factor $|V_{td}/V_{ts}|^2$ in the SM, and no significant signal has yet been established. By the end of Run 4, and assuming the SM predictions, LHCb will reach a 40% precision on the ratio $R \equiv \mathcal{B}(B^0 \to \mu^+\mu^-)/\mathcal{B}(B_s^0 \to \mu^+\mu^-)$, a very powerful observable to constrain the flavour structure of models beyond the SM. The CMS experiment

will attain a similar statistical sensitivity. However the hadron particle identification capabilities, valuable for suppressing background and characterising residual contamination, the superior mass resolution of LHCb, will be invaluable in obtaining the control of systematic uncertainties that will be essential for these measurements in the longer term. After Phase-II of LHCb the precision on the ratio R will be $\sim$20% and, together with the expected similar CMS sensitivity [42] on the same timescale, the combined reach should be $\sim$14%, putting strong constrains on viable NP models, as shown in Fig. 2.2. Recent improvements in the LHCb analysis [5] may lead to an even better performance. Moreover the large B_s^0 yield will allow the study of new observables such as the effective lifetime in the $\mu^+\mu^-$ mode, where LHCb is in the process of publishing a proof-of-concept measurement [5], and *CP* asymmetries. These observables will be particularly crucial for discriminating between NP models in the event that effects beyond the SM are observed.

An important complementary test of the SM is the search for the lepton-flavour-violating process $\tau^- \to \mu^+\mu^-\mu^-$. It has a negligible SM rate, but in many theories [43–46] beyond the SM this branching ratio can be in the region $(10^{-9} - 10^{-8})$. The current experimental limit [47–49], $\mathcal{B}(\tau^- \to \mu^+\mu^-\mu^-) < 1.2 \times 10^{-8}$, is at the starting point of this range, and Belle II will probe exactly this interesting region of sensitivity when accumulating up to 50 ab^{-1} at the $\Upsilon(4S)$. The LHC produces τ leptons, primarily in the decay of heavy flavour hadrons, with a cross-section five orders of magnitude larger than at Belle II. This compensates for the higher background levels and lower integrated luminosity, and means that a Phase-II Upgrade of LHCb would also be able to probe down to $\mathcal{O}(10^{-9})$, and independently confirm any Belle-II discovery or significantly improve the combined limit. The proposed improvements to the calorimeter during the Phase-II Upgrade (see Sec. 4.3.3) will be helpful in suppressing backgrounds such as $D_s^+ \to \eta(\mu^-\mu^+\gamma)\mu^+\nu_\mu$, and enabling LHCb to make best use of its statistical power.

2.3 Precision tests of the CKM paradigm

The SM does not predict the values of the weak flavour-couplings, and so all matrix elements must be measured experimentally. However, the unitary nature of the CKM matrix, and the assumptions of the SM, impose relations between the elements that are often expressed graphically in the complex plane as the so-called unitarity triangle. The angle γ of this triangle is of particular interest, because it can be determined extremely cleanly from measurements of *CP* asymmetries and relative rates in the $B^- \to Dh^-$ ($h = K, \pi$) family of decays. The theoretical uncertainty on the interpretation of the physical observables in terms of γ is five orders of magnitude smaller than the attainable experimental precision, even at the end of the Phase-II period. For this reason, ever more precise measurements of γ will remain very well-motivated for the foreseeable future, and provide a reference determination (not affected by possible contributions from NP in loops) of the apex of the unitarity triangle against which all other measurements of the triangle can be compared. The degree-level uncertainty in γ after Run 4, extrapolated from the current LHCb measurements [7], will be achieved mainly through the analysis of $B^- \to DK^-$ decays. With the Phase-II LHCb Upgrade this uncertainty will be reduced to around 0.4°, which will provide a very stringent test of new phases contributing in B decays. This extrapolation is in fact conservative, as it neglects the increased power that will come from modes involving neutrals, such as $D^0 \to \pi^+\pi^-\pi^0$, which will be reconstructed with higher efficiency using the improved Phase-II calorimeter (see Sec. 4.3.3), or high-multiplicity modes which will gain from

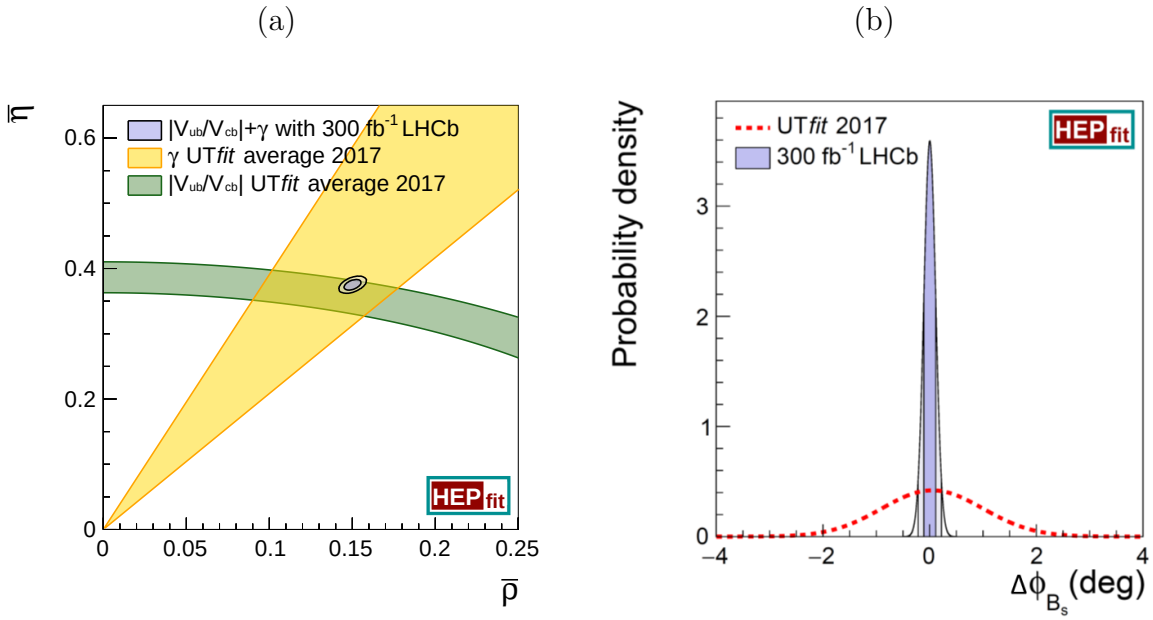

Figure 2.3: Current experimental constraints and Phase-II LHCb reach in the (a) $\bar{\rho} - \bar{\eta}$ plane, where Belle-II measurements and developments in lattice QCD will also contribute to the knowledge of $|V_{ub}/V_{cb}|$, and for (b) NP contributions to ϕ_s (dark blue 68%, light blue 95%) [52].

improvements in the low-p_{T} tracking efficiency (see Sec. 4.2.3). In parallel to these studies of tree-level processes, it will be essential to improve the measurement of γ in channels where virtual loops play a significant role, for example $B_s^0 \to K_{\mathrm{S}}^0\pi^+\pi^-$ and $B_s^0 \to K^-\pi^+\pi^0$, and the family of $B \to h^+h^-$ modes ($h = \pi, K$), already studied to great effect in Run 1 [50].

LHCb can also measure the magnitude of V_{ub}, and is uniquely able [51] to determine this quantity in the semileptonic decay modes of B_s^0, B_c^+, and Λ_b^0 hadrons, several of which will require the statistical reach of the Phase-II Upgrade to achieve the most interesting precision. Measurements of $|V_{ub}|$ in different processes can also be used to constrain the fraction of left-handed and right-handed couplings, and in general different decay modes lead to differently shaped constraints in this 2D space. Furthermore, the lattice-QCD inputs required for these measurements have very different systematic uncertainties for each process. Because of this, measurements of $|V_{ub}|$ by LHCb will play a particularly important role in global tests of the CKM paradigm and proposed NP extensions of it. The reconstruction of semi-leptonic decays relies on the kinematical constraint provided by the vector between the primary and decay vertices, and will be improved in quality if the material in the RF foil surrounding the VELO detector can be reduced or eliminated (see Sec. 4.1). The impact of Phase-II LHCb measurements in the $\bar{\rho} - \bar{\eta}$ plane, which defines the apex of the unitarity triange, is shown in Fig. 2.3(a).

With the detector improvements described in Chapter 4, time-dependent analyses will be possible with a pileup of $\mathcal{O}(50)$ and a very precise measurement of ϕ_s in the CKM unitary triangle can be performed at the Phase-II Upgrade. The uncertainty on ϕ_s after Run 4, as extrapolated from the current LHCb measurements [8], is expected to be 9 mrad, based mainly on the time-dependent analysis of the decay $B_s^0 \to J/\psi\phi$. If new phases affect B_s^0 and B^0

mixing differently, it could very well be that a comparison of loop-dominated processes in B_s^0 and B^0 mixing with tree-level measurements will show different levels of NP contributions. With the Phase-II LHCb Upgrade a precision of $\sim$4 mrad will be attainable using $B_s^0 \to J/\psi\phi$ only. Including other measurements from other modes (for example, $B_s^0 \to J/\psi\pi^+\pi^-$) the uncertainty on ϕ_s will become better than $\sim$3 mrad, which is at the same level as the precision on the indirect determination of ϕ_s from tree-level measurements. This determination will impose severe constraints on any possible NP contribution to the phase, as shown in Fig. 2.3(b).

In order to interpret properly the time-dependent analysis of $B_s^0 \to J/\psi\phi$ in terms of ϕ_s, the size of any potential contributions from doubly Cabibbo-suppressed penguin decays must be determined, for example using control channels such as $B^0 \to J/\psi\rho^0$ [53] and $B_s^0 \to J/\psi\bar{K}^{*0}$ [54], which benefit from the hadron identification capabilities of LHCb. With the data accumulated after the Phase-II Upgrade, it is expected that the effect of such penguin diagrams will be known with a precision better than 1.5 mrad. Moreover, studies of the weak phase in complementary $b \to s\bar{s}s$ decay modes such as $B_s^0 \to \phi\phi$, where current measurements [55] are very limited by statistics, will be able to reach sensitivities of $\sim$8 mrad with the Phase-II Upgrade sample. Similar improvements will be possible in the related charmless decays $B_s^0 \to K^-\pi^+K^+\pi^-$, $B_s^0 \to K_S^0 h^+h^-$ ($h = \pi, K$) and $B_s^0 \to K^+K^-\pi^0$, where the improved capabilities of the Phase-II ECAL will play an important role. Furthermore, LHCb will continue to make important CKM tests in the B^0 system; for example the Phase-II Upgrade will allow LHCb to measure $\Delta\Gamma_d$ with sufficient precision to be potentially sensitive to a non-zero value, even at the predicted SM level.

In the SM, the *CP* asymmetries in semileptonic neutral B mesons decays are predicted [56] to be very small: $a_{sl}^d = (-4.7 \pm 0.6) \times 10^{-4}$ and $a_{sl}^s = (2.22 \pm 0.27) \times 10^{-5}$. The LHCb measurements with Run-1 data have reached a precision of $\sigma(a_{sl}^d) = 3.6 \times 10^{-3}$ and $\sigma(a_{sl}^s) = 3.3 \times 10^{-3}$ [57, 58], which are at least an order of magnitude larger than the SM uncertainties. The hints for discrepancies with the SM shown by previous Tevatron results [59] have not been confirmed, but given the size of the uncertainties there is still room for sizable NP contributions. Hence there is a clear motivation to perform these measurements with a much larger data sample, in particular since the systematic uncertainties are dominated by detector asymmetries, which are limited by the statistical size of the control samples and therefore expected to scale with the integrated luminosity. With the expected data set collected at a Phase-II Upgrade it will be possible to reach a precision close to the SM value for a_{sl}^d.

2.4 Lower $p_{\rm T}$ signatures

Following the Phase-I LHCb Upgrade in LS3, the experiment will be fully read out at 40 MHz, allowing for a very flexible full software trigger. This, in addition to the excellent detector resolution, opens up new analysis possibilities. An illustrative example is the search for dark photons using the inclusive dimuon mass spectrum [60]. Until now both direct and indirect searches have failed to discover Weakly Interacting Massive Particles (WIMPs), and so alternative explanations are motivated to explain the nature of dark matter. One popular paradigm involves a dark sector, which couples to the SM only through a dark photon, which shares quantum numbers, and therefore mixes, with the SM photon. In Fig. 2.4 the LHCb potential to look for such dark photons is shown in the plane of the mass of the dark photon vs. the coupling strength. The improvement in knowledge from accumulating an integrated luminosity of 300 fb^{-1} is shown; in particular, the sensitivity in the region below m_ϕ is much better than can be achieved at Belle

II. Related searches for Majorana neutrinos [61,62] and inflatons [63,64], which LHCb has already performed with Run-1 samples, are expected to remain background-free throughout the Phase-II period. As these types of NP particles can have a very wide range of lifetimes, the additional capabilities downstream of the magnet offered by the proposed TORCH detector (see Sec. 4.3.2) may lead to improvements in LHCb's sensitivity beyond a simple integrated-luminosity scaling.

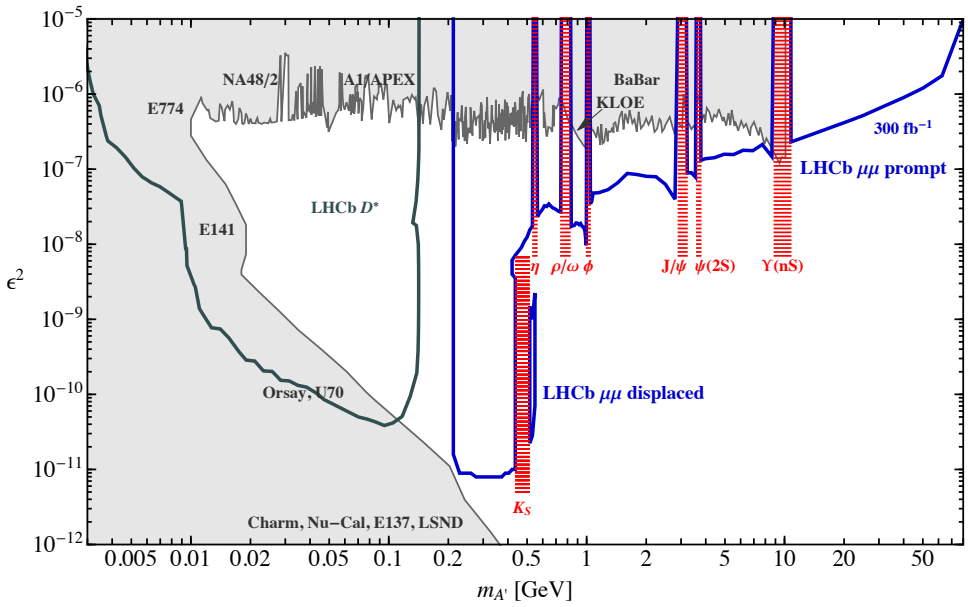

Figure 2.4: Bounds on dark photon mass ($m_{A'}$) and coupling (ϵ^2) compared to the anticipated LHCb reach for inclusive A' production in the dimuon channel. The contour assumes an integrated luminosity of 300 fb^{-1}. This plot is similar to that in Ref. [60], where a more detailed description of the different contributions to this figure can be found.

The software trigger will also allow LHCb to take full advantage of the enormous production rate of charm hadrons at the LHC, and collect the largest sample, by far, of charm decays ever recorded. If the full offline performance can be achieved in the trigger during the Phase-II Upgrade, LHCb will collect over two orders of magnitude more $D^0 \to h^+h^-$ and $D^0 \to K^0_S h^+h^-$ decays ($h = \pi, K$), than Belle II, allowing it to probe indirect CP violation with a precision of 10^{-5} and measure charm-mixing parameters with a precision of 10^{-4}. CP-violation in mixing-related phenomena are predicted to be very small, $\mathcal{O}(10^{-4})$ or less [65], and therefore improved measurements have excellent discovery potential for observing NP contributions. Effects of CP violation in decay are less cleanly predicted, and could be as large as $\mathcal{O}(10^{-3})$ [66], close to the current levels of sensitivity. If current hints [67] are confirmed, or if other signals emerge with Run-II or Phase-I data, it will be possible to launch a comprehensive survey of such effects in charm decays with the Phase-II Upgrade. The expected impact that the Phase-II data samples will have on the knowledge of the charm-mixing and indirect CP-violation parameters is shown in Fig. 2.5. In addition, the flexible nature of the LHCb trigger will allow a wide range of other three- and four-body decay modes to be studied, and will also permit a thorough exploration of the charm-baryon sector.

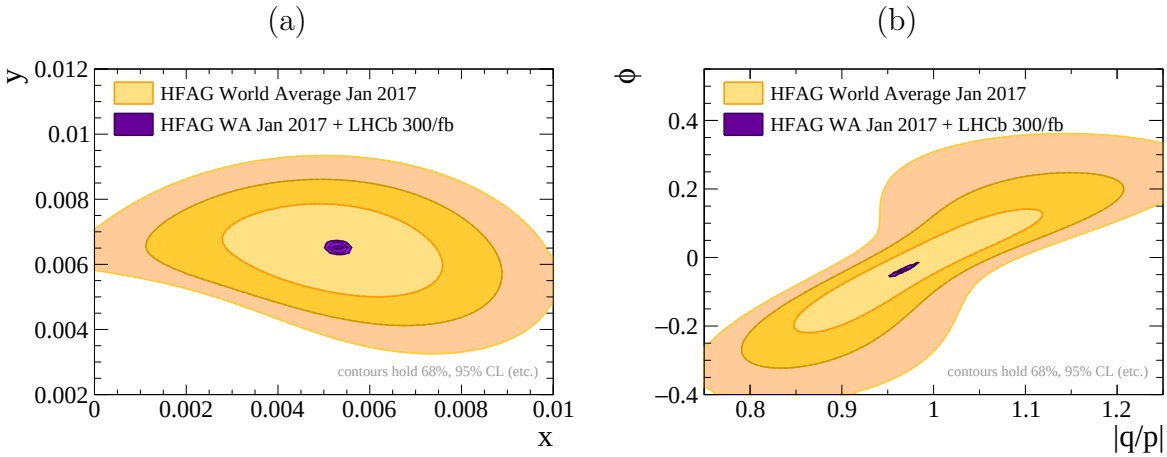

Figure 2.5: A projection of the improvement in the knowledge of the charm sector that will come from the Phase-II Upgrade: (a) mixing parameters (in a study that allows for *CP* violation); (b) the quantities ϕ and $|q/p|$, which parametrise indirect *CP*-violation in charm.

LHCb has a unique reach for rare decays of strange hadrons, and has already produced world-best results in the search for $K^0_S \to \mu^+\mu^-$ [68] and made studies of the decay $\Sigma^+ \to p\mu^+\mu^-$ [69]. The Phase-II Upgrade and the Phase-I/-II software trigger will allow LHCb to observe $K^0_S \to \mu^+\mu^-$ down to its SM decay rate and make similarly sensitive measurements for the decays of other charged hadrons. Possible improvements from augmenting the trigger with additional downstream capabilities (see Sec. 5.7) may bring further gains in performance over what is expected from the baseline Phase-I system. One additional very interesting physics possibility [70] is to study the spin precision of particles in the dipole magnet and hence determine the electric dipole moment (EDM) of the Λ baryon, and to measure the magnetic dipole moment (MDM) of both Λ and $\bar{\Lambda}$ baryons as a test of CPT symmetry. Sensitivities at $10^{-19}\,e\,\text{cm}$ and 100 ppm will be achievable for the EDM measurement and CPT test, respectively, at the Phase-II Upgrade. Even higher precision may be achievable by adding new tracking stations in the magnet region, as discussed in Sec. 4.2.3.

2.5 Exotic hadrons and spectroscopy

The LHC is an extremely rich laboratory for the study of exotic hadrons, and this opportunity has been exploited by LHCb to great effect during Run 1. Highlights include the demonstration of the four-quark nature of the $Z_c(4430)^+$ resonance [71] and the observation of the $P_c(4380)^+$ and $P_c(4450)^+$ pentaquark states [10]. These examples also show the need for a 'critical mass' of signal events, to allow for the thorough amplitude analyses which are essential to gain full understanding of the observed resonant structures. A key priority for future LHCb data taking is to establish other possible exotic multiplets, which can contain a large number of states in the pentaquark picture. Neutral isospin partners of the P_c^+ resonances, however, cannot be detected in $J/\psi n$ final states, implying the need for studying the fully hadronic decay modes $\Lambda_c^+ D^{(*)-}$ accessible through $\Lambda_b^0 \to \Lambda_c^+ D^{(*)-} K^{*0}$ decays.

The Phase-II Upgrade will have an unprecedented sensitivity for exotic hadron studies, whether directly produced in the pp collisions, or produced in the decays of beauty hadrons where high-statistics amplitude analyses will allow the resonant nature of these states to be determined. Some especially important examples are the precision studies of exotic hadrons which decay into doubly-charmed final states that can be accessed only in B_c^+ decays, or searches for doubly-heavy hadrons such as bc-baryons, which will not be accessible at any other experiment in the foreseeable future. It is also important to emphasise that the enhanced attributes of the Phase-II Upgrade, in particular the improved calorimeter (see Sec. 4.3.3), and the greater acceptance to soft particles that will be brought by the Magnet Stations (see Sec. 4.2.3), will be very beneficial for the multibody final states, many of which involve neutral particles, for example $\Lambda_b^0 \to \eta_c p K^-$ and $\Lambda_b^0 \to \chi_{cJ} p K^-$.

The Phase-II Upgrade of LHCb will also allow for ever more precise measurements of heavy flavour production. The improved calorimeter will greatly expand LHCb's sensitivity to those hadrons whose decays primarily involve neutral particles, while the additional statistical reach will allow precise double-differential measurements of the pair-production of various types of hadrons [72] to be performed for the first time. Such measurements, and related searches for the associated production of three or more given hadrons, will play an invaluable role in constraining pp production models in the forward region.

2.6 Forward and high-$p_{\rm T}$ physics

LHCb has already produced results [73] that show the ability to discriminate effectively between c-jets and b-jets. For instance, for a jet with $p_{\rm T} > 20\,{\rm GeV}/c$ a c-jet tag efficiency of $6\,(20)\%$ is achieved for a b-jet tag efficiency of $1\,(10)\%$. This initial performance, which is the best of any LHC experiment, is expected to improve further in the forthcoming years, as the sophistication of the tagging algorithms increases. If this level of discrimination can be maintained (or even improved) in the Phase-II Upgrade, there will be a very interesting potential to search for $H^0 \to c\bar{c}$, where the Higgs is produced in association with weak bosons. Preliminary studies suggest that the experimental sensitivity would approach that required to see this process at the SM rate.

LHCb has demonstrated that it can make a valuable contribution to the study of electroweak-boson production at the LHC [74–86]. In the measurement of cross-sections the experiment benefits from the most precise luminosity measurement ever achieved at a bunched-beam hadron collider [87], an achievement that can be largely attributed to the SMOG gas-imaging system [88, 89], which is unique to LHCb. The forward region is where the fraction of quark-initiated processes is largest as a consequence of the relative decline of the gluon with respect to the valence-quark Parton Distribution Function (PDF) at high x. This property gives LHCb certain advantages, for example in minimising the dilution associated with the knowledge of the incoming fermion direction in Z-boson production in the measurement of the effective weak-mixing angle. The collaboration has published the most precise determination of this observable at the LHC [11], and the prospects for the evolution of this important measurement with larger samples are promising. In general, measurements of boson production in the forward region provide valuable constraints on PDFs; conversely, a measurement of the W-boson mass, m_W, at LHCb will have a different dependence on PDF uncertainties to those at central rapidities, and hence will be complementary to the measurements performed at ATLAS and CMS [90], bringing

an improvement in knowledge above that which comes from two central-rapidity experiments alone.

The high rate of top-quark production at the LHC compensates for the limited acceptance of LHCb for decays of very massive objects [91, 92]. The Phase-II Upgrade will allow LHCb to make precise measurements of the double-differential top-production cross-section in the forward region, which will be a powerful input for constraining the PDFs used to calculate the expected Higgs cross-sections at the LHC. In addition, the dominance of quark-initiated top-production processes at forward rapidities [93] means that the Phase-II Upgrade will give LHCb an ideal opportunity to measure top-quark pair asymmetries [94], which may be very sensitive to NP contributions. While a 5σ observation of a non-zero asymmetry may be possible with data taken up to Run 4 [95], a Phase-II Upgrade will be essential to go beyond the simple observation, and allow precise studies to differentiate NP effects from those of the SM.

2.7 Ion and fixed target physics

The excellent particle-identification attributes, forward acceptance and good efficiency for low-$p_{\rm T}$ signals provide LHCb with unique and powerful capabilities for pA and AA physics, as already demonstrated in several publications [13, 96–99]. The very high granularity and extended instrumentation of the Phase-II detector will allow the experiment to access AA collisions at higher centralities than with the current detector, and make LHCb a perfectly adapted experiment for these studies, should there be a strong motivation for pursuing heavy-ion measurements in Run 5 and beyond.

The gas-injection SMOG system of LHCb, originally installed for luminosity measurements, also allows LHCb to function as a fixed-target experiment, adding further breadth to the LHC programme. Data have been taken with a variety of noble gases, and measurements are underway of relevance for both nuclear physics and particle astrophysics. There have been proposals from within the collaboration [70] and also the external community [100], identifying important measurements that can be conducted in fixed-target mode at the LHC, such as the measurement of the EDM and MDM of charm baryons. Discussions are ongoing as to whether it is possible to integrate these exciting ideas into the ongoing LHCb physics programme.

2.8 Summary and sensitivity to key flavour observables

The Phase-II Upgrade of LHCb will both enable a significant improvement in statistical reach for observables already under study, and will also allow complementary observables in highly suppressed processes to be measured with good precision for the first time. The broad programme of measurements will provide high sensitivity in the search for effects beyond the SM, and allow for a detailed characterisation of any NP that is discovered. Table 2.1 summarises the physics reach of the Phase-II Upgrade for several key topics that have been discussed in this chapter.

The immense statistical power of the Phase-II Upgrade will present outstanding opportunities in hadron spectroscopy, where LHCb has already made major discoveries. The capabilities of the experiment are also very well suited to making major contributions to new particle searches, and precise measurements in electroweak physics, QCD and even the Higgs sector. The fully software-based trigger system, unique at the LHC, will give the experiment great flexibility in adjusting to whatever physics possibilities will emerge at the HL-LHC.

Table 2.1: Summary of prospects for Phase-II measurements of selected flavour observables.

Topics and observables	Experimental reach	Remarks
EW Penguins		
Global tests in many $b \to s\mu^+\mu^-$ modes with full set of precision observables; lepton universality tests; $b \to dl^+l^-$ studies	*e.g.* 440k $B^0 \to K^*\mu^+\mu^-$ & 70k $\Lambda_b^0 \to \Lambda\mu^+\mu^-$; Phase-II $b \to d\mu^+\mu^-$ $\approx$ Run-1 $b \to s\mu^+\mu^-$ sensitivity.	Phase-II ECAL required for lepton universality tests.
Photon polarisation		
$\mathcal{A}^\Delta$ in $B_s^0 \to \phi\gamma$; $B^0 \to K^*e^+e^-$; baryonic modes	Uncertainty on $\mathcal{A}^\Delta \approx 0.02$; $\sim 10k$ $\Lambda_b^0 \to \Lambda\gamma$, $\Xi_b \to \Xi\gamma$, $\Omega_b^- \to \Omega\gamma$	Strongly dependent on performance of ECAL.
$\boldsymbol{b \to cl^-\bar{\nu}_l}$ **lepton-universality tests**		
Polarisation studies with $B \to D^{(*)}\tau^-\bar{\nu}_\tau$; τ^-/μ^- ratios with B_s^0, Λ_b^0 and B_c^+ modes	*e.g.* 8M $B \to D^*\tau^-\bar{\nu}_\tau$, $\tau^- \to \mu^-\bar{\nu}_\mu\nu_\tau$ & $\sim 100k$ $\tau^- \to \pi^-\pi^+\pi^-(\pi^0)\nu_\tau$	Additional sensitivity expected from low-p tracking.
$\boldsymbol{B_s^0, B^0 \to \mu^+\mu^-}$		
$R \equiv \mathcal{B}(B^0 \to \mu^+\mu^-)/\mathcal{B}(B_s^0 \to \mu^+\mu^-)$; $\tau_{B_s^0 \to \mu^+\mu^-}$; CP asymmetry	Uncertainty on $R \approx 20\%$ Uncertainty on $\tau_{B_s^0 \to \mu^+\mu^-} \approx 0.03$ ps	
LFV τ decays		
$\tau^- \to \mu^+\mu^-\mu^-$, $\tau^- \to h^+\mu^-\mu^-$, $\tau^- \to \phi\mu^-$	Sensitive to $\tau^- \to \mu^+\mu^-\mu^-$ at 10^{-9}	Phase-II ECAL valuable for background suppression.
CKM tests		
γ with $B^- \to DK^-$, $B_s^0 \to D_s^+K^-$ *etc.*	Uncertainty on $\gamma \approx 0.4^\circ$	Additional sensitivity expected
ϕ_s with $B_s^0 \to J/\psi K^+K^-$, $J/\psi\pi^+\pi^-$	Uncertainty on $\phi_s \approx 3$ mrad	in CP observables from Phase-II
$\phi_s^{s\bar{s}s}$ with $B_s^0 \to \phi\phi$	Uncertainty on $\phi_s^{s\bar{s}s} \approx 8$ mrad	ECAL and low-p tracking.
$\Delta\Gamma_d/\Gamma_d$	Uncertainty on $\Delta\Gamma_d/\Gamma_d \sim 10^{-3}$	Approach SM value.
Semileptonic asymmetries $a_{\rm sl}^{d,s}$	Uncertainties on $a_{\rm sl}^{d,s} \sim 10^{-4}$	Approach SM value for $a_{\rm sl}^d$.
$\lvert V_{ub}\rvert/\lvert V_{cb}\rvert$ with Λ_b^0, B_s^0 and B_c^+ modes	*e.g.* $120k$ $B_c^+ \to D^0\mu^-\bar{\nu}_\mu$	Significant gains achievable from thinning or removing RF-foil.
Charm		
CP-violation studies with $D^0 \to h^+h^-$, $D^0 \to K_{\rm S}^0\pi^+\pi^-$ and $D^0 \to K^\mp\pi^\pm\pi^+\pi^-$	*e.g.* 4×10^9 $D^0 \to K^+K^-$; Uncertainty on $A_\Gamma \sim 10^{-5}$	Access CP violation at SM values.
Strange		
Rare decay searches	Sensitive to $K_{\rm S}^0 \to \mu^+\mu^-$ at 10^{-12}	Additional sensitivity possible with downstream trigger enhancements.

Chapter 3

Machine considerations

Interaction Point (IP) 8, at which LHCb is located, is not designed for high luminosity operation. To raise the instantaneous luminosity significantly beyond $2 \times 10^{33}\,\mathrm{cm}^{-2}\mathrm{s}^{-1}$ requires changes both to the optics and to the shielding of the machine elements.

3.1 Luminosity projections

The default value of β^* for the LHCb Phase-I Upgrade is 3 m, which without levelling permits a maximum luminosity of around $1 \times 10^{34}\,\mathrm{cm}^{-2}\mathrm{s}^{-1}$ at start of fill. In order to collect substantially more data per year than in Phase-I operation it will be necessary to reduce β^* to 2 m or below.

Table 3.1 shows the data sets that could be collected each year in various scenarios [101, 102]. Results are given for the case where the luminosity is levelled by beam separation at values of 1 and $2 \times 10^{34}\,\mathrm{cm}^{-2}\mathrm{s}^{-1}$, and where no levelling is applied. In some scenarios it will not be possible to maintain the target luminosity throughout the fill, and so the extent of the levelling time is also indicated. For comparison an entry is also provided for Phase-I operation, with levelling at $2 \times 10^{33}\,\mathrm{cm}^{-2}\mathrm{s}^{-1}$. The fill length has been optimised to maximise the amount of integrated luminosity delivered to IP1 and IP5. The results assume an external crossing angle in the horizontal plane of 500 μrad. As the crossing angle at the IP also includes the bend induced by the spectrometer dipole, the instantaneous luminosity achievable and overall performance differs for negative and positive magnet polarity, hence results are shown for each setting. The calculated numbers do not account for beam-beam effects, which may degrade the performance, particularly for negative polarity (that is when the spectrometer reduces the external crossing angle, resulting in a smaller crossing angle at the IP).

It can be seen that, given the assumptions of the calculations, at $\beta^* = 2$ m it will be possible to collect around four times more data per year than in Phase I, and with $\beta^* = 1$ m and operating at the most favourable polarity, it will be possible to collect an annual sample that is more than seven times larger. The loss in integrated luminosity to ATLAS and CMS from the additional burn-off caused by operating IP8 at higher luminosity is small, never exceeding 5% [102]. The impact on beam lifetime and quality needs to be further studied to confirm the above numbers.

Operating at low values of β^* implies a big external crossing angle and large beam sizes in the region of the triplets and the superconducting dipole D1. The minimum value of β^* that is attainable will be determined by the aperture either in the triplets or in the TCCM (a copper block which masks D1 from injection-kicker malfunctions). The constraints imposed by the

Table 3.1: Integrated luminosity projections at IP8 per year for different values of β^* and settings of the LHCb dipole polarity ($-$ and $+$). Results are shown for different target luminosities for levelling, and also without levelling. The maximum instantaneous luminosity achievable at each setting is also given. The study assumes a performance efficiency of 50% and a minimum turn-around time of three hours [103].

β^*	Maximum $\mathcal{L}$		Target levelling $\mathcal{L}$	Fill length		Levelling time		$\int \mathcal{L}\,dt$	
[m]	[$\times 10^{34}\,\mathrm{cm^{-2}s^{-1}}$]		[$\times 10^{34}\,\mathrm{cm^{-2}s^{-1}}$]	[h]		[h]		[$\mathrm{fb^{-1}/yr}$]	
	$-$	$+$		$-$	$+$	$-$	$+$	$-$	$+$
3	1.04	0.78	0.20	8.1	8.1	8.1	8.1	10	10
2	1.53	1.04	1.00	7.7	7.8	2.8	0.4	39	31
2	1.53	1.04	/	7.6	7.8	/	/	43	31
1	2.90	1.66	1.00	7.5	7.6	6.0	3.5	48	42
1	2.90	1.66	2.00	7.3	7.5	2.3	0	73	48
1	2.90	1.66	/	7.2	7.5	/	/	80	48

TCCM can be loosened if it will be possible to replace it with a new absorber with movable jaws. During injection the external crossing angle must be applied in the horizontal plane, and the baseline scenario is that it remains in the same plane at flat top. The value assumed for the calculations shown in Table 3.1 is close to the largest feasible, taking into account the limits in the corrector strength. The preliminary indications are that with this baseline scheme a β^* of 2 m is attainable, while allowing the possibility of inverting the polarity of the LHCb spectrometer.

A possible alternative option would be to switch the external crossing angle into the vertical plane at flat top [104]. This configuration could allow the value of β^* to be reduced below 2 m, but still above 1 m. Studies are required to assess the feasibility and robustness of this scheme for operation at high bunch population.

Operation at high luminosity and with small β^* at IP8 will enhance beam-beam effects, which have the potential to reduce the dynamic aperture and therefore lower the integrated luminosities from the values given in Table 3.1, and also degrade the performance at IPs 1 and 5. Detailed simulations, benefitting from the ever-increasing knowledge of the performance of the current machine, are underway to answer these questions [105].

3.2 Energy deposition and shielding issues

In order to operate IP8 at high luminosity it will be necessary to insert additional shielding components for the machine elements, as are already present at IP1 and IP5. In particular a TAS (Target Absorber) will be required to protect the upstream inner triplet from quenching, and to limit its radiation dose. Further away from the IP it will be necessary to install TANs (Target Absorber Neutrals) to shield the recombination dipoles D2 from high-energy neutral particles, and TCLs (Target Collimator Long) to protect the cold magnets in the matching sections from collision debris. Modifications are already foreseen during LS2 to allow for $2 \times 10^{33}\,\mathrm{cm^{-2}s^{-1}}$ operation. These include the addition of a mini-TAN [106] close to each beam-recombination dipole. However the protection that these components provide is not validated for higher

luminosities.

Space constraints make it problematic to insert a TAS on the right side of IP8 (RB86) of the same design as exists in IP1 and IP5. A promising alternative solution would be to modify the first compensator dipole (MBXWS) to perform this shielding function also, by filling the air gap around the vacuum chamber with tungsten [107, 108]. With this in place the heating load on the triplet quadrupoles and long-term radiation dose would be suppressed and approach the acceptable regime. However the precise values of these quantities will depend on the choice of crossing angle. On the left side of IP8 (RB84) the additional shielding walls could be modified to incorporate a TAS element. In this case the impact from the increased radiation levels on the installed services and tunnel ventilation and access must be evaluated, although preliminary studies have uncovered no show-stopper. A successful optimisation of the shielding will allow the lifetime of the quadrupoles to be extended to that of the inner triplets currently in place at the high luminosity IPs, which is designed to be $300\,\mathrm{fb}^{-1}$. These magnets at IP1 and IP5 will be removed during LS3, in preparation for the HL-LHC, and then could be subjected to a detailed inspection that would yield valuable information for the future operation of IP8 at high luminosity, and perhaps open the possibility of running beyond the currently accepted lifetime.

It is also necessary to review the shielding configuration of the entire experimental cavern, to ensure that there is adequate protection for the cryogenic equipment, experimental services and electronics. Studies are required to evaluate the possible effects of high luminosity operation, and to find mitigation options.

For the purposes of this document it is assumed that Phase-II operation will be at luminosities of up to $2 \times 10^{34}\,\mathrm{cm}^{-2}\mathrm{s}^{-1}$, with an annual data yield of 4 to 7 times larger than that of Phase I, and a cumulative baseline goal of $300\,\mathrm{fb}^{-1}$.

Chapter 4

Detector challenges and candidate solutions

Performing flavour physics at a luminosity of $2 \times 10^{34}\,\mathrm{cm}^{-2}\mathrm{s}^{-1}$ presents significant experimental challenges. The mean number of interactions per crossing is around $\mu = 50$, which leads to much higher particle multiplicities and rates than is the case for the Phase-I Upgrade. Radiation damage also becomes a greater concern for certain sub-detectors. In this chapter these detector challenges are discussed in more detail and possible solutions are presented. These solutions can be accommodated within the existing footprint of the spectrometer while maintaining, in general, the current arrangement of sub-systems. At very high pileup fast-timing information becomes an essential attribute for suppressing combinatorics and enabling time-dependent *CP*-violation measurements, and so this capability becomes a design feature for several detector components. A number of the proposed changes are intended to provide an improved intrinsic performance, aside from the gain that arises from the larger data samples which higher luminosity will bring. Sub-detectors that fall into this category include the electromagnetic calorimeter, and a system of tracking stations that could be installed on the side-faces of the magnet. The layout of the Phase-II Upgrade is shown in Fig. 4.1.

4.1 Vertex Locator

The physics programme of LHCb is predicated on a highly performant vertex detector with fast pattern-recognition capabilities, excellent vertex resolution and sufficient radiation hardness to maintain these attributes over the full detector lifetime. The move to the higher luminosity operation of the Phase-II Upgrade necessitates the construction of a new Vertex Locator (VELO), which, as with the Phase-I Upgrade [17], will be based on high-granularity pixels operated in vacuum in close proximity to the LHC beams. The principal challenges of the Phase-II Upgrade vertex detector are achieving performant operation in a high pile-up environment, under high-radiation conditions and with the required readout data rate.

Tracking performance

At an instantaneous luminosity of $2 \times 10^{34}\,\mathrm{cm}^{-2}\mathrm{s}^{-1}$, the average number of visible proton-proton interactions per crossing in LHCb is $\mu = 50$, producing a total of 1500–3500 charged particles

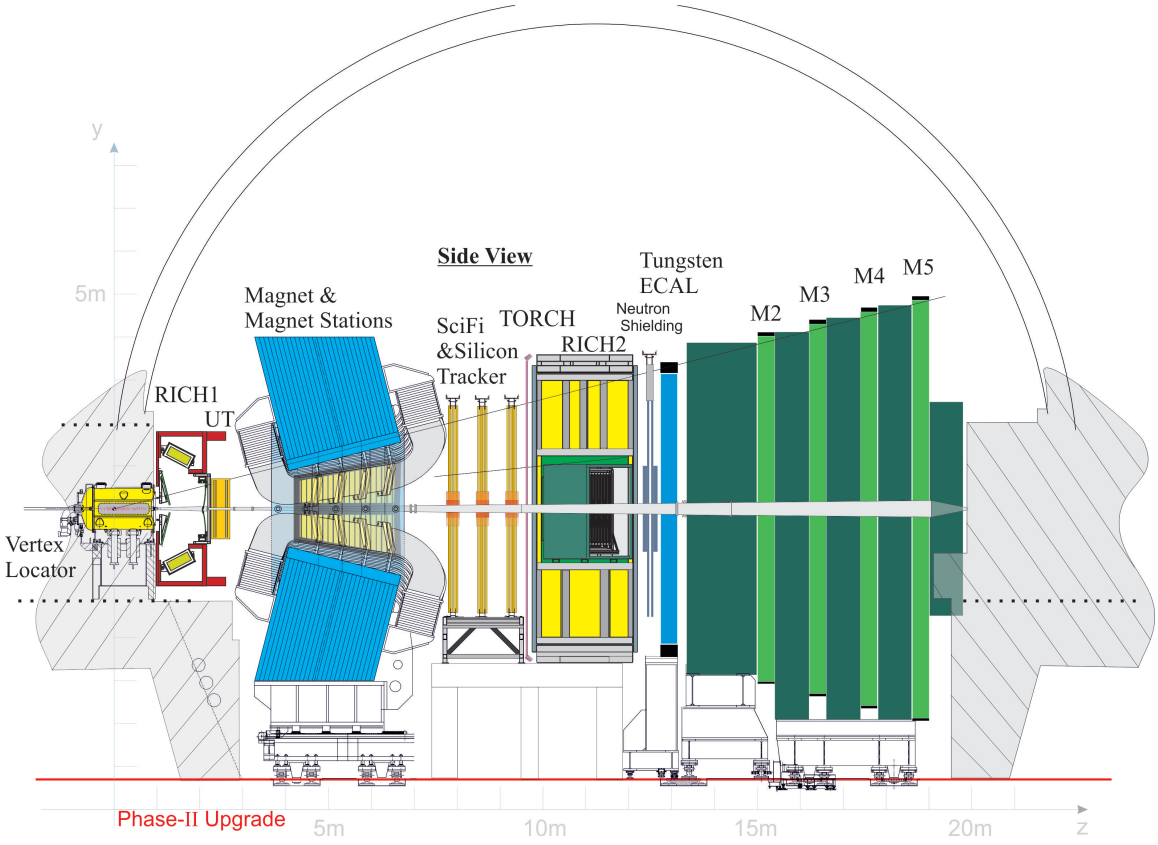

Figure 4.1: Schematic side view of the Phase-II detector.

within the LHCb acceptance from the initial interactions alone. These high multiplicities lead to challenging conditions for track and vertex reconstruction. Using the Phase-I Upgrade VELO detector design as a baseline, the performance of a number of potential modifications to the detector geometry and materials has been evaluated at the proposed Phase-II luminosity, and their effects on the final physics performance studied using full Monte Carlo simulations. Figure 4.2 summarises the tracking performance of the baseline (Phase-I) design under luminosities expected in the Phase-I and Phase-II Upgrade eras. The mean rate of reconstructing ghost tracks in the VELO alone from spurious hit combinations increases dramatically from 1.6% to 40% for the increased luminosity, even after tight track-quality requirements are imposed to limit the rate of these ghosts. There is a corresponding reduction in tracking efficiency, with the integrated value within the LHCb acceptance falling from ∼99% to ∼96%. There is also a modest degradation in the impact parameter (IP) resolution, driven by the effect of the lowered tracking efficiency on the primary vertex (PV) resolution.

These losses in performance can be almost entirely recovered with a small number of design improvements. Most notably, by decreasing the pixel pitch from 55 µm to 27.5 µm and reducing the sensor silicon thickness from 200 µm to 100 µm, the ghost rate can be reduced back down to 2% while retaining a tracking efficiency of 96%, to choose one working point. Another potential design improvement would be the reduction of material. In the current and Phase-I Upgrade

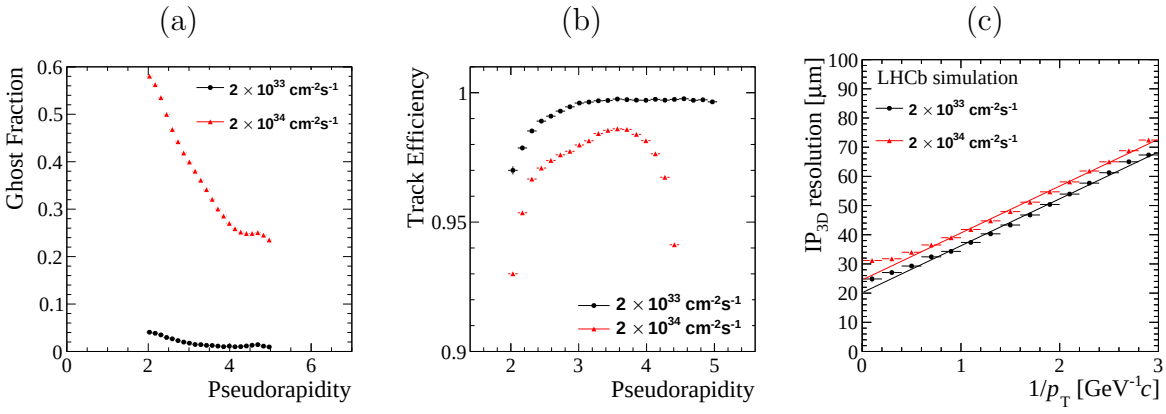

Figure 4.2: Simulated performance of the Phase-I Upgrade VELO design, with no further improvements, at the design luminosity (black points) and at the proposed Phase-II upgrade luminosity (red points): (a) ghost rate vs. pseudorapidity; (b) tracking efficiency vs. pseudorapidity; (c) IP resolution vs. $1/p_{\mathrm{T}}$.

designs the VELO sensors are located in a secondary vacuum, surrounded by a thin metal shield which suppresses wakefields from the beam. This RF foil gives the largest contribution to the material budget, however alternative designs can be considered, such as a system of wires, which would reduce this contribution to a negligible value. Such a change would result in a significant improvement in the IP resolution, particular at lower momentum, and also have the benefit of reducing the ghost rate even further. Figure 4.3 repeats the tracking performance plots for these two scenarios: (1) smaller pixels and thinner silicon; (2) these improvements plus the removal of the RF foil. In both cases the pattern recognition algorithms developed for the Phase-I Upgrade have been coarsely optimised for the new conditions by scanning the parameter space for the most important tuneable thresholds. Additional gains are almost certainly possible from a more comprehensive redesign of the track-finding software. Furthermore, the addition of fast-timing information, discussed below in the context of vertex association, will also bring potential improvements in track finding (see *e.g.* Ref. [109]).

Pile-up and 4D readout

The large number of multiple interactions per beam crossing at Phase-II presents particular problems for the operation of a heavy flavour experiment. The selection of beauty and charm hadron samples is based on their flight distance, as determined by the VELO. This measurement requires the correct association of the production (PV) and decay vertices of the heavy flavour hadron. Using a Phase-I Upgrade design detector 13% of b-hadron decays would be mismatched to the wrong PV at an average pile-up of $\mu = 50$, which would limit the possibilities to perform time-dependent CP-asymmetry measurements, as well as increase the combinatoric background levels. If the time information of the track hit is known within a resolution of 200 ps, a performance already achieved by NA62 [110], the mismatch is reduced to the current levels (1%). Figure 4.4 shows a preliminary study on how this mismatch fraction depends on the time resolution of the hits. Consequently R&D on achieving high-granularity 4D spatial and timing information in the VELO in this high-radiation environment is clearly well motivated.

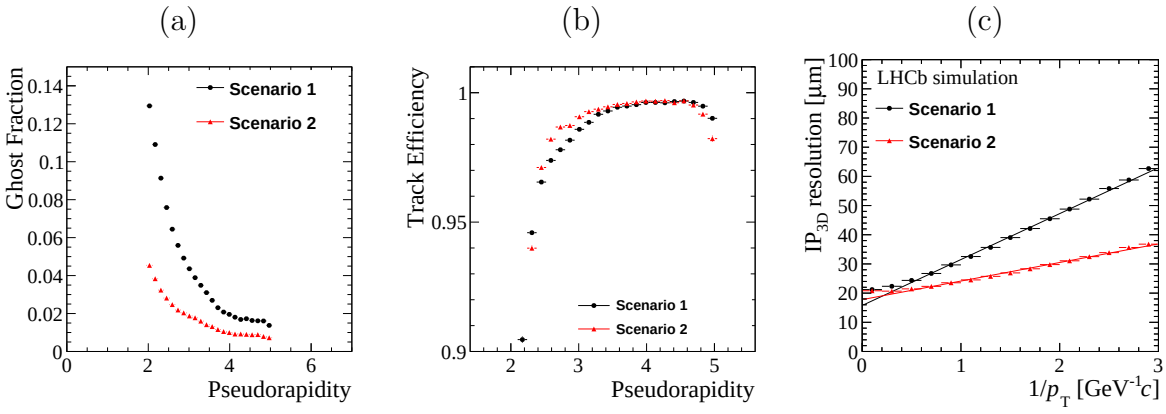

Figure 4.3: Simulated performance of two prospective Phase-II Upgrade VELO designs at $2\times10^{34}\,\mathrm{cm}^{-2}\mathrm{s}^{-1}$ based on the Phase-I upgrade model: (a) ghost rate vs. pseudorapidity; (b) tracking efficiency vs. pseudorapidity; (c) IP resolution. Scenario 1 (black points) includes pixels with one quarter of the area of the Phase-I pixels, and a reduced sensor thickness. Scenario 2 also includes removal of the RF foil separating the VELO and beam vacua.

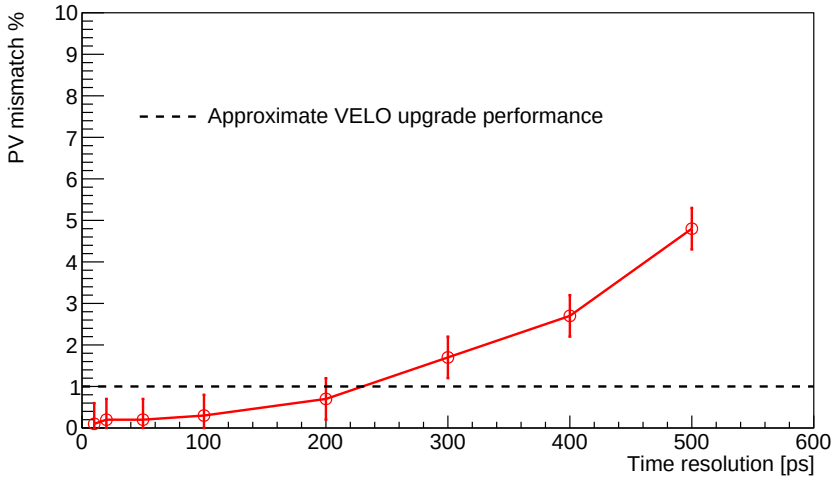

Figure 4.4: Fraction of b-hadron decays mismatched to the wrong PV as a function of the time resolution per hit at a luminosity of $2\times10^{34}\,\mathrm{cm}^{-2}\mathrm{s}^{-1}$. The horizontal dashed line shows the approximate performance of the Phase-I Upgrade VELO at $2\times10^{33}\,\mathrm{cm}^{-2}\mathrm{s}^{-1}$. The hit information used as input to the study is obtained from a sample of simulated events assuming the layout of the Phase-I Upgrade VELO.

Radiation environment

The anticipated radiation fluence at the silicon sensors could be maintained at levels where current technologies achieve sufficient signal to noise ratios by increasing the inner radius from 5 to 11 mm, at the cost of a degradation in the impact parameter resolution, from 50% to 100% depending on the track pseudorapidity. A better solution, from the point of view of physics performance, would be to design 'hot-swap' mechanics to allow the replacement of modules in the end-of-year technical stops. The total number of modules in the Phase-I Upgrade VELO is only

52, so regular replacement is not prohibited from financial or construction-effort considerations, though the access in a high radiation area must be carefully evaluated.

Other considerations

Preliminary discussions are underway on the potential future evolution of the VeloPix ASIC [111], developed for the Phase-I upgrade, in the framework of the Timepix/Medipix chip family.

The optimisation studies for the design will also investigate the option of installing the smallest achievable granularity of pixels and additional dedicated timing planes with larger timing pads. These timing planes would be larger in size than the space-point modules to provide geometrical coverage with fewer planes.

An R&D programme will be instigated to investigate the challenges and develop the design of the Phase-II Upgrade VELO. Progress in technology and understanding may allow additional enhancements to be considered in areas such as pixel granularity, sensor thickness, RF-shielding, and the utility of an additional magnetic field to eliminate low-p background at trigger level.

4.2 Tracking system

The tracking system of the Phase-I LHCb Upgrade [19] comprises one tracking station (Upstream Tracker, UT) located upstream, and three tracking stations (T1-T3) at the downstream side of the magnet. In conjunction with the VELO, these stations provide a high precision momentum measurement for charged particles, which results in an excellent mass resolution when reconstructing hadron decays. They also measure the track directions of the charged particles as input to the particle identification systems, notably the photon-ring searches in the RICH detectors. The increased occupancies of the Phase-II Upgrade will require a comprehensive reoptimisation of the tracking system. Technology considerations are described below but two general design challenges for the Phase-II Upgrade tracking design are identified.

- **Track segment matching** The matching of the correct track segments upstream and downstream of the magnet must be achieved. This will be addressed through the study of the layout in the Upstream Tracker and magnet region and the use of timing information (see Secs. 4.1 and 4.3.2).
- **Occupancy** The higher occupancy in the central region of the detector will be addressed with finer segmentation in the tracking stations.

In addition, the potential to improve the low-momentum tracking acceptance of the experiment is considered. This may be achieved through installing a new tracking system on the side walls of the dipole magnet.

4.2.1 Upstream Tracker

The Upstream Tracker (UT) of the Phase-I Upgrade is an important element in track reconstruction, and replaces the TT detector in the current experiment. Tracks in LHCb have long segments in the VELO and the downstream tracker but these are 7 m apart. The UT provides space-points that facilitate the effective matching of these track segments in a high multiplicity environment, reducing the rate of false tracks. The addition of further tracking stations in the

Table 4.1: Potential layout for tracking stations in the Inner, Middle and Outer tracker (IT, MT and OT) regions. The IT dimensions are similar to the current LHCb IT. The installation schedule is discussed in Sec. 5.2. The SciFi will be modified in LS3 before replacement in LS4.

	Outer dimension	Surface area (12 layers)	Installation schedule
Beam-pipe hole	$\varnothing$ 0.23 m		
IT	1.1×0.4 m^2	3.4 m^2	LS3
MT	3.2×0.8 m^2	16.9 m^2	LS4
SciFi, OT	6.5×4.8 m^2	340 m^2	LS2, LS4

Phase-II Upgrade will be studied as part of the overall tracking optimisation. The UT also significantly improves the momentum resolution of the tracks. Furthermore, the majority of K^0_S and Λ particles decay after the VELO, and thus the experiment's efficiency for such channels is boosted significantly by the presence of the UT. Finally, UT information can be used in the trigger to reject soft particles and speed up the tracking by a significant factor.

The UT covers an area of approximately 2 m^2 and is composed of four layers of single-sided silicon-microstrip detectors. The magnetic field bends tracks in the horizontal plane (along the X coordinate). Therefore, in order to measure the track momentum, the strips run vertically (Y). The middle two planes labelled U and V are at 5° angles to the vertical in order to provide stereo measurements, allowing the Y coordinate also to be determined. The majority of the area is covered with silicon strip sensors of 100 cm^2 area and 190 µm strip pitch, with the central region using half-length and half-pitch sensors. The increased occupancies and data rates of the Phase-II upgrade will mandate a reduced device-segmentation in some regions. For an integrated luminosity of 300 fb^{-1} a maximum fluence at the innermost edge of the silicon sensors of 3×10^{15} n$_{eq}$/cm^2 is anticipated, rapidly decreasing with the distance from the beam axis. This is well within the capabilities of established sensor designs, and may also be achievable with the emerging technology of HVCMOS. Synergy with devices suitable for the inner part of the downstream tracking stations will be exploited where possible.

4.2.2 Main tracking stations

Both the current experiment and the Phase-I Upgrade utilises three downstream tracking stations (T1,T2,T3), each composed of four layers of detectors. This sub-system provides the track segments after the magnet and is thus a primary tracking device of the experiment that provides momentum resolution for the tracks, in conjunction with the VELO and UT. The detector is a large downstream tracker covering a surface of 30 m^2 per layer, and consequently a key challenge for the Phase-II Upgrade is providing the required performance at a core-cost compatible with the funding envelope that is envisaged for the experiment.

The current LHCb experiment uses a mixed-technology solution based on silicon-strip detectors in the inner region and straw-tube detectors in the outer region. The Phase-I Upgrade uses a scintillating-fibre tracker (SciFi) to cover the full acceptance. This is based on 2.5 m long scintillating fibres with a diameter of 250 µm, readout by silicon photomultipliers (SiPM). This tracking system is expected to be highly efficient during the Phase-I Upgrade [19]. For the Phase-II Upgrade Inner, Middle and Outer Tracker regions are considered, as shown in Fig. 4.5, with the dimensions given in Table 4.1, using a mixed technology solution.

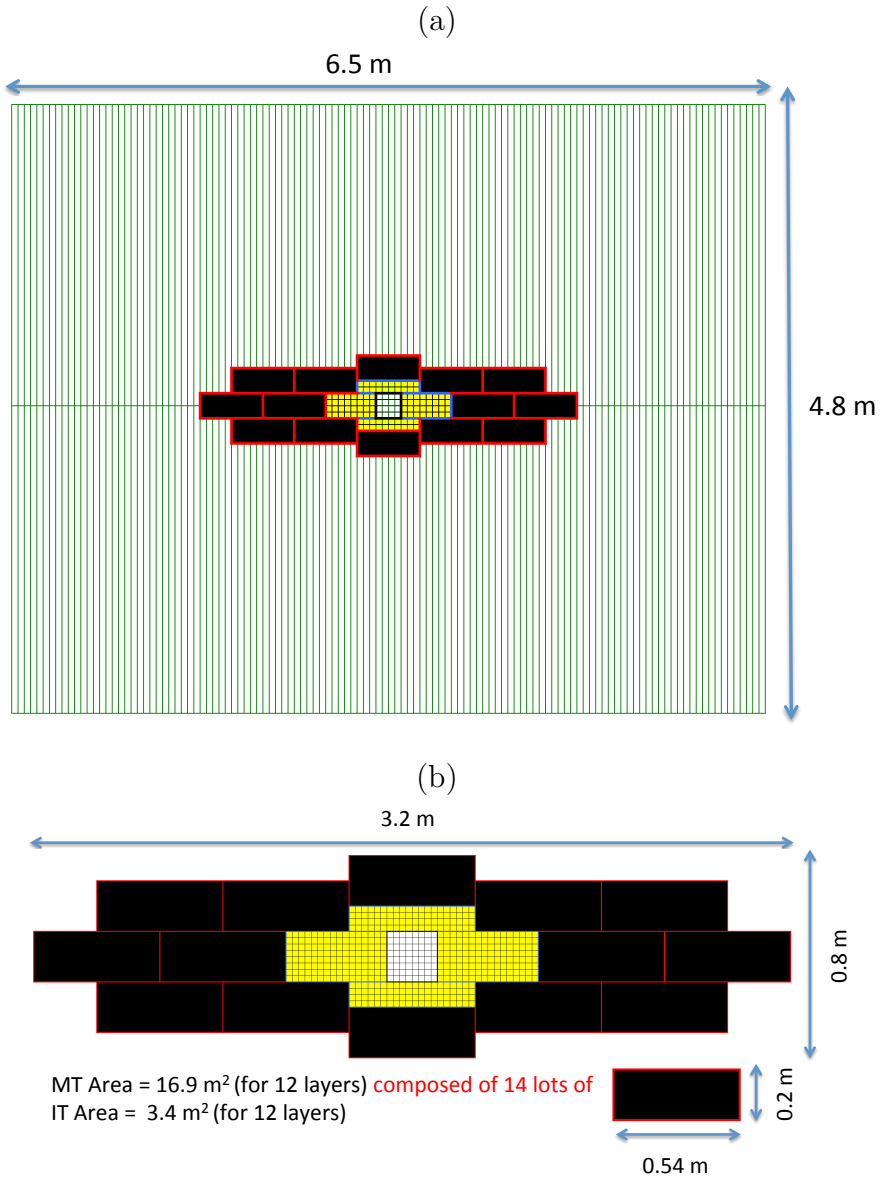

Figure 4.5: A potential layout for the tracking stations with one layer of the Outer, Middle and Inner (OT, MT, IT) trackers for the Phase-II Upgrade: (a) the OT region is covered with vertical scintillating fibres, following the design of the Phase-I Upgrade detector; (b) the IT and MT silicon region, where one black outlined cell of the IT has dimensions typical of HVCMOS reticles ($25 \times 25\,\mathrm{mm}^2$), and the $540 \times 200\,\mathrm{mm}^2$ red outlined elements of the Middle Tracker can be tiled with sensors similar to those in the UT of the Phase-I Upgrade.

The future development of the novel and cost-effective scintillating fibres will be a primary candidate technology for covering the outer region of the tracking stations. The radiation hardness of the system is likely the primary challenge. Detailed studies for both the SiPMs and the fibres are required. The SiPMs remain a rapidly developing technology. The fibre performance degrades

primarily from the change of transparency of the polystyrene and starts to suffer significantly above 100 Gy. A simulation study will be performed to assess the effect on the tracking system. The maximum occupancy in the proposed Outer Tracker region at Phase-II luminosities can be kept similar to that at the inner part of the Phase-I Upgrade SciFi fibres. The occupancy can also be reduced, and resolution improved, by using smaller diameter fibres; a modest reduction to 200 µm can already be anticipated.

The occupancy in the hottest areas of the Phase-II tracker necessitates the use of longitudinally segmented devices in the Inner and Middle regions. Preliminary studies show that partitioning the Inner and Middle regions within an area of around $1.4\,\mathrm{m}^2$ would reduce the fake track rate in the Outer region of the tracker to a manageable level at Phase-II luminosities.

The required radiation tolerance and occupancy conditions at the Phase-II Upgrade suggest silicon detectors as the natural candidate technology for the Inner and Middle regions. A vertical segmentation of the order of a few cm is required in the Inner region. A segmentation of 10 cm is sufficient in the Middle region. The sensor requirements are comparable with those of the ATLAS Phase-II Upgrade microstrip tracker for LS3 [112]. In addition to conventional silicon-detector designs, the application of HVCMOS designs in this region appears promising.

4.2.3 Low momentum tracking: the Magnet Stations

It is desirable to extend the LHCb tracking acceptance for low momentum particles, in order to take fuller advantage of the opportunities offered by the HL-LHC. Particles with momenta below $\sim$1 GeV/c are swept outside the LHCb acceptance by the magnetic field of the dipole. These particles leave hits in the upstream detectors of the VELO and UT but the low magnetic field in this region gives rise to a momentum measurement of poor precision ($\Delta p/p$ 15 – 20%). Instrumenting the internal surfaces of the magnet in the bending plane, as illustrated in Fig. 4.6(a), will allow the momentum of these particles to be measured with similar precision to tracks that reach the downstream tracker. Coverage of a surface area of around $2\,\mathrm{m}^2$ in each of the four stations (left/right, top/bottom) is required. Hence these Magnet Stations (MS) would enhance the capabilities of the detector at a relatively modest cost.

A wide range of topics in the LHCb physics programme would gain from this initiative. Many-body final states in beauty and charm decays commonly contain one or more low-momentum particles and thus could be reconstructed with significantly improved efficiency. The expanding study-area of strange mesons and baryons would benefit due to the low momenta of the products originating from the decays of these lower mass particles. The reconstruction efficiency will improve for decays where a final-state particle is produced at or near threshold. This includes the collaboration's primary sample of D^0 mesons, which arise from $D^* \to D^0\pi^+$ decays and are flavour-tagged for CP-violation studies using the charge of the near-threshold ('slow') π^+ meson. As illustrated in Fig. 4.6(b) this flavour-tagged charm sample can be increased by $\sim$40% in size by the inclusion of Magnet Station information. Flavour tagging of B decays using the same-side kaon tagger will be improved through the access to lower momenta particles from this detector.

The implementation will require careful consideration of the mechanical constraints but a preliminary study suggests a solution will be feasible. The minimal clearance between the magnet and the LHCb acceptance is 105 mm. The design must work around the rods and cables supporting the beampipe. The movement of the magnet coils and yoke under the effect of the magnetic field must be taken into account.

A promising solution is to construct the detector from scintillating fibres, readout by SiPMs.

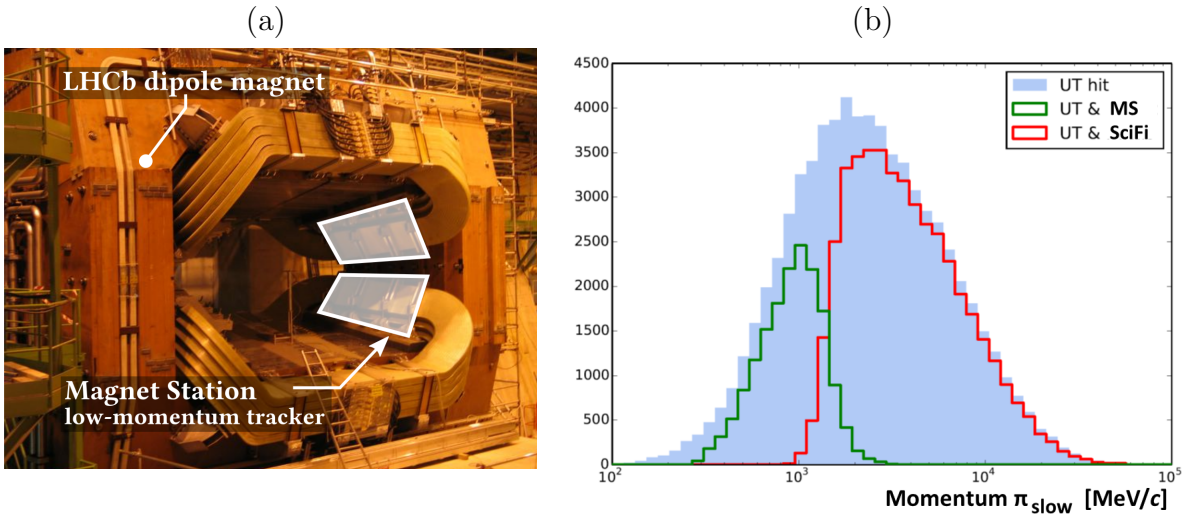

Figure 4.6: (a) the LHCb dipole magnet, with the white outline indicating the area to be covered by this device. A symmetrical module will cover the opposite face of the magnet. (b) the momenta spectra in LHCb simulation of slow pions from the decay $D^* \to D^0\pi^+$ that leave hits in the UT, Magnet Stations (MS) and SciFi.

The SiPMs can be located outside the acceptance at the side of the yoke in a region of lower neutron fluence, routing the photon signals with clear fibres. This design utilises the extensive knowledge and experience in the collaboration of this technology and re-use of fabrication facilities and readout electronics designs. A spatial resolution of the order of a mm is sufficient to obtain the required momentum resolution. The use of a stereo arrangement of layers will be implemented to achieve the required Y segmentation. Preliminary studies show that the pattern recognition will be able to cope with the occupancy in Phase-II Upgrade conditions. The tracks from signal channels are distributed across the vertical acceptance of the modules, while background tracks from secondary interactions are predominantly close to the mid-plane of the device. Consequently a small gap between the chambers, as indicated in Fig. 4.6, reduces the occupancy significantly. The expected lifetime of the fibres in Phase-II Upgrade conditions is under study.

4.3 Particle identification and downstream fast-timing detectors

4.3.1 RICH system

The RICH system plays a central role in the current LHCb physics programme, and will continue to do so for both the Phase-I and Phase-II Upgrades. The challenge of operating in the fierce environment of $2 \times 10^{34}\,\mathrm{cm}^{-2}\mathrm{s}^{-1}$ can be overcome through a natural evolution of the optics, photodetectors and readout of the existing two-RICH system. The necessary modifications will take full advantage of ongoing developments in photodetector and mirror technology. Here the main aspects of the Phase-II system are outlined, with emphasis on RICH 1, where detailed studies have already been performed. More information may be found in Ref. [113].

Occupancy is highest in the central region of the RICH-1 photodetectors, rising to around

30% per pixel per bunch crossing for the current experiment. This value, considered to be an upper limit for successful pattern recognition, will be maintained in the Phase-I Upgrade by increasing the focal length of the spherical focusing mirror by a factor $\sqrt{2}$, hence spreading out the rings in the imaging plane [18]. The pixel areas of the two systems are similar, being 6.3 mm^2 and 6.8 mm^2 for the current HPDs and Phase-I MaPMTs, respectively. The occupancy can be kept at the same level during Phase II by employing a photodetector, for instance a SiPM-based technology, with pixel area of $\sim$1 mm^2, and further increasing the focal length from 1.9 m to 2.0 m (larger increases cannot be accommodated within the available space). In order to restrict the total number of channels, a larger pixel size could be deployed outside the hottest region. A complementary approach to limit the effective occupancy would be to use a two-bit electronics, able to record multiple hits, or to use fast-timing information to allow the association of hits to specific interactions.

From basic assumptions it can be shown that good pattern recognition requires that the RICH system satisfies the relation $(\sigma_\theta \cdot f) \lesssim \sqrt{A_p}$, where σ_θ is the single-photon Cherenkov-angle resolution, f the focal length of the mirror, and A_p the pixel area. The already-discussed modifications to RICH 1 then imply a requirement of $\sigma_\gamma \lesssim 0.5$ mrad, which is three times smaller than the resolution of the current detector, and better than that foreseen in Phase I. The contribution to this uncertainty from the finite pixel size will decrease significantly, but corresponding reductions are also required on the components associated with the chromatic dispersion and also the spread in photon-emission point.

The chromatic dispersion is more pronounced at low wavelengths, therefore the associated single-photon Cherenkov-angle uncertainty can be minimised by choosing a photodetector with a quantum efficiency that is optimised for visible light. SiPMs fulfill this criterion, possessing typical efficiencies of almost 80% at green wavelengths. This is shown in Fig. 4.7, in comparison with the HPDs used in the current experiment, and the MaPMTs that will be installed in the Phase-I Upgrade. Such a response would lead to a chromatic uncertainty less than half that of the MaPMT case. A filter can be employed to reduce this uncertainty still further. A cutoff at 400 nm would reduce the chromatic uncertainty to 0.18 mrad, while suppressing the photoelectron yield by a factor of two. It is anticipated that photocathodes with green-peaked response will also become available for MaPMTs and Micro-Channel Plate (MCP) PMTs, making these photodetectors suitable technologies for regions in which their pixel size can be matched to the occupancy requirements.

The emission-point uncertainty can be suppressed by reducing the tilt of the spherical mirror. The tilts of 316 mrad and 259 mrad in the current and Phase-I detectors, respectively, are chosen to ensure that the intermediate flat mirror lies outside the acceptance. For the Phase-II experiment it is proposed to insert a lightweight composite flat mirror *inside* the acceptance, which will allow the tilt to be reduced to 140 mrad, thereby reducing the emission-point uncertainty to a negligible value. Advances in mirror technology, themselves partly driven by the demands of the evolving LHCb RICH system, mean that it will be possible to construct such a mirror with a thickness of around 1%X_0. Although this mirror will reduce the effective radiator length, the overall number of detected photoelectrons will remain at an acceptable level. A possible design is shown in Fig. 4.8, and compared to that of the current detector. The new design remains within the footprint of the existing and Phase-I systems. (Although the diagram includes the same magnetic shielding as is being assembled for the Phase-I Upgrade, this may not be required if SiPMs, a technology insensitive to magnetic fields, are adopted for the full photodetector plane.)

Table 4.2 compares the contributions to the Cherenkov angle resolution in the current, Phase-I

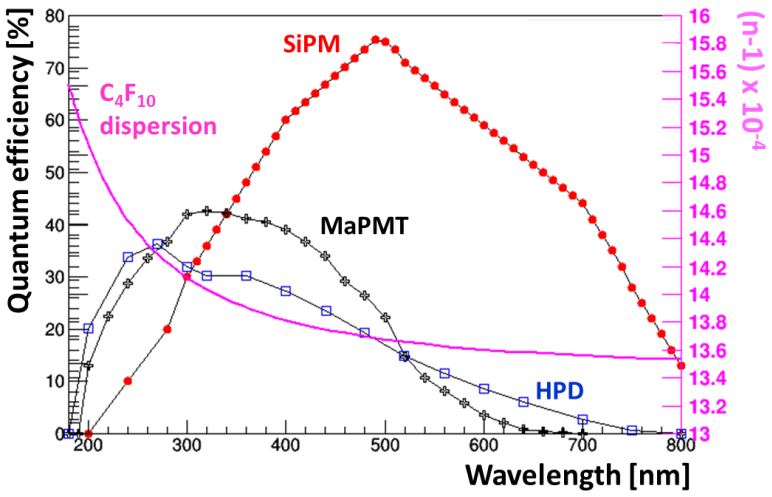

Figure 4.7: Dispersion curve for C_4F_{10}, together with the quantum-efficiency dependence on wavelength for typical HPDs, MaPMTs and SiPMs.

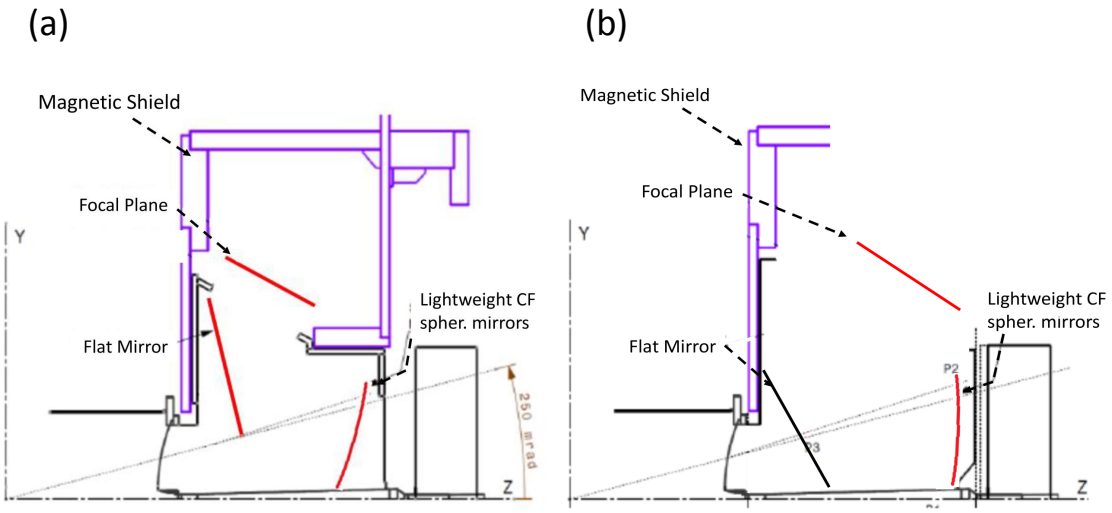

Figure 4.8: RICH 1 layout for (a) current detector, (b) proposed Phase-II detector.

and Phase-II detectors. The sum of the three components is also shown, as is the total number of photoelectrons expected for saturated rings. The RICH-2 values assume similar developments as have been discussed for RICH 1. It can be seen that for both detectors the intrinsic resolution can be improved by a factor of three to four, which will both facilitate the performance of the particle identification and also improve the π–K separation for rings close to saturation.

Fast timing with a resolution of better than 100 ps, as provided by *e.g.* MCPs (see Sec. 5.4)

Table 4.2: Mean number of photoelectrons expected for saturated rings, $N_{\rm pe}$, and contributions to the Cherenkov angle resolution for single photons, σ_γ, for the current detectors and the Phase-I and Phase-II Upgrades (numbers from current and Phase I taken from Ref. [114]). The range in $N_{\rm pe}$, and in the chromatic and total resolution for RICH 1 in Phase II corresponds to whether or not filters are employed to exclude the higher frequency light. The RICH-2 Phase-II values are with filters.

	RICH 1			RICH 2		
	Current	Phase I	Phase II	Current	Phase I	Phase II
$N_{\rm pe}$	32	42	60–30	24	22	30
σ_γ [mrad]						
Chromatic	0.84	0.58	0.24–0.18	0.48	0.31	0.10
Pixel	1.04	0.44	0.15	0.35	0.19	0.07
Emission	0.76	0.37	0.10	0.27	0.27	0.05
Total	1.60	0.78	0.30–0.24	0.65	0.45	0.13

would be a useful attribute, enabling photons to be associated with their correct interaction vertex. Simulation studies are required to quantify the benefits of such a capability. However, as will be discussed in Sec. 5.3, coarser resolution than this is also valuable for rejecting certain classes of background.

4.3.2 Fast-timing detectors: the TORCH

The importance of being able to measure the arrival time of charged particles with a precision of a few tens of ps has already been discussed within the context of the VELO in Sec. 4.1. This attribute is equally valuable downstream of the dipole magnet, with the added challenge that covering the acceptance of the spectrometer in this region requires a large-area detector of $\sim$30 m^2. A promising technology for meeting this need is a TORCH (Time Of interally Reflected CHerenkov light) detector, an innovative time-of-flight (ToF) system based on internally-reflected Cherenkov light produced by traversing charged particles in a $\sim$1 cm thick quartz radiator [115].

A schematic of the TORCH detector intended for LHCb is shown in Fig. 4.9. It could be located just in front of RICH 2, at around 9.5 m from the interaction point. The system aims to achieve a timing resolution of $\sim$70 ps per photon, and to collect around 30 photoelectrons per track, yielding a net precision on each track of $\sim$15 ps. Attaining this level of performance requires that the direction of the incident particles is known to around 1 mrad, which is well within the capabilities of the LHCb tracking system. Micro-Channel Plate (MCP) PMTs are the most promising technology for achieving the necessary timing resolution, and meeting the other requirements of the system. As reported in Sec. 5.4, there has been good progress in R&D for all aspects of the TORCH, including MCP development. A half-sized module will be constructed this year and evaluated in a test beam, and later possibly with collision data on the periphery of LHCb itself.

Fast-timing information in the downstream region will bring many benefits, including the following examples.

1. Fast timing will be a powerful and necessary weapon in suppressing the rate of ghost

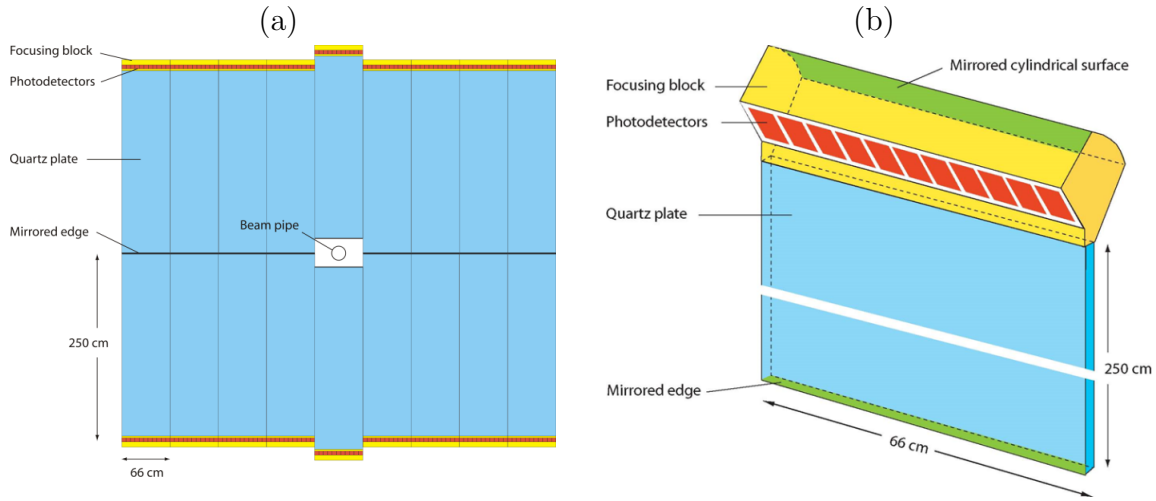

Figure 4.9: Schematic of TORCH detector for LHCb: (a) Front-on view of full detector; (b) View of single module showing focusing block and photodetector plane.

tracks that occur through the mismatching of track candidates found in the VELO and UT, with candidates found in the downstream tracker, referred to as 'T-tracks'. Studies indicate that in events with 50 interactions, when using the matching algorithms developed for the Phase-I Upgrade, this category of ghosts will reach around 50% of the number of correct associations. A sufficiently precise time stamp for the downstream candidates would allow for comparison with the timestamp from the VELO, thereby enabling incorrect matches from different interactions to be rejected (see Fig. 4.10(a)). A timing detector sensitive to the direction of the incident particles, such as the TORCH, would also suppress T-track ghosts arising from the incorrect association of hits in the downstream tracker (see Fig. 4.10(b)).

2. Two-thirds of K^0_S mesons, and a higher proportion of Λ baryons, decay after the VELO and so could only be time-stamped by the TORCH. This information would allow these long-lived particles to be assigned to the correct interaction, thereby reducing combinatorics.

3. The design specifications of the TORCH are such to enable particle identification through ToF in the low-momentum region of 10 GeV/c and below, which is the threshold for positive identification of kaons in the C_4F_{10} radiator of RICH 1. Many important topics in the LHCb physics programme can be enhanced through the additional discrimination between pions, kaons and protons that the TORCH will bring in this regime. Examples include flavour tagging, *CP*-violation measurements involving high-multiplicity final states, and searches for exotic hadrons.

It should be noted that the particle identification capabilities of the TORCH will be equally valuable at the lower luminosities of the Phase-I Upgrade, making this detector an attractive project for installation in LS3, as discussed in Sec. 5.4.

In Sec. 4.3.3 fast-timing information is also proposed for the ECAL, obtained from silicon planes embedded between converter material, in order to suppress combinatoric background for

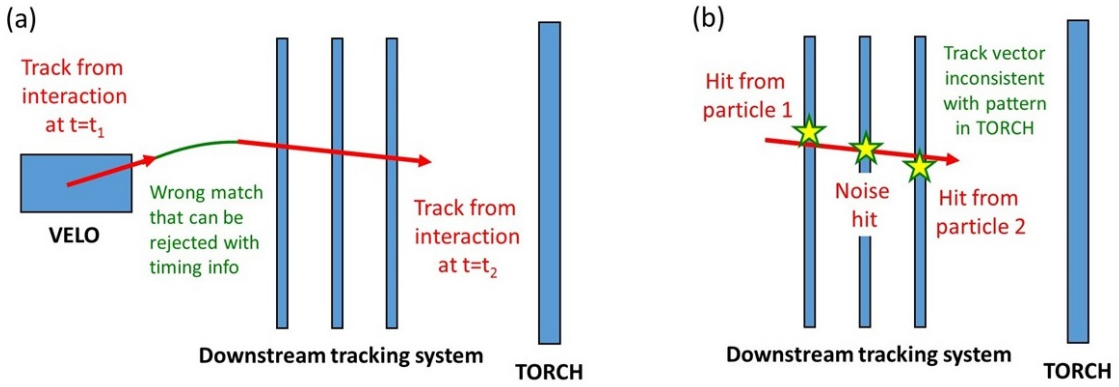

Figure 4.10: Categories of ghost tracks that may be suppressed with TORCH information: (a) wrongly matched VELO-UT and T tracks; (b) wrongly constructed T tracks.

in heavy-flavour studies for π^0 mesons and photons. The same detector will therefore provide fast-timing for charged particles. Further studies are required to ascertain the complementarity between these capabilities and those of the TORCH. It has also been suggested that the timing needs of the ECAL could be met by using the TORCH itself as part of the calorimeter system, situated behind a 1-2 X_0 converter plane, which would give the detector sensitivity to photons. Again, more studies are necessary to evaluate the feasibility of this option.

4.3.3 Calorimetry

The LHCb physics programme can be widened significantly in scope through installing a higher performant Electromagnetic Calorimeter (ECAL), and one adapted to the requirements of a high-luminosity environment. In particular, a rich range of measurements can be performed with final states involving π^0 and η mesons, electrons, and photons from loop-level transitions. There are many examples of individual processes to be studied, so only a short list can be provided here. In the domain of *CP*-violation measurements the angle ϕ_s can be probed with $B_s^0 \to J/\psi\,\eta^{(\prime)}$ decays; knowledge of the angle γ, which is primarily measured with $B^- \to DK^-$ decays, can be improved by including D-meson modes with π^0 mesons in the final state (also valuable for mixing and *CP*-violation studies in the charm system itself); the angle α can be measured through an isospin analysis of the decays $B^0 \to \rho^+\rho^-$ and $B^+ \to \rho^+\rho^0$, which thus far could only be performed at e^+e^- machines. Rare decay studies, that until now have been inaccessible at LHCb, include $B_s^0 \to \mu^+\mu^-\gamma$ and hadronic modes such as $B^+ \to K^+\pi^0$. High quality calorimeter information can be used to suppress $D_s^+ \to \eta(\mu^-\mu^+\gamma)\mu^+\nu_\mu$ decays, which are an important source of background in the search for $\tau^- \to \mu^+\mu^-\mu^-$. Precise studies of photon polarisation in radiative penguin decays such as $B_s^0 \to \phi\gamma$ will be possible, provided the experiment retains good sensitivity to high-$p_{\rm T}$ photons. Modes with electrons, such as $B^0 \to K^{*0}e^+e^-$ and $B^- \to K^-e^+e^-$, which are currently attracting much attention through lepton-universality measurements in loop-induced transitions, will remain a high priority. Searches for pentaquarks and other exotic hadronic states would be greatly enhanced using modes such as

$\Lambda_b^0 \to \eta_c p K^-$ and $\Lambda_b^0 \to \chi_{cJ} p K^-$, to give but two examples.

ECAL requirements and environment

The current LHCb ECAL, of lead-shashlik design, comprises cells ranging in dimension from $4 \times 4\,\mathrm{cm}^2$ in the innermost region, to $6 \times 6\,\mathrm{cm}^2$ and $12 \times 12\,\mathrm{cm}^2$ in the middle and outer regions, respectively. In order to combat the problems caused by overlapping clusters at high luminosity it will be necessary to change to an absorber with reduced Molière radius, such as tungsten, and adjust the cell size accordingly. A dimension of $2 \times 2\,\mathrm{cm}^2$ is a natural choice for the inner region, with further studies required to optimise the size for the other regions. This cell size also ensures that the two photons from π^0 mesons will form distinct, resolvable clusters in the kinematic regime where the bulk of b-hadron decays are reconstructed.

A further requirement, driven by the need to suppress combinatoric background when forming π^0 candidates and reconstructing b-hadron decays, is fast-timing information. The ability to measure the arrival time of particles incident on the calorimeter with a precision of a few tens of ps will allow clusters to be associated to one or a small number of primary vertices, which will be invaluable in reducing background. The importance of this attribute can be assessed from Fig. 4.11, which shows π^0 candidates formed from resolved photon clusters in Run-2 minimum-bias data. The spectrum is shown for events in which 1, 2, 3 and 4 primary vertices have been reconstructed. It can be seen that there is a significant degradation in signal to background as the pileup increases (as well as a slight worsening in resolution caused by overlapping showers). Sufficiently precise timing information will allow the combinatoric background from pileup interactions to be rejected. As discussed below, certain solutions to this problem, for example fast-timing silicon strips or pads, would also bring the benefit of precise spatial information.

The radiation profile in the calorimeter is highly non-uniform. It peaks in the cells closest to the beam pipe, and then falls off with an approximate inverse-square dependence. Figure 4.12 shows the expected dose as determined with the FLUKA package [116, 117] for the hottest region of the inner section in cubes of $5 \times 5 \times 5\,\mathrm{cm}^3$, plotted as a function of z, centred on $y = 0$ for different intervals in x. A correction factor has been applied to account for known differences between simulation and measurements performed after the exposure of Run 1. It can be seen that the innermost modules will experience a very high dose of around 240 Mrad/300 fb^{-1}. Those modules lying further away from the beampipe will accumulate much lower doses.

It may be challenging to optimise simultaneously energy resolution, robustness against radiation damage and cell size. Therefore it is important to ascertain what intrinsic performance is required from the ECAL to obtain sufficient resolution on the π^0 mass. A smearing exercise was conducted in simulation using photons from inclusive π^0-decays, assuming an energy resolution of the form $\sigma_E/E = \sigma_S/\sqrt{E(\mathrm{GeV})} \oplus \sigma_C$, with $\sigma_S = 7 - 15\%$ and $\sigma_C = 1 - 2\%$ [1]. In order to assess the impact of any improved spatial resolution that may become available, the exercise has been conducted assuming the use of spatial information from clusters formed in the current ECAL, and also assuming perfect knowledge of the photon impact point. The results of the study are shown in Table 4.3 and indicate that with improved spatial knowledge a resolution of around $6\,\mathrm{MeV}/c^2$ is attainable, assuming a stochastic term of 10%.

[1] The performance of the current LHCb ECAL can be parametrised by the relation $\sigma_E/E = 10\%/\sqrt{E(\mathrm{GeV})} \oplus 1.5\% \oplus 1\%/E[\mathrm{GeV}]\sin\theta)$.

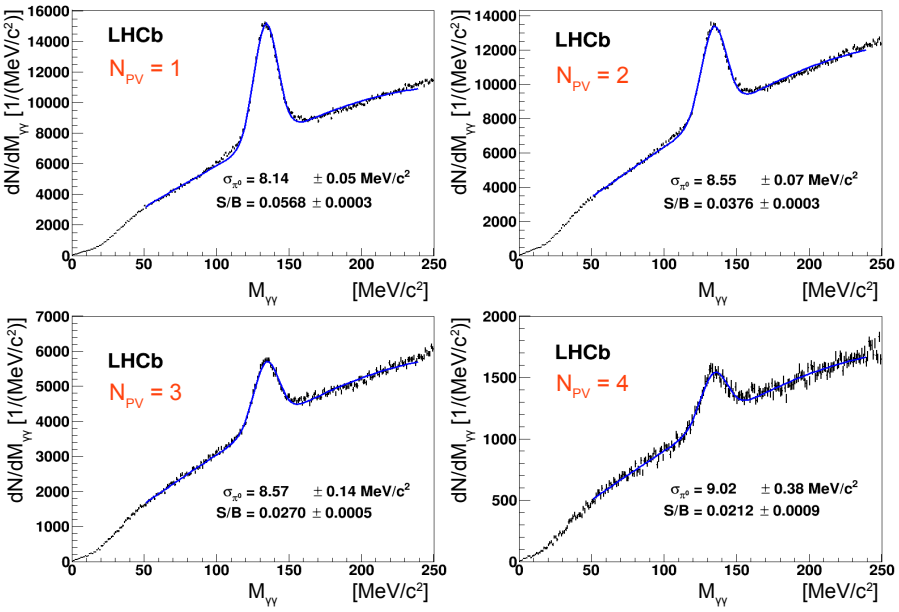

Figure 4.11: Reconstructed resolved π^0 candidates in Run-2 minimum-bias data, divided into sub-samples with different numbers of reconstructed primary vertices (N_{PV}). The mass resolution and signal-to-background ratio (S/B) is indicated for each sub-sample. The selection requires $p_{\mathrm{T}}(\gamma) > 300\,\mathrm{MeV}/c$ and $p_{\mathrm{T}}(\pi^0) > 550\,\mathrm{MeV}/c$.

Table 4.3: Resolutions in MeV/c^2 on the π^0 mass as determined from true $\pi^0 \to \gamma\gamma$ decays in LHCb simulation, where the photons are subjected to Gaussian smearing on the energy resolution of the form $\sigma_E/E = \sigma_S/\sqrt{E(\mathrm{GeV})} \oplus \sigma_C$. Results are shown for the case where the spatial information on the photon impact point is obtained from current cluster information, and with perfect knowledge.

	Spatial information from clusters		Perfect spatial knowledge	
	σ_C		σ_C	
σ_S	1%	2%	1%	2%
7%	7.5	8.2	4.2	5.2
10%	8.5	9.3	5.5	6.5
15%	10.5	11.3	8.0	8.9

Candidate technologies for the Phase-II ECAL

A suitable technology to meet the challenging requirements of the Phase-II ECAL is a modular sampling-calorimeter based on a tungsten or tungsten-alloy absorber. It should be around 25 X_0 in depth, as is the current detector, in order to contain the electromagnetic showers induced by particles from b-hadron decays, and hence will be significantly thinner in longitudinal extent

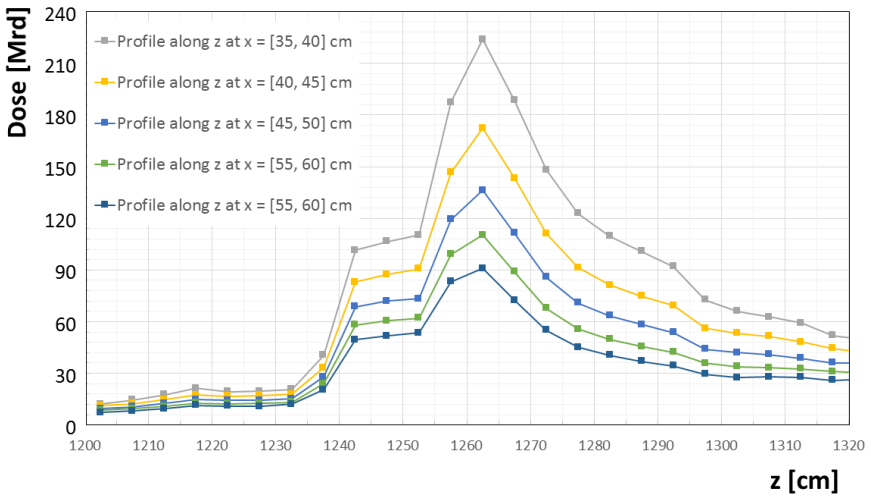

Figure 4.12: Accumulated radiation dose plotted against z in the vicinity of the ECAL for different regions of x, all close to the beampipe, at $y = 0$. The dose is calculated in $5 \times 5 \times 5\,\text{cm}^3$ cells and corresponds to an integrated luminosity of $300\,\text{fb}^{-1}$ at 14 TeV, determined with the detector layout of the Phase-I Upgrade.

than at present. This attribute brings several benefits, for example improved radiation hardness due to shorter wave guides. The cell area in the innermost region should be around $2 \times 2\,\text{cm}^2$; this small size is again benefial for radiation hardness.

Fast-timing and precise position information will be provided by three planes of silicon pads or strips, embedded between absorber layers or behind a single converter plane at the front of the module, or alternatively placed deeper in the detector to benefit from the larger signal at the shower maximum. The final choice of location requires optimisation with respect to the position and timing resolution that the silicon provides. Fast timing in a silicon detector operating in a beam-based experiment has been demonstrated by the NA62 Gigatracker, which has already achieved a resolution of better than 200 ps [110]. An order-of-magnitude better performance is aimed for by the CMS forward-calorimeter Phase-II Upgrade, which will use silicon pads for its active elements [118, 119]. Figure 4.13 shows the impact of fast timing in LHCb for 50 interactions per crossing, simulating the temporal and spatial distribution of interactions, and assuming both a 50 ps and a 20 ps Gaussian resolution for each of the three silicon planes of the ECAL. By placing a one-sigma window around arrival times corresponding to the interaction of interest, the mean number of incorrect primary vertices giving rise to background hits can be reduced to 2.7 with 50 ps resolution, and 1.1 with 20 ps.

The requirements on the spatial resolution to be provided by the silicon planes are under study. In the inner region pad sizes of $1\,\text{cm}^2$ or smaller located towards the front of the module will provide better sensitivity than the centre-of-gravity of the pure calorimeter clusters, and will be valuable for improving the resolution of the π^0 reconstruction and in discriminating between overlapping showers.

The precise design of the module will be decided after an appropriate programme of R&D,

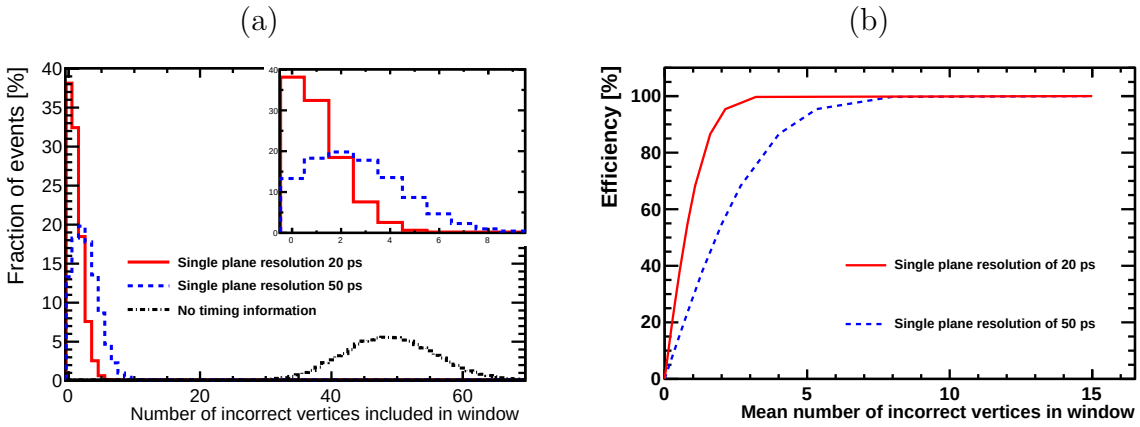

Figure 4.13: Impact of timing information on assigning ECAL clusters to PVs: (a) number of incorrect vertices passing selection; (b) efficiency of selection vs. number of incorrect vertices.

the first steps of which are outlined in Sec. 5.5. The choice of scintillator will be made after a careful evaluation of the possible effects of radiation. One possible geometry is to embed the wavelength shifters in chamfers at the corner of the cells, thereby avoiding the need to drill holes in the tungsten plates. Such an approach, based on the pioneering work described in Ref. [120] is sketched in Fig. 4.14(a). Another interesting possibility is to dispense with wavelength shifters and employ clear light-guides to improve the resultant photon yield. These light guides could be constructed of quartz to improve the radiation hardness of the module. This solution is shown schematically in Fig. 4.14(b).

Modules constructed of small tungsten cells, and containing silicon planes, are expected to be rather robust against radiation damage. The exact sampling ratio of the cells need to be studied, such that this robustness is optimised whilst at the same time satisfying the resolution requirements discussed above. It may be necessary to plan for the replacement of the innermost modules after a couple of years of data taking. This operation will be relatively straightforward in LHCb thanks to the detector's open geometry, although dedicated tooling will need to be developed.

Hadron calorimeter

The primary purpose of the Hadron Calorimeter (HCAL) is to give input to the hardware-trigger decision in the current detector, and also the so-called LLT (low level trigger) of the Phase-I Upgrade. However the LLT is only expected to be required in the early years of Run 3, when the HLT is still being commissioned, and hence the HCAL can be removed after this period. As described in Sec. 4.3.4, the liberated space can be used for augmenting the muon filter.

4.3.4 Muon system

The muon system for the Phase-I Upgrade will consist of four stations, labelled M2 through to M5, equipped with MWPCs. Station M2 is located directly behind the calorimeter and the other three stations are embedded in the muon filter, as shown in Fig. 4.15. Each station is divided

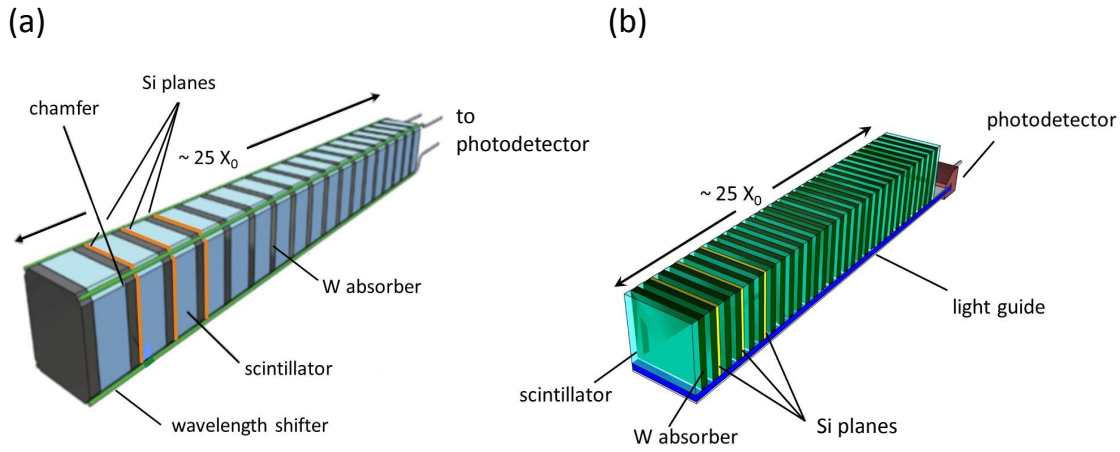

Figure 4.14: Two possible designs of a Phase-II ECAL module: (a) inspired by the sampling tungsten-scintillator calorimeter developed for CMS [120]; (b) including a clear light guide, and no wavelength shifting fibres.

into four regions, R1 through to R4, with the highest particle flux being in R1. The main changes with respect to the current system are the removal of station M1, needed only for the hardware trigger, new off-detector readout electronics, and additional shielding in the beam-pipe region.

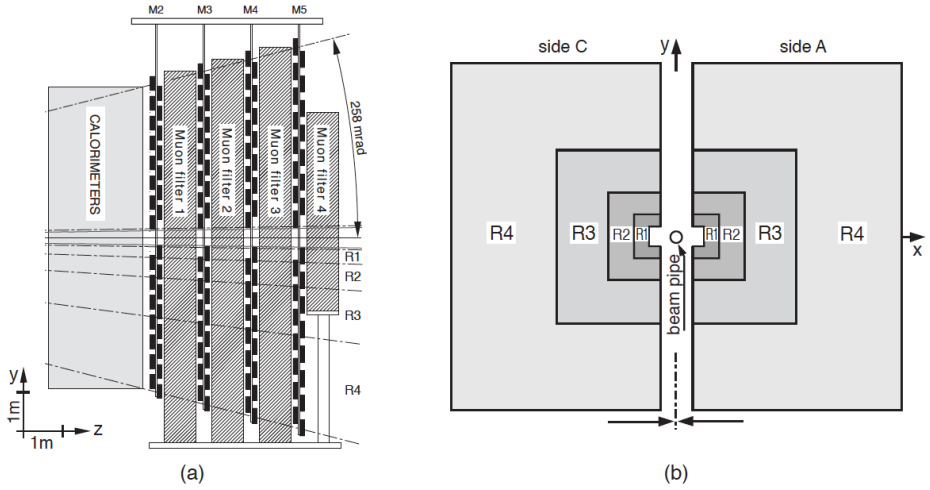

Figure 4.15: (a) Side view of the LHCb muon system for the Phase-I Upgrade. (b) Station layout with the four regions R1−R4 indicated.

At a luminosity of $2 \times 10^{34}\,\mathrm{cm}^{-2}\mathrm{s}^{-1}$ the maximum rate in M2R1, the region of highest flux,

would reach $6\,\mathrm{MHz\,cm^{-2}}$, with an average rate of about half this value. The maximum rates in the other critical regions would be around $1\,\mathrm{MHz\,cm^{-2}}$, $2\,\mathrm{MHz\,cm^{-2}}$ and $0.3\,\mathrm{MHz\,cm^{-2}}$, for M2R2, M3R1 and M3R2, respectively. Such conditions would lead to unacceptable dead time with the current chambers.

The high flux can be suppressed by replacing the HCAL with additional shielding. The full HCAL system occupies a depth of 1.7 m, and corresponds to 5.6 interaction lengths. Filling this space with iron would increase the material in front of M2 by an extra 4.4 interaction lengths. This additional shielding would suppress the rates in the muon chambers by around a factor two, while raising the minimum momentum for muon identification by about $1\,\mathrm{GeV}/c$.

In addition to the extra shielding, new chambers will be required in the hottest regions with their own customised frontend electronics. The requirements on these chambers are to sustain a rate of up to $3\,\mathrm{MHz\,cm^{-2}}$, high efficiency, and operational stability for an accumulated charge of $6\ \mathrm{C/\,cm^2}$ over 10 years of operation. The size of the logical pads will need to be two to four times smaller than those of the current detector, being $0.6 \times 0.8\,\mathrm{cm^2}$ in M2R1. A promising technology is the micro-resistive WELL detector (μ-RWELL) [121], a novel MPGD which has good prospects for satisfying all of these criteria. In the lower flux regions of M2R3 and M2R4 a modified MWPC with pad readout is a possible solution. Moreover, a robust consolidation phase is to be anticipated for the rest of the detector, with the replacement of MWPCs and frontend electronics that have degraded through ageing.

4.4 Trigger and data processing

The removal of the hardware trigger, and the consequent readout, event-building and processing of all interactions at the crossing rate of the LHC, is the distinguishing paradigm shift of the Phase-I Upgrade. The trigger and online scheme for this project is detailed in Ref. [20]. A fully software-based trigger brings maximal benefits in terms of efficiency and flexibility for physics performance, and hence will be retained for Phase-II operation. No fundamental change in architecture will be required for the online system, where the increased data rate can be accommodated by the addition of new links, readout boards and servers. If the throughput rate exceeds a critical value then re-designs of the readout board and event builders will be required.

The strategy for the software and the computing of the Phase-I Upgrade are currently under development, and will be presented in a Technical Design Report (TDR) at the end of 2017. One key aspect of this programme is the design of a new event model and thread-safe software framework, which will enable the experiment to make full use of modern multicore processors. The possible deployment of GPUs, accelerators and other highly performant new processor-technologies is also under active consideration.

The order-of-magnitude growth in data volume for Phase-II operation, and consequent increased demands in processing power and offline storage, will present significant challenges. It is expected that these can be largely met by the solutions adopted for Phase-I, which will be flexible and scalable, in conjunction with the steady advances in computing hardware that will take place throughout the 2020s. A thorough assessment of the requirements and effectiveness of candidate solutions will be made once the Phase-I Software and Computing TDR has been written. One important ingredient in this study will be to assess the beneficial impact of fast-timing information, which will help in speeding-up reconstruction through the suppression of combinatoric background and wrong associations.

Chapter 5

Next steps

Establishing solutions to the challenges of running at high luminosity requires a programme of focused detector R&D, accompanied by appropriate simulation studies. Although high luminosity operation will not begin until after LS4, it is sensible to construct a project plan that takes full advantage of the two and a half years of shutdown scheduled for LS3. In some cases detector modifications, and even installation of new components, can be envisaged that will already bring physics gains for the second period of operation at $2 \times 10^{33}\,\mathrm{cm}^{-2}\mathrm{s}^{-1}$. Furthermore, the experience gained from modifying and then operating even restricted regions of the detector, for example parts of the RICH-1 photodetector plane or a single VELO station, will be invaluable in preparing for the full Phase-2 Upgrade. Finally, the long duration of LS3 provides an ideal opportunity for executing large-scale and time-consuming work, for example the replacement of the HCAL with an additional muon filter, or the installation of new machine elements, such as TAN and TAS shielding.

In the following pages R&D plans are sketched out for each sub-system, together with possible goals for LS3. In most cases these goals are relatively modest, and so well-matched to the restricted level of resources that are available on this timescale. Several larger-scale projects are proposed, and here a priority list will be established after further studies of the physics benefits, and discussions with the relevant funding agencies. It is already evident, however, that a replacement of the most critical regions of the ECAL is required at this time due to radiation damage, and that significant gains to the physics reach of the experiment can be achieved by upgrading with a higher-performant technology. Hence this activity can already be considered a necessary project for LS3. The complete list of activities currently under consideration, and how these would evolve for full Phase-2 operation, is given in Table 5.1.

Responsibilities have been assigned within the sub-systems in order to oversee the R&D programmes leading up to LS3. Studies performed this year will allow a 'Framework Technical Design Report' providing detailed planning to be presented in the near future. More information on selected projects will be made available in separate documents, depending on the scale and complexity of the LS3 goals.

In parallel with work on the detector design it is essential that machine studies continue on the best approach to operating IP8 at high luminosity, and the radiation implications for the machine elements and the experimental cavern. Close collaboration will be maintained between LHCb and the accelerator experts in order to achieve progress in these areas.

Table 5.1: Summary of the modifications under consideration for LS3, and those for Phase-II (LS4). Priorities will be assigned for the LS3 activities after further studies.

Detector	LS3	Phase-II
VELO	Deployment of prototype modules	New detector with fast timing
Tracking	Insert silicon IT, modify SciFi; install MS	Silicon UT and IT, SciFi OT
RICH	New photodetectors for selected regions; use of timing information	New optics; full replacement of photodetectors
TORCH	Installation for low-p hadron identification	Higher granularity photodetectors
CALO	Tungsten sampling modules installed in inner region	New modules in middle and outer regions
Muon	Replace HCAL with iron shielding; installation of high-rate chambers	Complete chamber installation
Trigger and data processing	Adiabatic software improvements; review of offline processing; installation of downstream track-finding processor	Expansion/replacement of links, readout boards and servers

5.1 VELO

The VELO system will be replaced in LS4 for the Phase-II Upgrade. Major modifications are not anticipated in LS3 and the system designed for the LHCb Phase-I Upgrade is expected to perform with high efficiency throughout Runs 3 and 4 [17]. If available on the timescale of LS3, the opportunity would exist to incorporate prototype detectors in available slots in the VELO, mostly likely in two stations backwards of the nominal interaction point. These detectors would allow a technology test in the LHC environment and provide timing information that would be beneficial for primary-vertex reconstruction during the second period of Phase-I operation. Valuable experience would be gained, without the need for significant modifications to the detector cabling and services.

The preparation of a radiation-hard VELO system utilising timing information and potentially incorporating advancements such as smaller pixels and operation without an RF foil, as described in Sec. 4.1, will be a highly challenging project requiring R&D on a range of elements. The critical components of the R&D programme towards the Phase-II detector system are described below.

Design studies

Simulation studies will be performed to direct the technology development programme. The relative advantages of timing performance and reduced pixel size must be evaluated, as there will be an inevitable trade-off between these factors in the ASIC design. The VELO is a principal element of the tracking and its design will be studied as part of an overall optimisation of the Phase-II tracking system. The potential benefits of adding a further dipole field in the VELO region will also be evaluated.

ASIC

The Phase-I Upgrade VeloPix ASIC is based on $55 \times 55\,\mu m^2$ pixels, designed in an 130 nm CMOS process. It uses 25 ns timing resolution to associate hits to their LHC beam crossing. It provides continuous triggerless readout with binary hit information and has a maximum data rate of 20 Gbps.

An ultimate ASIC for the Phase-II Upgrade would have timing resolution better than 200 ps per pixel. The pixel size would be reduced; an aggressive goal would be to aim at a quarter area of the current pixels, $27.5 \times 27.5\,\mu m^2$. Continuous triggerless readout would again be required, consequently leading to a maximum data rate of up to 200 Gbps, depending on the inner radius of the system. Development of such a chip has synergy with future trends in ASICs developed for medical applications, in particular tomography scans, protein crystallography, powder diffraction and high resolution X-ray imaging. The Medipix collaboration is embarking on the design of a Timepix4 chip, which may share a number of the features that are required for this Phase-II Upgrade ASIC. This Timepix4 will be designed in the 65 nm CMOS process. This smaller feature size allows the analogue front-end size to be reduced somewhat, but the digital design will require more space to allow timing information to be included. It seems feasible that a reduction of the pixel size in this process to 40 µm may be achievable.

Two approaches are possible for the timing: either to integrate the Time-to-Digital Converter (TDC) together with the analogue front-end directly in the pixel cell, or to send the discriminator signal to the end-of-column area outside the pixel matrix. The first solution has the advantage of a direct evaluation of the timing without further transmission, while the second requires a distribution of a precise clock inside the pixel matrix. Time-walk compensation will be essential, via a Constant-Fraction-Discriminator or Time-Over-Threshold technique, bringing further complexity to the pixel cell. The ADCs will operate at speeds of 50 GHz or above, and suitable techniques must be found to limit the power consumption. The global ASIC design will be modelled around an approach of grouping the pixels into larger superpixel clusters, with alternating digital and analogue circuits. This will allow the sharing of resources and data compression on the pixel level, while isolating the circuits from each other. It will probably be advantageous to incorporate Through Silicon Vias (TSVs) into the fast ASIC design, facilitating access to the pixels and simplifying the overall hybrid assembly. It will be of great interest to include an interposer layer between the ASIC and the silicon, allowing for differences in pitch or layout between the sensor and the ASIC segmentation. This may permit the data concentrators to be placed in subsections of the chip, easing congestion, as well as allowing an even pixel size on the sensor with no need for elongated sections.

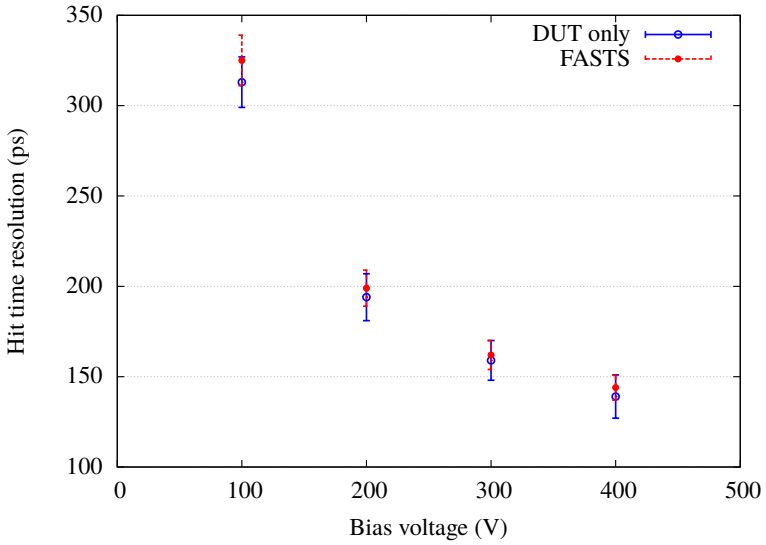

Figure 5.1: Test-beam results of the silicon pixel detector developed by NA62. Average time resolution, as calculated with two methods, is shown as a function of sensor bias-voltage across all pixels in the device. Reproduced from Ref. [122].

Sensor

Achieving simultaneous timing and spatial resolution characteristics from the pixel sensors at high irradiation-levels requires dedicated R&D. The sensor must provide a signal capable of matching the speed available from the electronics. The baseline solution will remain a thin, highly-segmented device. Thin detectors will optimise the slew rate, allow for high electric fields and give the best radiation-hardness performance. The finely-segmented pixels will provide the necessary position resolution, in particular after irradiation, and present the lowest capacitances and leakage currents to the readout electronics. Detector operation in electron collection mode will be mandatory. Conventionally designed silicon sensors may provide a reasonable resolution for this application, as demonstrated by the NA62 collaboration [110] and shown in Fig. 5.1. R&D studies are required to investigate how the timing performance evolves after heavy irradiation. In order to achieve more ambitious timing resolutions below 100 ps it may be necessary to adopt an engineered approach. Dedicated designs such as Low-Gain Avalanche Detectors (LGAD) [123] function by adding an extra doping layer to the readout side, providing an avalanche region to boost the signal. A best performance of 27 ps has recently been achieved for a $1.4 \times 1.4\,\mathrm{mm}^2$ pixel size [124] using a Silicon-on-Insulator (SoI) design and a 50 µm thin sensor. The additional gain of the LGAD detectors is not currently robust against irradiation. Alternative approaches use as a baseline epitaxial or micro-machined (3D) technology sensors [125]. The development of such sensors combining high spatial resolution and timing is of benefit across a wide range of high energy physics experiments, and significant work is already underway in the context of the CERN RD50 collaboration and elsewhere.

A schematic showing a possible layout of a hybrid pixel-sensor detector is shown in Fig. 5.2.

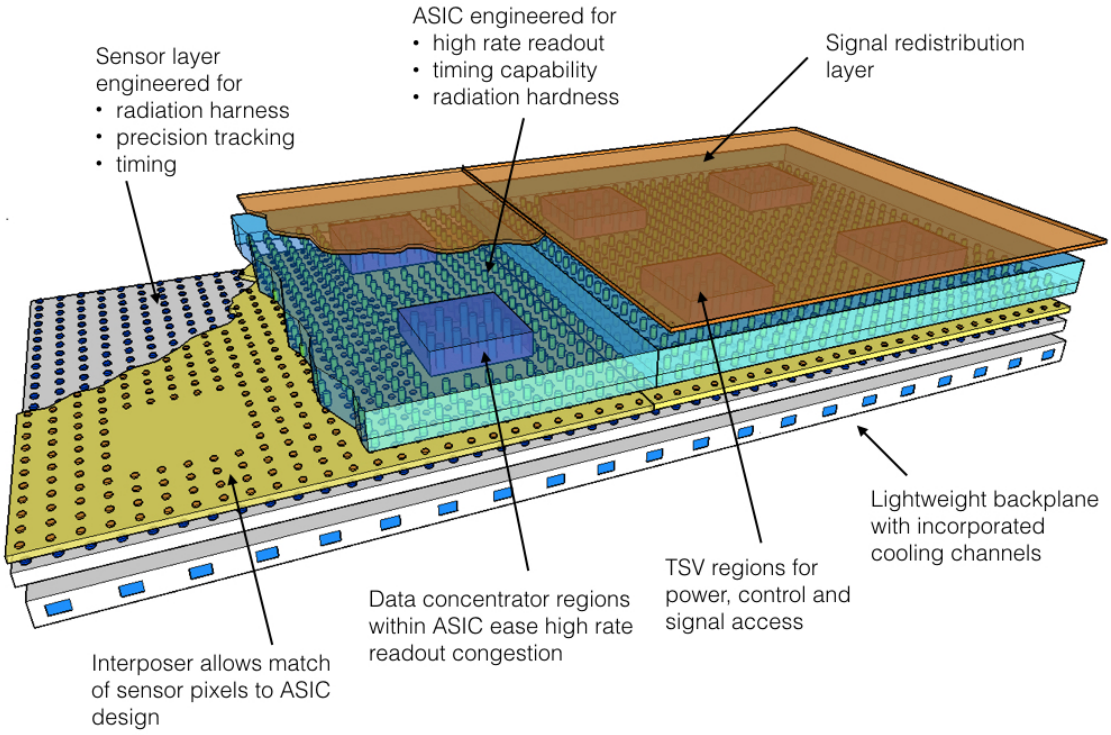

Figure 5.2: Conceptual layout illustrating the technologies that will be explored for the fast-timing hybrid pixel module.

Mechanical system

There are two critical challenges for the VELO mechanical system that require dedicated programmes of R&D.

The first relates to the RF foil, that is the thin corrugated aluminium shield which encapsulates each detector half. The RF foil serves to minimise electrical coupling between VELO components and LHC beams and provides a surface free of abrupt changes in geometry which would generate heat and peturb both the VELO electronics and the beam parameters. It also provides a non-evaporable getter (NEG) coating, which contributes to the control of dynamic vacuum effects and separates the high-vacuum region of the LHC beam-pipe from the volume containing the detectors. The RF foils are the single largest contributor to the material in the VELO and of particular importance as the foil is before the first measured point. Solutions which reduce the material contribution of the foil, by extending the thinning programme already underway for the Phase-I Upgrade, or using alternative materials such as CFRP composites may enable a reduction of material. Based on the experience gained with LHC operation, it may also be possible to consider alternative solutions, such as a system of wires or an ultralight tube to guide the beam mirror currents, combined with with local cryo-pumping to remove outgassing.

The second critical mechanical challenge is to design into the system from the outset the ability to gain relatively easy access to the silicon sensors. The radiation environment is such that replacement, or rotation to more or less irradiated positions, of silicon sensors is a likely corollary of Phase-II operations, in particular in the light of the need for radiation hardness for both the spatial and timing performance of the sensors. In the current mechanical system access to the sensors is not foreseen on a regular basis and requires a complex and time-consuming intervention procedure. In Phase-II the sensor-base mounting, vacuum boxes and mounting of the electronics and services must be designed under the assumption of facilitating access to the silicon modules in End-of-Year Technical Stops.

5.2 Tracking system

The LHCb tracking system for the Phase-II Upgrade comprises detectors upstream and downstream of the LHCb magnet, and utilises silicon and scintillating-fibre based detectors. During LS3 there will be an opportunity to install selected components of this system, which will improve the physics reach of the Phase-I Upgrade. Plans are outlined below on the assumption that this attractive option will be adopted, although variations on this approach can be envisaged. There are significant synergies between the R&D programmes required for each sub-system.

Goals for LS3

The mixed technology solution of the downstream tracking stations naturally suggests a staging scenario for construction, making optimal use of the LS3 shutdown. The performance of the tracking system in the Phase-I Upgrade will benefit from the addition of the Inner Tracker in LS3. This will improve the performance of the detector through the reduction of the false-track rate, increased track-finding efficiency and potential improvements in the speed of track reconstruction. Furthermore, a small very inner region of the LHCb acceptance which remains uninstrumented in the Phase-I Upgrade SciFi design could be recovered, leading to an additional gain in track reconstruction efficiency.

The design shown in Fig. 4.5 respects the module dimensions of the Phase-I Upgrade SciFi. The Middle Tracker spans the width of six SciFi modules, the Inner Tracker two modules. Sufficient fibres may be available from after the current Phase-I Upgrade construction to allow the necessary fibre mats to be made in readiness for the insertion of the Inner Tracker in LS3. The Middle silicon tracker and revised tracker for the Outer region will then be constructed for insertion in LS4, in readiness for Phase-II Upgrade operation.

The primary elements of the required initial R&D programme are described below. The proposed Magnet Stations, based on scintillating fibre technology and intended to extend the low momentum particle tracking capabilities of the experiment, are also to be installed in LS3.

Design studies

A comprehensive optimisation study of the tracking detectors for the Phase-II Upgrade will be performed, informing the design of the upstream and downstream tracking regions, optimised in tandem with that of the VELO. The key performance parameters are: the efficiency of the track finding procedure inside the LHCb acceptance and the corresponding rate of ghost tracks; the precision of the reconstructed track momentum; the precision of the reconstructed track

impact parameter; and the speed of the pattern-reconstruction and track-finding algorithms. The optimisation will also incorporate the effects on particle identification, notably on the determination of track slopes for the RICH and TORCH detectors, and the reconstruction efficiency for the relatively long-lived K^0_S and Λ particles which predominantly decay outside the VELO acceptance. Design drivers of the performance include the occupancy of the tracking detectors and the matching of track stubs in the upstream and downstream elements of the tracking system. These are controlled by the granularity of the designed system and the potential for time tagging (see Sec. 4.3.2) to complement the high spatial and time resolution anticipated for the Phase-II Upgrade VELO. The number and location of the stations will be revisited to ensure good matching between the VELO, UT, MS and IT/MT/OT regions. Detailed designs for the Magnet Stations will also be produced, determining the resolution, occupancy and light yields anticipated in the fibres and the corresponding effects on the track-finding efficiency.

High granularity silicon detectors

The inner part of the Phase-II Upgrade UT and the IT will require the granularity of short strips and this is where the initial research will focus, as these sensors will be required for IT installation during LS3. The requirements are matched by existing silicon sensor technologies. In addition to conventional short microstrip sensors the emerging technologies of High Voltage (HV)/High Resistance CMOS may be applicable and an R&D programme on this technology is proposed. CMOS based devices now dominate the market for image sensors and large scale production capacity is available at significantly lower cost than for the standard silicon devices currently used in high energy physics. These CMOS detectors can combine detection and processing capabilities in a single lower cost and thinner device, allowing higher resolution systems for the same number of readout channels. Monolithic active pixel sensors combine the sensor and processing in one integrated device, while CMOS active sensors can include the sensor and analogue processing in the sensor while connecting to an external chip for the digital elements of the processing. The CHESS HV-CMOS R&D programme [126] of the ATLAS experiment has demonstrated low noise (< 100 e^-) sensors with a granularity exceeding that required for LHCb, and most critically has demonstrated the radiation tolerance at the level required for the LHCb Phase-II tracking application.

Scintillating fibres

The installation of the Inner Tracker in LS3 requires the construction of the corresponding shorter fibre modules for the Scintillating Fibre tracker to accommodate this system. It is anticipated that this construction will occur directly after the completion of the construction for the Phase-I Upgrade. The construction will thus fully benefit from the production and quality-control expertise and infrastructure and provide consistency with the remaining elements of the tracker. Two of the ten or twelve modules in each layer of the SciFi will be prepared to allow the modifications to occur in LS3.

The design and preparation of the Magnet Stations is also proposed to be based on this technology. The additional technique required in the production of this detector is the join of the scintillating fibres to clear fibres, which is a well-established procedure. The clear fibres route the photons to the SiPMs which are located in a low-background region at the side of the magnet yoke.

The existing R&D programme of the collaboration on scintillating fibres will be continued to facilitate the development of the Phase-II Upgrade Outer Tracker. The radiation tolerance of the SiPM is a key element of this programme. The SiPM radiation damage (dark count rate) is proportional to the 1 MeV neutron fluence. The radiation damage is mitigated by cooling, and the Phase-I Upgrade system is cooled to -40°C. It may be possible to operate at somewhat lower temperatures, with -50°C a realistic target. The neutron shielding of the system can be further optimised. In addition there are hopes that the light yield of scintillating fibres suitable for LHCb applications will continue to improve, and so the existing close collaboration with industry for both fibres and SiPMs will be maintained. The light attenuation after irradiation requires a dedicated simulation-study to guide the overall system design. The utilisation of fibres with smaller diameters will also be considered. These have a shorter attenuation length, are likely to be more affected by quality control issues in the variation of the diameter ('bumps'), and are more delicate in handling and winding. Hence it is currently envisaged to employ fibres with only a modest reduction in diameter, and indeed the thinest fibre currently produced by the manufacturer of the SciFi fibres is 200 µm. Large area scintillating-fibre trackers are a relatively new technology for high energy physics and further improvements can be anticipated on the timescale of the Phase-II Upgrade.

5.3 RICH system

It will not be feasible to implement any significant changes to the optics of the RICH system during LS3, however replacement of a limited, but critical, region of the photodetector plane can be envisaged, along with minor changes to the readout. These modifications would both improve the particle identification performance during Run 4, and constitute important intermediate steps towards the full Phase-II detectors.

As shown in Fig. 5.3, there are two symmetric regions in the RICH-1 photodetector plane, each of approximately $50 \times 25\,\mathrm{cm}^2$, where the occupancy is significantly higher than elsewhere. Long Shutdown 3 provides an ideal opportunity to replace the MaPMTs in this vital area (or a horizontal band encompassing this area) with a first iteration of the photodetector that will be used in the Phase-II Upgrade. If the chosen technology is SiPM based, the greatest challenge will be to integrate the necessary cooling services within the existing space. The new device will have improved granularity and a photocathode that exhibits highest sensitivity in the visible spectrum. As can be seen from Table 4.2, the pixel and chromatic uncertainties will dominate the photon resolution for the baseline Phase-I RICH-1 counter. The new devices will therefore allow these uncertainties to be reduced in the most important regions of the photodetector planes, and also significantly reduce occupancy, thereby benefiting the overall performance. The experience gained will be invaluable in optimising the final version that will be installed during LS4. The LS3-installed devices can then be moved to the outer regions of the photodetector plane.

It should also be noted that within the next few years new versions of the Phase-I MaPMTs are expected to become available, also with photocathodes optimised for the visible spectrum. These tubes are natural candidates for populating the lower occupancy regions of the two RICHes. In Run 4 it will be possible to install a limited number of these devices and evaluate their performance during operation.

During LS3 it is intended to modify the existing frontend electronics to reduce the readout gate from 25 ns to ∼1 ns. The motivation for this change is apparent from Fig. 5.4, which shows

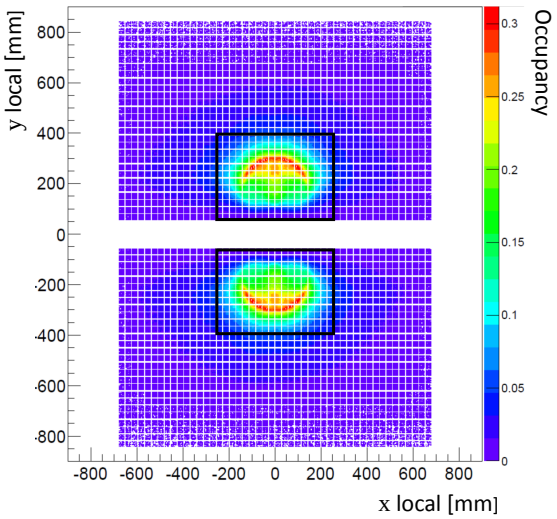

Figure 5.3: Simulation of the photodetector planes for the Phase-I MaPMT-equipped RICH 1, showing occupancy per bunch crossing at an instantaneous luminosity of $2 \times 10^{33}\,\mathrm{cm}^{-2}\mathrm{s}^{-1}$. The black boxes indicate the regions that could be replaced by new photodetectors during LS3.

the arrival time of photons at the photodetector plane, according to Monte Carlo simulation, integrated over many events. The photons from the single particles arrive coherently within a few ns. There is significant background at different times, however, from photons directly impinging on the detector plane, secondary reflections, scintillation light and from out-of-time particles. By selecting those photons in the signal window it is estimated that the signal-to-background ratio can be enhanced by almost a factor two, thereby improving the performance of the pattern recognition for the Phase-I system.

A vigorous R&D programme will now begin to develop the photodetectors, readout and mirror technology necessary for high luminosity operation, with the intention of implementing the above improvements during LS3, and being ready to evolve towards the fill Phase-II RICH system a few years later.

5.4 TORCH

The attributes discussed in Sec. 4.3.2 that make TORCH an exciting proposition for LHCb operation at luminosities of $10^{34}\,\mathrm{cm}^{-2}\mathrm{s}^{-1}$ can also be exploited during the Phase-I Upgrade era, in particular its low-momentum particle-identification capabilities. Hence it can be considered as an attractive potential project for installation in LS3. To this end, R&D is already well advanced [127], in readiness for a full proof-of-principle by the end of 2018.

As a first demonstration of the TORCH principle, a scaled-down prototype of a TORCH module has been constructed, shown in Fig.5.5. The optical components of this small-scale demonstrator constitute a quartz radiator plate of dimensions $350 \times 120 \times 10\ \mathrm{mm}^2$ and a focusing block, read out by a single customised MCP photodetector. The anode pad structure of the MCP has been designed by an industrial partner, Photek UK, with a granularity of 128×8

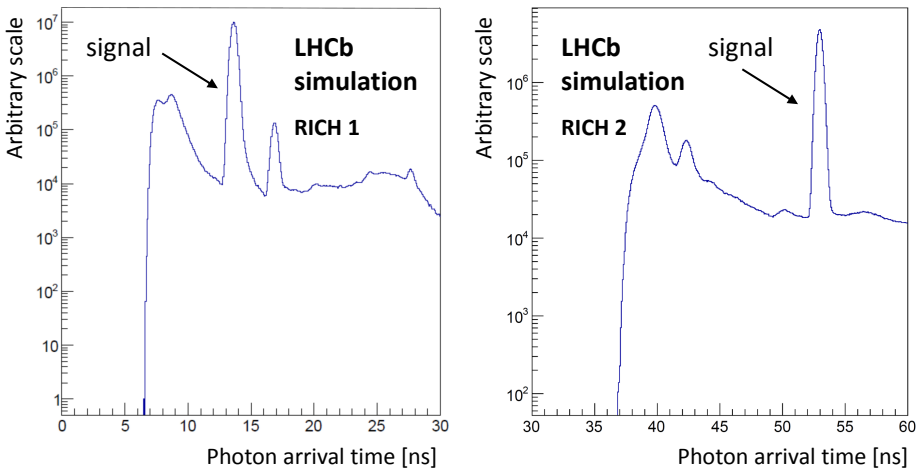

Figure 5.4: Simulation study showing arrival time, with respect to the *pp* interaction, of photons at the photodetector planes of RICH 1 and RICH 2. The events have been simulated with the current geometry at a luminosity of $2 \times 10^{33}\,\mathrm{cm}^{-2}\mathrm{s}^{-1}$.

effective pixels, suitable for for operation at Phase-I luminosities, over a 2-inch square tube.

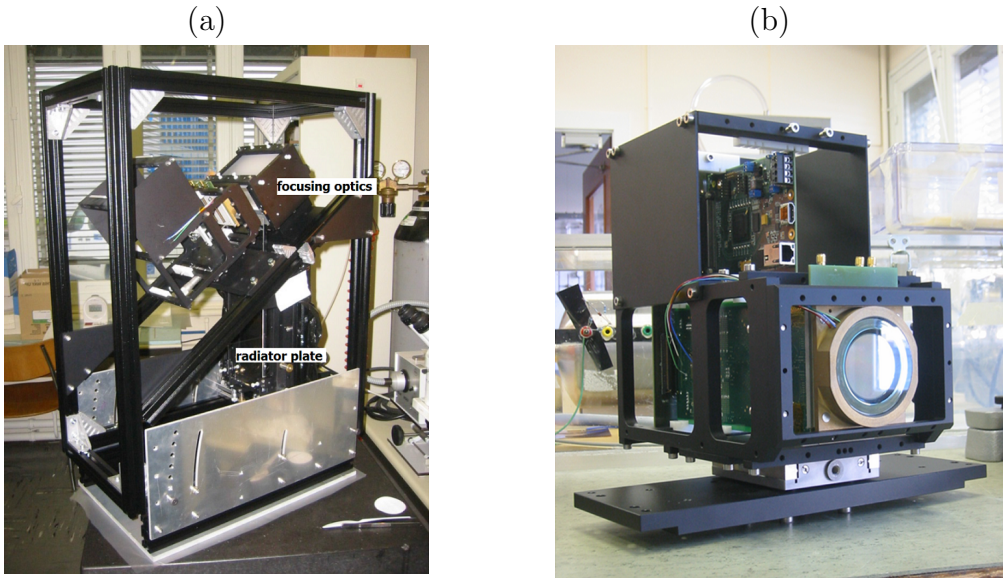

Figure 5.5: The small-scale TORCH module demonstrator: (a) the TORCH radiator and optics mechanical vessel; (b) the MCP photodetector and readout electronics.

The final MCP PMTs will have square format with high active area ($> 80\%$), have radiation tolerance (integrated charge) beyond $5\,\mathrm{Ccm}^{-2}$ using an Atomic Layer Deposition (ALD) technique [128], and an excellent intrinsic time resolution of $\sim$30 ps [129]. The tube has 64×64 pixel pads of dimension 0.75 mm wide on a 0.88 mm pitch. In order to achieve 128×8 effective

granularity, eight pixels are connected together in the coarse direction and charge sharing is used between pads in the fine direction. This also halves the total number of readout channels. The MCP is read out by customised 32-channel electronics which provides a time and amplitude measurement [130], crucial for achieving the desired timing and spatial resolution of the TORCH detector.

The demonstrator has been tested in the CERN T9 test-beam, and the performance of the MCP and readout electronics evaluated. An MCP hit map from 5 GeV/c incident pions is displayed in Fig.5.6, showing the arrival time of detected Cherenkov photons as a function of position in the MCP column. The curved lines show Monte Carlo expectations. The three distinct regions of the distribution correspond to zero, one and two reflections, respectively, off the side edges of the radiator plate as the photons propagate to the focusing block. The time-projection measurements from these data show that a resolution of ∼85 ps is achieved after corrections have been made for time-walk effects, the integral non-linearity of the TDC, and quadrature subtraction of the start-time uncertainty [131]. The measurements are close to the 70 ps that has been targeted for single photons.

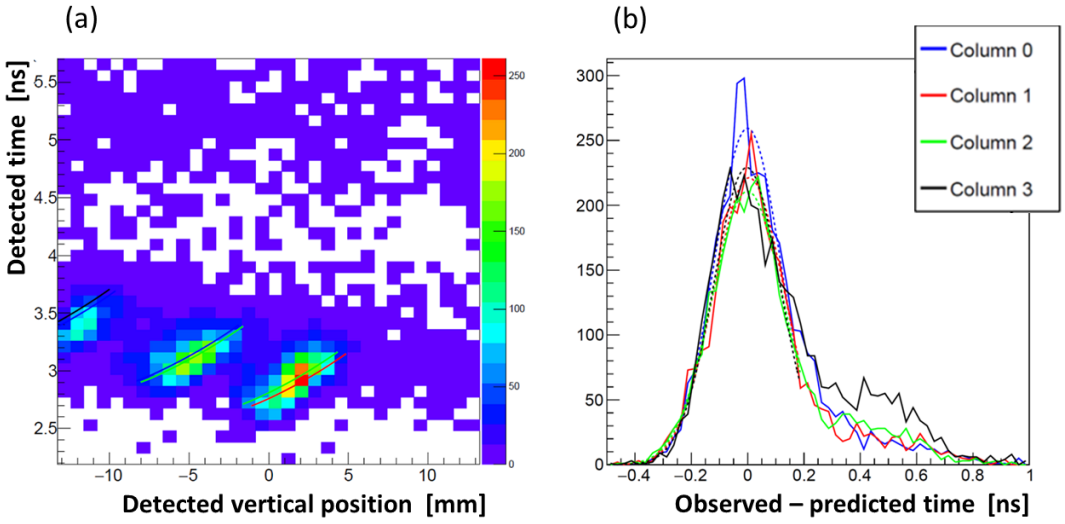

Figure 5.6: TORCH testbeam results: (a) arrival time of detected Cherenkov photons as a function of position in the MCP column; (b) projected time distribution.

A half-length TORCH module is currently under construction, following on from the successful experience with the demonstrator. This module will have a single $1250 \times 660 \times 10\,\mathrm{mm}^3$ quartz radiator plate, and a focusing block which accommodates ten MCP PMTs of the final design. The radiator plate and focusing block have been ordered from industry. All ten MCPs and readout electronics will be delivered in the first half of 2017.

Following beam-tests which will proceed towards the end of the year, it is proposed to install the TORCH half-module in the LHCb experiment during the 2017/18 End-of-Year Technical Stop. A candidate location, shown in Fig.5.7, is adjacent to the electromagnetic calorimeter. Here the module will see low-momentum particles bent at large angles by the dipole magnet, without impinging on the acceptance volume typically used in physics analysis. The priority will

be to test the time-of-flight particle identification capabilities of TORCH, however there is also the possibility to investigate its capability to time photons, by placing $\sim 1\,X_0$ of lead in front of the module.

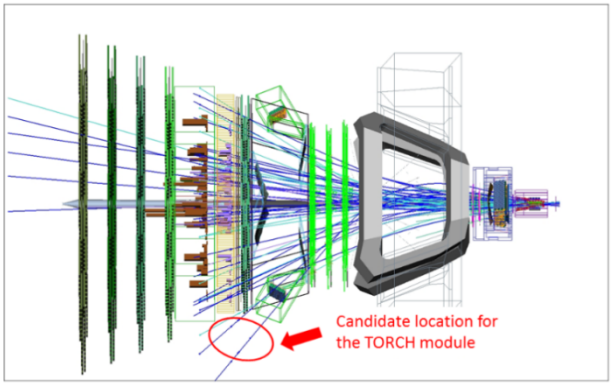

Figure 5.7: A possible location of the TORCH half-sized module in LHCb.

In looking ahead to the next steps required to build a TORCH detector for installation in LHCb in LS3, one important consideration is the procurement of the quartz radiator for the full-scale detector. This could naturally follow the design of the current prototype module, but an alternative option is to re-use some of the radiator bar-boxes from the BaBar DIRC detector, which are currently in storage at SLAC. They have the required length, but are composed of smaller bars which would require suitably adapted optics [132]. The project has the exciting opportunity to borrow one such bar-box and, if it were to yield satisfactory results, the option of requesting an additional seven bar-boxes remains open, which would be sufficient to instrument around two-thirds of the TORCH area in LHCb.

5.5 ECAL

As already reported in the TDR for the Phase-I Upgrade of the particle identification systems [18], the innermost 32 modules of the ECAL will have suffered severe radiation damage by the time of LS3, and therefore need replacing. In that document it was stated that spare modules of the same design, which already exist, would be installed during this Long Shutdown. It is now proposed to replace the entire inner region with high granularity tungsten-based modules equipped with fast-timing capabilities and excellent spatial resolution, as discussed in Sect. 4.3.3. The inner region is marked out in Fig. 5.8 and would require around 175 modules to populate, each containing 36 cells of $2 \times 2\,\text{cm}^2$. Depending on the module design, it might be possible to install the pure calorimeter elements first, and leave the timing planes for insertion in a later shutdown, although it is preferrable to have full functionality in place for Run 4.

In addition to installing a high performant new technology in the most critical region of the ECAL, other modifications can be implemented at low cost that will improve the overall physics reach of the experiment. The modules removed from the inner region that are still functioning well, and the available spares, can be re-deployed in the middle region, and the middle-region

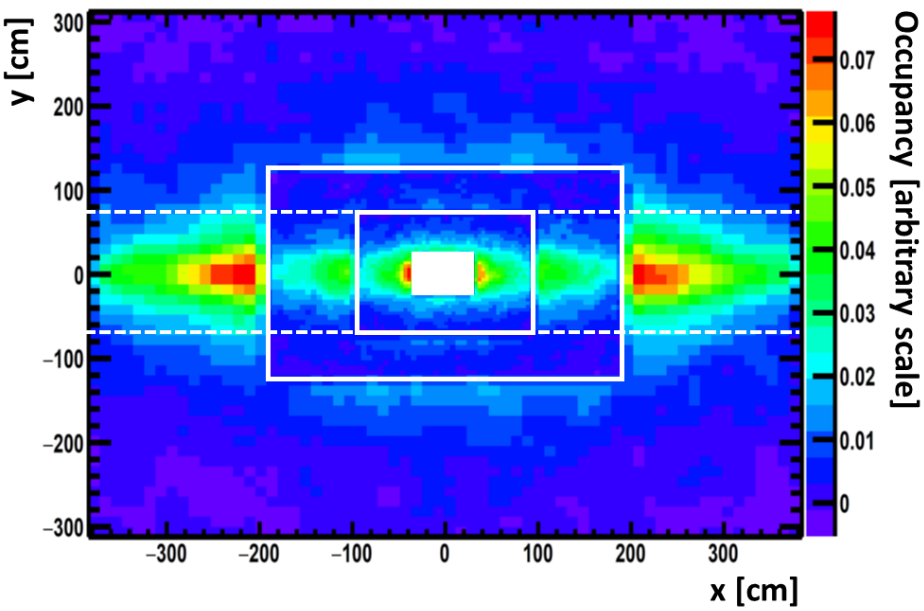

Figure 5.8: Distribution of occupancy across current ECAL. The solid lines indicate the inner, middle and outer regions. The dotted horizontal lines indicate the region that could be modified during LS3.

modules in turn placed in the outer region (if necessary, it will be possible to manufacture additional modules at the original production centres). This rearrangement of modules would be performed in the horizontal band in which the particle flux is highest, and hence would reduce the occupancy throughout. This scheme is sketched in Fig. 5.8. In b-hadron decays to final states involving a single π^0 meson emitted within the acceptance, the photons fall into this horizontal band with around 50% probability. The timing information that will become available in the inner region will suppress with high efficiency background from pile-up interactions during the $\mu = 5$ operation of Run 4. Therefore, the proposed intervention will both lay the foundations for the full Phase-II ECAL, and also bring a significant improvement in physics performance for Run 4, which will be invaluable in preparing the physics programme of the high-luminosity era.

Initial R&D will pursue in parallel the pure calorimeter aspects of the module design, and also the fast-timing capabilities provided by the silicon planes. Concerning the former, the first priorities will include the optimisation of the scintillating-light output and the performance of different scintillators and light-guide materials; the construction of module prototypes and evaluation in test beams; and radiation hardness tests. The silicon studies will focus on performance versus different wafer thicknesses and geometry, the evaluation of various readout solutions, and the optimal location of the planes within the module.

5.6 Muon system

The extended time available during LS3 provides an ideal opportunity to dismantle the HCAL and replace it with additional iron shielding, in order to reduce the rates in the muon system. Either custom-cut iron slabs may be purchased, or existing material may be adapted for this purpose. A promising possibility is to make use of the iron slabs from the magnet of the OPERA experiment at Gran Sasso underground laboratory [133]. There are a sufficient number of OPERA slabs to meet the needs of LHCb, and preliminary engineering designs indicate that with some re-machining they are suitable for the muon shielding. One possible scheme is shown in Fig. 5.9. INFN have been notified of this interest.

Figure 5.9: A possible design of the new muon filter, making use of the iron slabs from the OPERA magnet.

Test beam studies are already underway of μ-RWELL detectors in the framework of INFN R&D on new detector technologies. The preliminary results are very promising, showing a rate capability, as measured with X-rays, up to several MHz/ cm^2 with very limited gain loss (see Fig. 5.10), and a time resolution around 5 ns. This year prototypes will be designed and constructed suitable for operating in the very high-rate of region of M2R1 during the Phase-II era. The development of a customized frontend electronics is also under consideration, based on the VFAT3 [134] front-end ASIC designed for the CMS GEM detectors. It is feasible that new chambers could be installed already during LS3. Simulation studies have begun to understand the benefits in physics performance from the improved chambers, and the effect of having the shielding installed already for $2 \times 10^{33}\,\mathrm{cm}^{-2}\mathrm{s}^{-1}$ operation in Run 4.

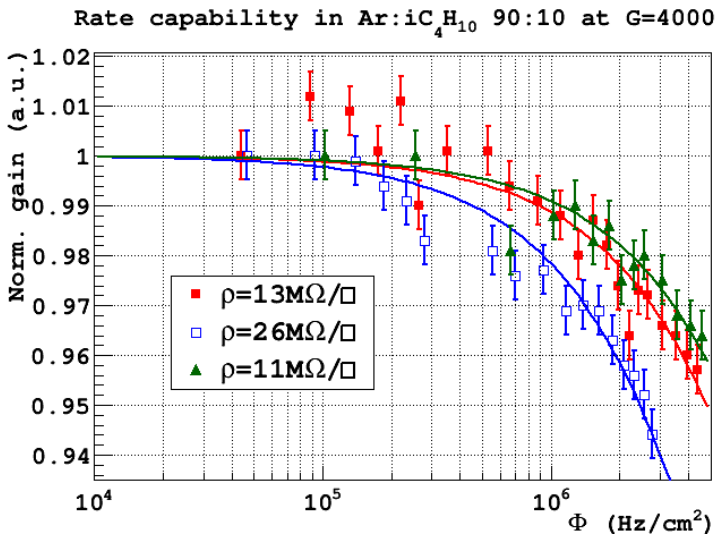

Figure 5.10: Rate capability of μ-RWELL detectors, measured with X-rays, at a gain of 4000 and using an Ar/iC$_4$H$_{10}$=90%/10% gas mixture, for different values of surface resistivity.

5.7 Trigger and data processing

Although the trigger strategy of both the Phase-I and Phase-II Upgrades will remain firmly software based, studies are underway to learn what benefits could accrue by adding dedicated processors to help solve specific low-level tasks. One example is to find tracks downstream of the magnet at the earliest trigger level. This capability is not part of the baseline trigger scheme, as proposed in Ref. [20], on account of the significant CPU time required to execute the search. Not having access to this information limits efficiency for decay modes with downstream tracks that cannot easily be triggered through another signature, for example channels containing a K^0_S meson and less than two prompt charged hadrons, for example $D^0 \to K^0_S K^0_S$, $D^+_s \to K^0_S \pi^+$, $D^+ \to K^0_S K^+$ *etc.* The same is true for decays involving Λ baryons and long-lived exotic particles. A system of specialised processors may be used to find rapidly the downstream tracks through look-up tables, and present these tracks to the software trigger in parallel with all the raw detector information in the event [135]. This 'retina' scheme, shown schematically in Fig. 5.11(a) can be run in a manner compliant with the online architecture and, if demonstrated to bring significant physics benefits, could be considered for installation in LS3. An ongoing R&D programme has already demonstrated the feasibility of fast track-finding with such a processor-based approach. Figure 5.11(b) shows a demonstrator system in the laboratory [136].

The Phase-I Upgrade computing model will provide a framework in which the software of the experiment can evolve adiabatically throughout the HL-LHC era. During Long Shutdown 3 there will be sufficient time to refine aspects of this model following the experience of Run 3, and to take advantage of ongoing commercial developments. One such possibility is the increased use of commercial clouds, rather than full reliance on GRID-based processing. Another is the wide-scale deployment of GPUs and similar technologies, which are already under evaluation for Phase-I applications.

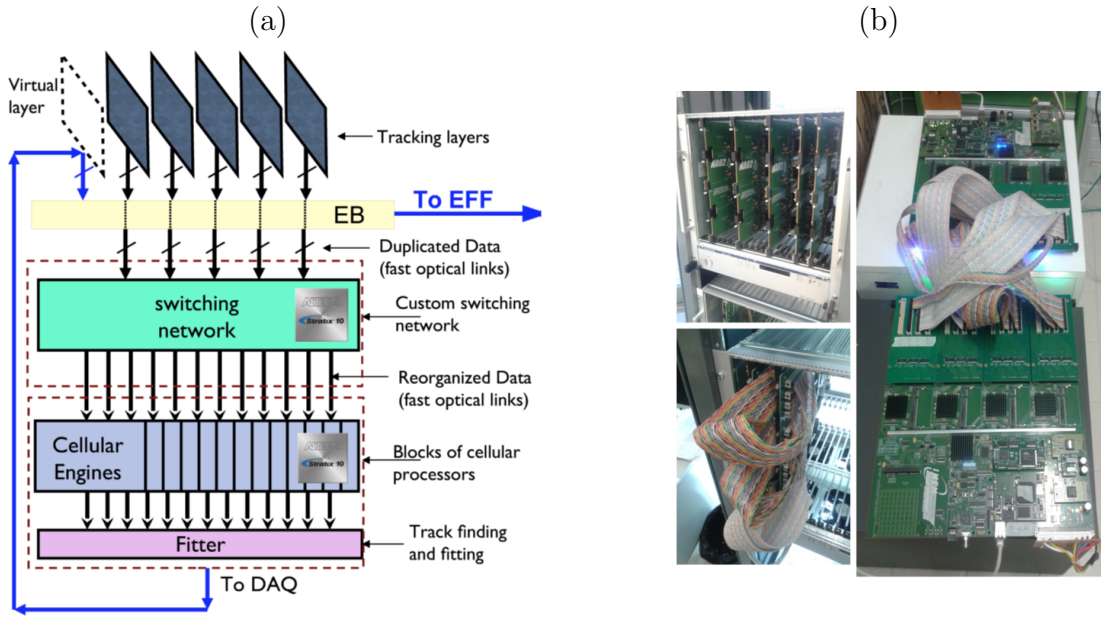

Figure 5.11: Track finding with the retina scheme: (a) schematic showing how the retina system could find downstream tracks in LHCb and inject them into the Event Filter Farm (EFF) where the software trigger is executed (EB refers to the event builder); (b) a successfully running proof-of-concept demonstrator.

Acknowledgements

We express our gratitude to our colleagues in the CERN accelerator departments for the studies they have performed in the preparation of this document, and many frutiful discussions. We thank the technical and administrative staff at the LHCb institutes. We acknowledge support from CERN and from the national agencies: CAPES, CNPq, FAPERJ and FINEP (Brazil); NSFC (China); CNRS/IN2P3 (France); BMBF, DFG and MPG (Germany); INFN (Italy); FOM and NWO (The Netherlands); MNiSW and NCN (Poland); MEN/IFA (Romania); MinES and FASO (Russia); MinECo (Spain); SNSF and SER (Switzerland); NASU (Ukraine); STFC (United Kingdom); NSF (USA). We acknowledge the computing resources that are provided by CERN, IN2P3 (France), KIT and DESY (Germany), INFN (Italy), SURF (The Netherlands), PIC (Spain), GridPP (United Kingdom), RRCKI and Yandex LLC (Russia), CSCS (Switzerland), IFIN-HH (Romania), CBPF (Brazil), PL-GRID (Poland) and OSC (USA). We are indebted to the communities behind the multiple open source software packages on which we depend. Individual groups or members have received support from AvH Foundation (Germany), EPLANET, Marie Skłodowska-Curie Actions and ERC (European Union), Conseil Général de Haute-Savoie, Labex ENIGMASS and OCEVU, Région Auvergne (France), RFBR and Yandex LLC (Russia), GVA, XuntaGal and GENCAT (Spain), Herchel Smith Fund, The Royal Society, Royal Commission for the Exhibition of 1851 and the Leverhulme Trust (United Kingdom).

References

[1] *The European strategy for particle physics update 2013*, CERN-Council-S/106.

[2] LHCb collaboration, R. Aaij *et al.*, *First evidence for the decay $B^0_s \to \mu^+\mu^-$*, Phys. Rev. Lett. **110** (2013) 021801, arXiv:1211.2674.

[3] LHCb collaboration, R. Aaij *et al.*, *Measurement of the $B^0_s \to \mu^+\mu^-$ branching fraction and search for $B^0 \to \mu^+\mu^-$ decays at the LHCb experiment*, Phys. Rev. Lett. **111** (2013) 101805, arXiv:1307.5024.

[4] CMS and LHCb collaborations, V. Khachatryan *et al.*, *Observation of the rare $B^0_s \to \mu^+\mu^-$ decay from the combined analysis of CMS and LHCb data*, Nature **522** (2015) 68, arXiv:1411.4413.

[5] LHCb collaboration, R. Aaij *et al.*, *Measurement of the $B^0_s \to \mu^+\mu^-$ branching ratio and effective lifetime and search for $B^0 \to \mu^+\mu^-$ decays*, LHCb-PAPER-2017-001, in preparation.

[6] LHCb collaboration, R. Aaij *et al.*, *Observation of D^0–$\overline{D}^0$ oscillations*, Phys. Rev. Lett. **110** (2013) 101802, arXiv:1211.1230.

[7] LHCb collaboration, R. Aaij *et al.*, *Measurement of the CKM angle γ from a combination of LHCb results*, JHEP **12** (2016) 087, arXiv:1611.03076.

[8] LHCb collaboration, R. Aaij *et al.*, *Precision measurement of CP violation in $B^0_s \to J/\psi K^+K^-$ decays*, Phys. Rev. Lett. **114** (2015) 041801, arXiv:1411.3104.

[9] LHCb collaboration, R. Aaij *et al.*, *Measurement of the CP-violating phase ϕ_s in $\overline{B}^0_s \to J/\psi \pi^-\pi^-$ decays*, Phys. Lett. **B736** (2014) 186, arXiv:1405.4140.

[10] LHCb collaboration, R. Aaij *et al.*, *Observation of $J/\psi p$ resonances consistent with pentaquark states in $\Lambda^0_b \to J/\psi p K^-$ decays*, Phys. Rev. Lett. **115** (2015) 072001, arXiv:1507.03414.

[11] LHCb collaboration, R. Aaij *et al.*, *Measurement of the forward-backward asymmetry in $Z/\gamma^* \to \mu^+\mu^-$ decays and determination of the effective weak mixing angle*, JHEP **11** (2015) 190, arXiv:1509.07645.

[12] LHCb collaboration, R. Aaij *et al.*, *Measurements of prompt charm production cross-sections in pp collisions at $\sqrt{s} = 13$ TeV*, JHEP **03** (2016) 159, arXiv:1510.01707.

[13] LHCb collaboration, R. Aaij *et al.*, *Measurement of two-particle correlations in proton-ion collisions at* $\sqrt{s_{NN}} = 5\ TeV$, Phys. Lett. **B762** (2016) 473, arXiv:1512.00439.

[14] LHCb collaboration, *Expression of Interest for an LHCb Upgrade*, CERN-LHCC-2008-007.

[15] LHCb collaboration, *Letter of Intent for the LHCb Upgrade*, CERN-LHCC-2011-001.

[16] LHCb collaboration, *Framework Technical Design Report for the LHCb Upgrade*, CERN-LHCC-2012-007.

[17] LHCb collaboration, *LHCb VELO Upgrade Technical Design Report*, CERN-LHCC-2013-021.

[18] LHCb collaboration, *LHCb Particle Identification Upgrade Technical Design Report*, CERN-LHCC-2013-022.

[19] LHCb collaboration, *LHCb Tracker Upgrade Technical Design Report*, CERN-LHCC-2014-001.

[20] LHCb collaboration, *LHCb Trigger and Online Upgrade Technical Design Report*, CERN-LHCC-2014-016.

[21] M. Nayak, *SuperKEKB, BEAST and Belle-II prospects*, Beauty 2016, Marseille, France, May 2016.

[22] F. Bordry, *Outline LHC schedule until 2035*, presentation to the CERN Science Policy Committee, June 2015.

[23] LHCb collaboration, R. Aaij *et al.*, *LHCb detector performance*, Int. J. Mod. Phys. **A30** (2015) 1530022, arXiv:1412.6352.

[24] W. Altmannshofer and D. M. Straub, *Implications of* $b \to s$ *measurements*, arXiv:1503.06199. 50th Rencontres de Moriond electroweak interactions and unified theories, La Thuile, Italy, March 2015.

[25] LHCb collaboration, R. Aaij *et al.*, *Angular analysis of the* $B^0 \to K^{*0}\mu^+\mu^-$ *decay using* $3\,fb^{-1}$ *of integrated luminosity*, JHEP **02** (2016) 104, arXiv:1512.04442.

[26] LHCb collaboration, R. Aaij *et al.*, *Angular analysis and differential branching fraction of the decay* $B_s^0 \to \phi\mu^+\mu^-$, JHEP **09** (2015) 179, arXiv:1506.08777.

[27] LHCb collaboration, R. Aaij *et al.*, *Differential branching fraction and angular anaysis of* $\Lambda_b \to \Lambda^0\mu^+\mu^-$ *decays*, JHEP **06** (2015) 115, arXiv:1503.07138.

[28] LHCb collaboration, R. Aaij *et al.*, *Angular analysis of the* $B^0 \to K^*e^+e^-$ *decay in the low-*q^2 *region*, JHEP **04** (2015) 064, arXiv:1501.03038.

[29] LHCb collaboration, R. Aaij *et al.*, *Angular analysis of charged and neutral* $B \to K\mu^+\mu^-$ *decays*, JHEP **05** (2014) 082, arXiv:1403.8045.

[30] LHCb collaboration, R. Aaij *et al.*, *Differential branching fractions and isospin asymmetries of* $B \to K^*\mu^+\mu^-$ *decays*, JHEP **06** (2014) 133, arXiv:1403.8044.

[31] LHCb collaboration, R. Aaij *et al.*, *Test of lepton universality using $B^+ \to K^+\ell\ell$ decays*, Phys. Rev. Lett. **113** (2014) 151601, arXiv:1406.6482.

[32] LHCb collaboration, R. Aaij *et al.*, *Measurement of the phase difference between the short- and long-distance amplitudes in the $B^+ \to K^+\mu^+\mu^-$ decay*, arXiv:1612.06764, submitted to Eur. Phys. J. C.

[33] S. Descotes-Genon, L. Hofer, J. Matias, and J. Virto, *On the impact of power corrections in the prediction of $B \to K^*\mu^+\mu^-$ observables*, JHEP **12** (2014) 125, arXiv:1407.8526.

[34] N. Serra, R. Silva Coutinho, and D. van Dyk, *Measuring the breaking of lepton flavour universality in $B \to K^*\ell^+\ell^-$*, arXiv:1610.08761.

[35] B. Capdevila *et al.*, *$B \to K^*(\to K\pi)\ell^+\ell^-$ theory and the global picture: What's next?*, arXiv:1609.01355. 4th Large Hadron Collider Physics Conference (LHCP 2016) Lund, Sweden, June 2016.

[36] B. Capdevila, S. Descotes-Genon, L. Hofer, and J. Matias, *Hadronic uncertainties in $B \to K^*\mu^+\mu^-$: a state-of-the-art analysis*, arXiv:1701.08672.

[37] LHCb collaboration, R. Aaij *et al.*, *First measurement of the photon polarization in radiative B_s^0 decays*, Phys. Rev. Lett. **118** (2016) 021801, arXiv:1609.02032.

[38] BaBar collaboration, J. P. Lees *et al.*, *Measurement of an excess of $\bar{B} \to D^{(*)}\tau^-\bar{\nu}_\tau$ decays and implications for charged Higgs bosons*, Phys. Rev. **D88** (2013) 072012, arXiv:1303.0571.

[39] Belle collaboration, A. Bozek *et al.*, *Observation of $B^+ \to \bar{D}^{*0}\tau^+\nu_\tau$ and evidence for $B^+ \to \bar{D}^0\tau^+\nu_\tau$ at Belle*, Phys. Rev. **D82** (2010) 072005, arXiv:1005.2302.

[40] LHCb collaboration, R. Aaij *et al.*, *Measurement of the ratio of branching fractions $\mathcal{B}(\overline{B}^0 \to D^{*+}\tau^-\overline{\nu}_\tau)/\mathcal{B}(\overline{B}^0 \to D^{*+}\mu^-\overline{\nu}_\mu)$*, Phys. Rev. Lett. **115** (2015) 111803, arXiv:1506.08614.

[41] B. Dutta and Y. Mimura, *Enhancement of $\mathcal{B}(B_d \to \mu^+\mu^-)/\mathcal{B}(B_s \to \mu^+\mu^-)$ in supersymmetric unified models*, Phys. Rev. D **91** (2015) 095011, arXiv:1501.02044.

[42] CMS collaboration, *Study of $B \to \mu^+\mu^-$ decays as a physics benchmark for the CMS Phase-II upgrade*, CMS PAS FTR-14-015.

[43] K. S. Babu and C. Kolda, *Higgs mediated $\tau \to 3\mu$ in the supersymmetric seesaw model*, Phys. Rev. Lett. **89** (2002) 241802, arXiv:hep-ph/0206310.

[44] A. Brignole and A. Rossi, *Lepton flavor violating decays of supersymmetric Higgs bosons*, Phys. Lett. **B566** (2003) 217, arXiv:hep-ph/0304081.

[45] P. Paradisi, *Constraints on SUSY lepton flavor violation by rare processes*, JHEP **10** (2005) 006, arXiv:hep-ph/0505046.

[46] C. Hays, M. Mitra, M. Spannowsky, and P. Waite, *Prospects for new physics in $\tau \to l\mu\mu$ at current and future colliders*, arXiv:1701.00870.

[47] LHCb collaboration, R. Aaij *et al.*, *Search for the lepton flavour violating decay* $\tau \to \mu^-\mu^+\mu^-$, JHEP **02** (2015) 121, arXiv:1409.8548.

[48] K. Hayasaka *et al.*, *Search for lepton flavor violating tau decays into three leptons with 719 million produced* $\tau^+\tau^-$ *pairs*, Phys. Lett. **B687** (2010) 139, arXiv:1001.3221.

[49] BaBar collaboration, J. P. Lees *et al.*, *Limits on tau lepton-flavor violating decays in three charged leptons*, Phys. Rev. **D81** (2010) 111101, arXiv:1002.4550.

[50] LHCb collaboration, R. Aaij *et al.*, *Determination of* γ *and* $-2\beta_s$ *from charmless two-body decays of beauty mesons*, Phys. Lett. **B739** (2015) 1, arXiv:1408.4368.

[51] LHCb collaboration, R. Aaij *et al.*, *Determination of the quark coupling strength* $|V_{ub}|$ *using baryonic decays*, Nature Physics **11** (2015) 743, arXiv:1504.01568.

[52] Plots courtesy of Maurizio Pierini.

[53] LHCb collaboration, R. Aaij *et al.*, *Measurement of the CP-violating phase* β *in* $\overline{B}^0 \to J/\psi\,\pi^+\pi^-$ *decays and limits on penguin effects*, Phys. Lett. **B742** (2015) 38, arXiv:1411.1634.

[54] LHCb collaboration, R. Aaij *et al.*, *Measurement of CP violation parameters and polarisation fractions in* $B_s^0 \to J/\psi\,\overline{K}^{*0}$ *decays*, JHEP **11** (2015) 082, arXiv:1509.00400.

[55] LHCb collaboration, R. Aaij *et al.*, *Measurement of CP violation in* $B_s^0 \to \phi\phi$ *decays*, Phys. Rev. **D90** (2014) 052011, arXiv:1407.2222.

[56] M. Artuso, G. Borissov, and A. Lenz, *CP violation in the* B_s^0 *system*, Rev. Mod. Phys. **88** (2016) 045002, arXiv:1511.09466.

[57] LHCb collaboration, R. Aaij *et al.*, *Measurement of the semileptonic* CP *asymmetry in* $B^0 - \overline{B}^0$ *mixing*, Phys. Rev. Lett. **114** (2015) 041601, arXiv:1409.8586.

[58] LHCb collaboration, R. Aaij *et al.*, *Measurement of the* CP *asymmetry in* $B_s^0 - \overline{B}_s^0$ *mixing*, Phys. Rev. Lett. **117** (2016) 061803, arXiv:1605.09768.

[59] D0 collaboration, V. M. Abazov *et al.*, *Study of CP-violating charge asymmetries of single muons and like-sign dimuons in* $p\bar{p}$ *collisions*, Phys. Rev. **D89** (2014) 012002, arXiv:1310.0447.

[60] P. Ilten *et al.*, *Proposed inclusive dark photon search at LHCb*, Phys. Rev. Lett. **116** (2016) 251803, arXiv:1603.08926.

[61] LHCb collaboration, R. Aaij *et al.*, *Search for Majorana neutrinos in* $B^- \to \pi^+\mu^-\mu^-$ *decays*, Phys. Rev. Lett. **112** (2014) 131802, arXiv:1401.5361.

[62] LHCb collaboration, R. Aaij *et al.*, *Searches for Majorana neutrinos in* B^- *decays*, Phys. Rev. **D85** (2012) 112004, arXiv:1201.5600.

[63] LHCb collaboration, R. Aaij *et al.*, *Search for long-lived scalar particles in* $B^+ \to K^+\chi(\mu\mu)$ *decay*, arXiv:1612.07818, submitted to Phys. Rev. D.

[64] LHCb collaboration, R. Aaij *et al.*, *Search for hidden-sector bosons in $B^0 \to K^{*0}\mu^+\mu^-$ decays*, Phys. Rev. Lett. **115** (2015) 161802, arXiv:1508.04094.

[65] L. Silvestrini, *CHARM-2015 Theory Summary*, 2015. arXiv:1510.05797. 7th International Workshop on Charm Physics (Charm 2015) Detroit, USA, May 2015.

[66] I. I. Bigi, *Bridge between hadrodynamics & HEP: regional CP violation in beauty & charm decays*, arXiv:1608.06528. 38th International Conference on High Energy Physics (ICHEP 2016) Chicago, USA, August 2016.

[67] LHCb collaboration, R. Aaij *et al.*, *Search for CP violation in the phase space of $D^0 \to \pi^+\pi^-\pi^+\pi^-$ decays*, arXiv:1612.03207, submitted to Phys. Lett. B.

[68] LHCb collaboration, *Updated limit for the decay $K^0_S \to \mu^+\mu^-$* , LHCb-CONF-2016-012.

[69] LHCb collaboration, *Evidence for the rare decay $\Sigma^+ \to p\mu^+\mu^-$*, LHCb-CONF-2016-013.

[70] F. J. Botella *et al.*, *On the search for the electric dipole moment of strange and charm baryons at LHC*, arXiv:1612.06769.

[71] LHCb collaboration, R. Aaij *et al.*, *Observation of the resonant character of the $Z(4430)^-$ state*, Phys. Rev. Lett. **112** (2014) 222002, arXiv:1404.1903.

[72] LHCb collaboration, R. Aaij *et al.*, *Production of associated Υ and open charm hadrons in pp collisions at $\sqrt{s} = 7$ and 8 TeV via double parton scattering*, JHEP **07** (2016) 052, arXiv:1510.05949.

[73] LHCb collaboration, R. Aaij *et al.*, *Identification of beauty and charm quark jets at LHCb*, JINST **10** (2015) P06013, arXiv:1504.07670.

[74] LHCb collaboration, R. Aaij *et al.*, *Measurement of forward $W \to e\nu$ production in pp collisions at $\sqrt{s} = 8$ TeV*, JHEP **10** (2016) 030, arXiv:1608.01484.

[75] LHCb collaboration, R. Aaij *et al.*, *Measurement of the forward Z^0 boson production cross-section in pp collisions at $\sqrt{s} = 13$ TeV*, JHEP **09** (2016) 136, arXiv:1607.06495.

[76] LHCb collaboration, R. Aaij *et al.*, *Measurement of forward W and Z^0 boson production in association with jets in proton-proton collisions at $\sqrt{s} = 8$ TeV*, JHEP **05** (2016) 131, arXiv:1605.00951.

[77] LHCb collaboration, R. Aaij *et al.*, *Measurement of forward W and Z^0 boson production in pp collisions at $\sqrt{s} = 8$ TeV* , JHEP **01** (2016) 155, arXiv:1511.08039.

[78] LHCb collaboration, R. Aaij *et al.*, *Measurement of the forward Z^0 boson cross-section in pp collisions at $\sqrt{s} = 7$ TeV*, JHEP **08** (2015) 039, arXiv:1505.07024.

[79] LHCb collaboration, R. Aaij *et al.*, *Study of W boson production in association with beauty and charm*, Phys. Rev. **D92** (2015) 052012, arXiv:1505.04051.

[80] LHCb collaboration, R. Aaij *et al.*, *Measurement of $Z^0 \to e^+e^-$ production at $\sqrt{s} = 8$ TeV*, JHEP **05** (2015) 109, arXiv:1503.00963.

[81] LHCb collaboration, R. Aaij *et al.*, *Measurement of the Z^0 + b-jet cross-section in pp collisions at $\sqrt{s} = 7$ TeV in the forward region*, JHEP **01** (2015) 064, arXiv:1411.1264.

[82] LHCb collaboration, R. Aaij *et al.*, *Measurement of the forward W boson production cross-section in pp collisions at $\sqrt{s} = 7$ TeV*, JHEP **12** (2014) 079, arXiv:1408.4354.

[83] LHCb collaboration, R. Aaij *et al.*, *Study of forward Z^0+jet production in pp collisions at $\sqrt{s} = 7$ TeV*, JHEP **01** (2014) 033, arXiv:1310.8197.

[84] LHCb collaboration, R. Aaij *et al.*, *Measurement of the cross-section for $Z^0 \to e^+e^-$ production in pp collisions at $\sqrt{s} = 7$ TeV*, JHEP **02** (2013) 106, arXiv:1212.4620.

[85] LHCb collaboration, R. Aaij *et al.*, *A study of the Z^0 production cross-section in pp collisions at $\sqrt{s} = 7$ TeV using tau final states*, JHEP **01** (2013) 111, arXiv:1210.6289.

[86] LHCb collaboration, R. Aaij *et al.*, *Inclusive W and Z^0 production in the forward region at $\sqrt{s} = 7$ TeV*, JHEP **06** (2012) 058, arXiv:1204.1620.

[87] LHCb collaboration, R. Aaij *et al.*, *Precision luminosity measurements at LHCb*, JINST **9** (2014) P12005, arXiv:1410.0149.

[88] M. Ferro-Luzzi, *Proposal for an absolute luminosity determination in colliding beam experiments using vertex detection of beam-gas interactions*, Nucl. Instrum. Meth. **A553** (2005) 388.

[89] LHCb collaboration, R. Aaij *et al.*, *Absolute luminosity measurements with the LHCb detector at the LHC*, JINST **7** (2012) P01010, arXiv:1110.2866.

[90] G. Bozzi, L. Citelli, M. Vesterinen, and A. Vicini, *Prospects for improving the LHC W boson mass measurement with forward muons*, Eur. Phys. J. **C75** (2015) 601, arXiv:1508.06954.

[91] LHCb collaboration, R. Aaij *et al.*, *Measurement of the $t\bar{t}$, $W + b\bar{b}$ and $W + c\bar{c}$ production cross sections in pp collisions at $\sqrt{s} = 8$ TeV*, Phys. Lett. **B767** (2016) 110, arXiv:1610.08142.

[92] LHCb collaboration, R. Aaij *et al.*, *First observation of top quark production in the forward region*, Phys. Rev. Lett. **115** (2015) 112001, arXiv:1506.00903.

[93] R. Gauld, *Feasibility of top quark measurements at LHCb and constraints on the large-x gluon PDF*, JHEP **02** (2014) 126, arXiv:1311.1810.

[94] A. L. Kagan, J. F. Kamenik, G. Perez, and S. Stone, *Top LHCb Physics*, Phys. Rev. Lett. **107** (2011) 082003, arXiv:1103.3747.

[95] R. Gauld, *Leptonic top-quark asymmetry predictions at LHCb*, Phys. Rev. **D91** (2015) 054029, arXiv:1409.8631.

[96] LHCb collaboration, R. Aaij *et al.*, *Study of $\psi(2S)$ production cross-sections and cold nuclear matter effects in pPb collisions at $\sqrt{s_{NN}} = 5$ TeV*, JHEP **03** (2016) 133, arXiv:1601.07878.

[97] LHCb collaboration, R. Aaij *et al.*, *Observation of Z^0 production in proton-lead collisions at LHCb*, JHEP **09** (2014) 030, arXiv:1406.2885.

[98] LHCb collaboration, R. Aaij *et al.*, *Study of Υ production and cold nuclear matter effects in pPb collisions at $\sqrt{s_{NN}} = 5$ TeV*, JHEP **07** (2014) 094, arXiv:1405.5152.

[99] LHCb collaboration, R. Aaij *et al.*, *Study of J/ψ production and cold nuclear matter effects in pPb collisions at $\sqrt{s_{NN}} = 5$ TeV*, JHEP **02** (2014) 072, arXiv:1308.6729.

[100] J. P. Lansberg *et al.*, *A Fixed-Target ExpeRiment at the LHC (AFTER@LHC) : luminosities, target polarisation and a selection of physics studies*, PoS **QNP2012** (2012) 049, arXiv:1207.3507.

[101] Riccardo De Maria, *Optics aspects and impact on luminosity*, 5th Joint HiLumi LHC-LARP Annual Meeting, CERN, Switzerland, October 2015.

[102] Updated numbers provided by Gianluigi Arduini, December 2016, private communication.

[103] I. B. Alonso and L. Rossi, *High Luminosity Large Hadron Collider (HL-LHC) Technical Design Report, EU Deliverable D1-10.*, CERN-ACC-2015-0140.

[104] W. Herr and Y. Papaphilippou, *Alternative running scenarios for the LHCb experiment*, CERN-LHC-PROJECT-REPORT-1009.

[105] Y. Papaphilippou, *Operation with high luminosity LHCb*, 26th LARP Hi-Lumi Collaboration Meeting, SLAC, USA, May 2016.

[106] F. Sanchez Galan, *Update on Mini TAN and D2 protection for IP8*, 17th HL-LHC TCC, CERN, Geneva, 29 September 2016.

[107] F. Cerutti, *Energy deposition aspects for LHCb request*, 5th Joint HiLumi LHC-LARP Annual Meeting, CERN, Switzerland, October 2015.

[108] I. Efthymiopoulos, *Hardware changes around LHCb*, 5th Joint HiLumi LHC-LARP Annual Meeting, CERN, Switzerland, October 2015.

[109] N. Neri *et al.*, *4D fast tracking for experiments at high luminosity LHC*, JINST **11** (2016) C11040.

[110] M. Fiorini, *Operational experience with the NA62 Gigatracker*, 25th international workshop on vertex detectors, La Biodola, Italy, September 2016.

[111] M. van Beuzekom *et al.*, *VeloPix ASIC development for LHCb VELO upgrade*, Nucl. Instrum. Meth. **A731** (2013) 92.

[112] ATLAS Collaboration, *ATLAS Phase-II Upgrade Scoping Document*, Tech. Rep. CERN-LHCC-2015-020. LHCC-G-166, CERN, Geneva, Sep, 2015.

[113] C. D'Ambrosio, *The future of RICH detectors through the light of the LHCb RICH*, RICH 2016, Bled, Slovenia, September 2016.

[114] S. Easo, *Overview of LHCb RICH upgrade*, RICH 2016, Bled, Slovenia, September 2016.

[115] R. Forty and M. Charles, *TORCH: time of flight identification with Cherenkov radiation*, Nucl. Instrum. Meth. **A639** (2011) 173.

[116] T. T. Bohlen *et al.*, *The FLUKA code: developments and challenges for high energy and medical applications*, Nucl. Data Sheets **120** (2014) 211.

[117] A. Ferrari, P. R. Sala, A. Fasso, and J. Ranft, *FLUKA: a multi-particle transport code*, CERN-2005-10, INFN/TC-05/11, SLAC-R-773.

[118] P. Bloch, *The CMS endcap calorimeter upgrade*, 3rd ECFA high luminosity LHC experiments workshop, Aix-les-Bains, France, October 2016.

[119] Z. Gecse, *CMS high-graularity calorimeter R&D*, 3rd ECFA high luminosity LHC experiments workshop, Aix-les-Bains, France, October 2016.

[120] R. Becker *et al.*, *Proof-of-principle of a new geometry for sampling calorimetry using inorganic scintillator plates*, Journal of Physics: Conference Series **587** (2015) 012039, arXiv:1405.6202, CALOR 2014, Gissen, Germany, April 2014.

[121] G. Bencivenni, R. De Oliveira, G. Morello, and M. Poli Lener, *The micro-Resistive WELL detector: a compact spark-protected single amplification-stage MPGD*, JINST **10** (2015) P02009.

[122] G. Aglieri Rinella *et al.*, *Test-beam results of a silicon pixel detector with Time-over-Threshold read-out having ultra-precise time resolution*, JINST **10** (2015) P12016.

[123] G. Pellegrini *et al.*, *Recent technological developments on LGAD and iLGAD detectors for tracking and timing applications*, Nucl. Instrum. Meth. **A831** (2016) 24, arXiv:1511.07175.

[124] N. Cartiglia *et al.*, *Beam test results of a 16 ps timing system based on ultra-fast silicon detectors*, arXiv:1608.08681.

[125] S. Parker *et al.*, *Increased speed: 3D silicon sensors; fast current amplifiers*, IEEE Trans. Nucl. Sci. **58** (2011) 404.

[126] A. Affolder *et al.*, *Charge collection studies in irradiated HV-CMOS particle detectors*, JINST **11** (2016) P04007.

[127] Supported by the European Research Council, grant ERC-2011-AdG, 291175-TORCH.

[128] T. M. Conneely, J. S. Milnes and J. Howorth, *Extended lifetime MCP-PMTs: characterisation and lifetime measurements of ALD coated microchannel plates, in a sealed photomultiplier tube*, Nucl. Instrum. Meth. **A732** (2013) 388.

[129] TORCH collaboration, L. C. Garcia *et al.*, *Micro-channel plate photon detector studies for the TORCH detector*, Nucl. Instrum. Meth. **A787** (2015) 197.

[130] TORCH collaboration, R. Gao *et al.*, *Development of TORCH readout electronics for customised MCPs*, JINST **11** (2016) C04012.

[131] T. Gys, *The TORCH detector R&D: status and perspectives*, RICH 2016, Bled, Slovenia, September 2016.

[132] TORCH collaboration, K. Fohl *et al.*, *TORCH - Cherenkov and time-of-flight PID detector for the LHCb upgrade at CERN*, JINST **11** (2016) C05020.

[133] M. Ambrosio *et al.*, *The OPERA magnetic spectrometer*, IEEE Trans. Nucl. Sci. **51** (2004) 975, arXiv:physics/0409137.

[134] D. Abbaneo *et al.*, *Design of a constant fraction discriminator for the VFAT3 front-end ASIC of the CMS GEM detector*, JINST **11** (2016) P02009.

[135] A. Abba *et al.*, *A specialized processor for track reconstruction at the LHC crossing rate*, JINST **9** (2014) C09001, arXiv:1406.7220.

[136] R. Cenci *et al.*, *First results of an artificial retina processor prototype*, EPJ Web Conf. **127** (2016) 00005, Connecting the Dots 2016, HEPHY, Vienna, Austria, February 2016.